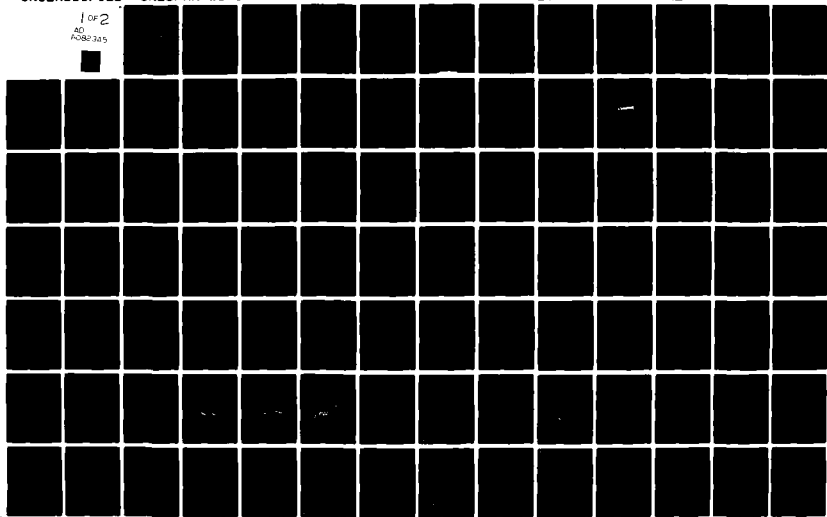


AD-A082 345

CALSPAN ADVANCED TECHNOLOGY CENTER BUFFALO NY AERODYN--ETC F/G 20/10
MEASUREMENT OF KINETIC RATES FOR CARBON MONOXIDE LASER SYSTEMS.(U)
NOV 79 J W RICH, R C BERGMAN, M J WILLIAMS F49620-77-C-0020
UNCLASSIFIED CALSPAN-WG-6021-A-3 AFOSR-TR-80-0207 NL

1 of 2

AD
A082345



AFOSR-TR- 80 - 0207

LEVEL

12
SR

AD A082345

**MEASUREMENT OF KINETIC RATES FOR
CARBON MONOXIDE LASER SYSTEMS**

J.W. Rich, R.C. Bergman, M.J. Williams
Aerodynamic Research Department

Calspan Advanced Technology Center
P.O. Box 400
Buffalo, N.Y. 14225

NOVEMBER 1979
CONTRACT NO. F49620-77-C-0020
FINAL SCIENTIFIC REPORT

DTIC
MAR 1980

Prepared for:
UNITED STATES AIR FORCE
PHYSICS DIVISION
OFFICE OF SCIENTIFIC RESEARCH
BOLLING AIR FORCE BASE, DC 20332

The views and conclusions contained in this document are those of the authors and should not be interpreted as necessarily representing the official policies or endorsements, either expressed or implied, of the Air Force Office of Scientific Research of the U.S. Government.

DDC FILE COPY

Approved for public release ;
distribution unlimited.

80 3 20 005

UNCLASSIFIED

SECURITY CLASSIFICATION OF THIS PAGE (When Data Entered)

REPORT DOCUMENTATION PAGE		READ INSTRUCTIONS BEFORE COMPLETING FORM
1. REPORT NUMBER (18) AFOSR TR-80-0207	2. GOVT ACCESSION NO. (9) Final Rept. Oct 76-30 8511	3. RECIPIENT'S CATALOG NUMBER
4. TITLE (and Subtitle) (6) MEASUREMENT OF KINETIC RATES FOR CARBON MONOXIDE LASER SYSTEMS	5. TYPE OF REPORT & PERIOD COVERED Final Report 10/76 - 10/30/79	6. PERFORMING ORG. REPORT NUMBER WG-6021-A-3
7. AUTHOR(s) (10) J. W. Rich, R. C. Bergman and M. J. Williams	8. CONTRACT OR GRANT NUMBER(s) F49620-77-C-0020	9. PERFORMING ORGANIZATION NAME AND ADDRESS Calspan Corporation Advanced Technology Center P. O. Box 400, Buffalo, New York 14225
10. CONTROLLING OFFICE NAME AND ADDRESS U.S. Air Force, Physics Division INP Office of Scientific Research Bolling Air Force Base, D.C. 20332	11. PROGRAM ELEMENT, PROJECT, AREA & WORK UNIT NUMBER 61102F (17) 162301/A1	12. SECURITY CLASS (of this report) Unclassified
13. MONITORING AGENCY NAME & ADDRESS (if different from Controlling Office) (12) 112	14. NUMBER OF PAGES 104	15. DECLASSIFICATION/DOWNGRADING SCHEDULE
16. DISTRIBUTION STATEMENT (of this Report) Approved for public release; distribution unlimited.		
17. DISTRIBUTION STATEMENT (of the abstract entered in Block 20, if different from Report)		
18. SUPPLEMENTARY NOTES		
19. KEY WORDS (Continue on reverse side if necessary and identify by block number) Vibrational Energy Transfer CO Lasers Molecular Electronic Excitation Laser Induced Chemistry		
20. ABSTRACT (Continue on reverse side if necessary and identify by block number) A continuous wave carbon monoxide laser is used to excite the vibrational mode of CO in gas mixtures flowing through an absorption cell. High steady-state excitation of the CO vibrational mode (0.3 eV/molecule) is achieved, while a translational-rotational temperature near 500 K is maintained by the steady flow of cold gas into the cell. These non-equilibrium conditions result in extreme vibration - vibration pumping, populating high-lying vibrational quantum levels (to $v = 42$) of CO. N_2 can also be pumped by vibrational		

391214

UNCLASSIFIED

SECURITY CLASSIFICATION OF THIS PAGE(When Data Entered)

20. Continued

energy transfer from CO. Using this experimental technique, the vibration-translation (V-T) deactivation rates for high vibrational quantum levels of carbon monoxide have been measured for collisions of carbon monoxide with argon at room temperature. The rates are quantum-state-resolved and have been measured for quantum levels from $V = 10$ up to $V = 42$.

At the highest levels of CO and CO/N₂ vibrational excitation, C₂ and CN molecules are formed, and are observed to fluoresce on various electronic band transitions, notably C₂ Swan ($A^3\Pi_g - X^3\Pi_u$) and CN violet ($B^2\Sigma^+ - X^2\Sigma^+$). Nitric oxide (NO) has been added to the vibrationally excited CO in the cell, and also has been observed to fluoresce on electronic bands (γ and β). The electronic fluorescence observed in these experiments appears to be created by vibration-to-electronic (V-E) transfer from the excited CO. Possible molecular electronic level laser action, pumped by such V-E processes, is discussed.

Accession for	
NTIS Serial	<input checked="" type="checkbox"/>
DEC TAB	<input type="checkbox"/>
Unannounced	<input type="checkbox"/>
Justification	
Re:	
Date:	
Author:	
Dist:	
A	

UNCLASSIFIED

SECURITY CLASSIFICATION OF THIS PAGE(When Data Entered)

TABLE OF CONTENTS

<u>Section</u>	<u>Page</u>
1 INTRODUCTION	1
2 EXPERIMENTAL METHOD.	4
2.1 APPARATUS	4
2.2 OPERATING CHARACTERISTICS	7
2.2.1 Conditions of Measurement.	7
2.2.2 Test Gases	9
2.2.3 Absorption Process	9
2.2.4 Laser Stabilization.	12
3 MEASUREMENT OF V-T RATES	17
3.1 MEASUREMENTS OF VIBRATIONAL POPULATION DISTRIBUTIONS.	17
3.1.1 CO-He Measurements	17
3.1.2 CO-Ar Measurements	17
3.1.3 Rotational Temperature Measurements.	20
3.1.4 Synthetic Spectrum Code.	27
3.2 REDUCTION OF CO-He AND CO-Ar V-T RATES AS FUNCTIONS OF VIBRATIONAL QUANTUM NUMBER	38
4 COMPUTER MODELING OF CELL KINETICS	53
5 CO DISSOCIATION AND C ₂ , CN FORMATION	64
5.1 C ₂ FORMATION.	64
5.2 EXPERIMENTS IN CO/N ₂ MIXTURES; CN FORMATION	70
5.3 DISCUSSION.	73
6 STUDIES OF V-E TRANSFER PROCESSES.	78
6.1 CO-NO V-E EXCHANGE.	78
6.2 MEASUREMENT OF NO EXCITED ELECTRONIC STATE POPULATIONS	85
6.3 V-E TRANSFER LASER CONCEPT.	86
REFERENCES	102

LIST OF FIGURES

<u>Figure</u>		<u>Page</u>
1	Schematic of Optical Pumping Apparatus	6
2	Absorption of Pump Laser Radiation. Spectral Dependence . .	11
3	Laser Stabilization; Broadband Power Lock-On	14
4	Laser Stabilization; Fast Sweep Mode	16
5	CO 1st Overtone Spectra for Selected Pressures of He Additive	19
6	CO 1st Overtone Spectra for Selected Pressures of Ar Diluent.	22
7	Rotational-Line Resolved $V = 1 \rightarrow 0$ R-Branch Spectrum, Precooled Gases.	25
8	Rotational-Line Resolved $V = 1 \rightarrow 0$ R-Branch Spectrum, Uncooled Gases	24
9	Determination of Rotational Temperature, Precooled Gases . .	25
10	Determination of Rotational Temperature, Uncooled Gases. . .	26
11	Comparison of Experimental and Computer-Generated Spectra. .	34
12	Measured Vibrational Population Distributions for Various He Concentrations.	36
13	Measured Vibrational Population Distributions for Various Ar Pressures	37
14	Reduction of Measured Distribution for CO-Ar Mixture, Case I	42
15	Reduction of Measured Distribution for CO-Ar Mixture, Case II.	43
16	Reduction of Measured Distribution for CO-Ar Mixture, Case III	44
17	Reduction of Measured Distribution for CO-Ar Mixture, Case IV.	45
18	CO-Ar V-T Transition Probability	47

LIST OF FIGURES (Cont'd)

<u>Figure</u>		<u>Page</u>
19	Reduction of Measured Distribution for CO-Ar-He Mixture, Case III	49
20	Reduction of Measured Distribution for CO-Ar-He Mixture, Case II.	50
21	CO-He V-T Transition Probability	51
22	Calculated Vibrational Energy for Selected Pressures of Ar Diluent.	58
23	Calculated CO Vibrational Population Distributions for Selected Pressures of Ar Diluent	59
24	Calculated Laser Pump Power Absorbed for Selected Pressures of Ar Diluent.	60
25	C ₂ Swan Bands (A ³ Π _g - X ³ Π _u) ΔV = 0 Sequence.	65
26	C ₂ Swan Bands (A ³ Π _g - X ³ Π _u) ΔV = +1 Sequence	66
27	C ₂ Swan Bands (A ³ Π _g - X ³ Π _u) ΔV = -1 Sequence	67
28	CN Violet Bands (B ² Σ ⁺ - X ² Σ ⁺), ΔV = 0 Sequence C ₂ Des Landres d'Azambuja (C'Π _g - b'Π _g) ΔV = 0 Sequence.	71
29	Effect of Flow Velocity on CN Violet Band Heading.	72
30	NO β and γ Bands, Excited by Transfer from Vibrationally Pumped CO.	80
31	CO ΔV = 2 Emission Spectra, for Several He Concentrations	81
32	NO β and γ Emission Spectra, for Several He Concentrations	83
33	CO and NO Energy Levels.	84
34	Energy Levels for Simplified V-E Transfer Laser Model	89
35	Estimated CO-NO β Transfer Laser Gain, T = 300°K	99
36	Estimated CO-NO β Transfer Laser Gain, T = 200°K	100
37	Estimated CO-NO β Transfer Laser Gain, T = 100°K	101

LIST OF TABLES

<u>Number</u>		<u>Page</u>
1	Typical Operating Conditions for V-T Rate Measurements. . . .	8
2	Operating Conditions for Series of CO - He V-T Rate Measurements.	18
3	Operating Conditions for Series of CO-Ar V-T Rate Measurements.	21
4	CO Molecular Spectroscopic Constants.	30
5	Einstein A Coefficients for Carbon Monoxide	31
6	Pump Laser Output Spectral Distribution Used In Modeling Calculations.	61
7	Mass Spectrographic Analysis of Precipitated Carbon	69
8	NO Electronic State Populations	87
9	Summary of Rate Data for CC/NO/Ar System.	97

Section 1
INTRODUCTION

The rates of energy transfer among the upper vibrational states of a molecule are often key processes in determining the kinetics of dissociation and the kinetics of other chemical reactions. Specifically, the thermal dissociation of diatomic molecules has long been regarded as one of the simplest examples of a collisionally induced gas phase reaction, and has been widely studied, both theoretically and experimentally.¹⁻⁶ In addition, the kinetic modeling of high power diatomic molecule lasers, such as the carbon monoxide laser,⁷⁻¹⁴ operating on the fundamental and overtone infrared bands, requires

1. Nikitin, E.E., Theory of Thermally Induced Gas Phase Reactions, Indiana Univ. Press, 1966.
2. Kieffer, J.H., Joosten, H.P.G., and Breshears, W.D., Chem. Phys. Lett. 30, 424 (1975).
3. Johnston, H. and Birks, K., Accounts Chem. Res. 5, 327 (1972).
4. Symposium on Current Status of Kinetics of Elementary Gas Reactions: Predictive Power of Theory and Accuracy of Measurement, J. Phys. Chem. 83, No. 1, 1979.
5. Bailey, W.F., and Guscadden, A., J. Physique Colloque C7 Supplement Aun 7, 40 July 1979.
6. Bailey, W.F., Ph.D. Thesis, Air Force Institute of Technology, Wright-Patterson Air Force Base, Ohio 1978.
7. Rich, J.W., Bergman, R.C., and Lordi, J.A., AIAA J. 13, 95 (1975).
8. Lordi, J.A., Falk, T.J., and Rich, J.W., "Analytical Studies of the Kinetics of Electrically Excited, Continuously Operating CO Flow Lasers", AIAA Paper No. 74-563, AIAA 7th Fluid and Plasma Dynamics Conference, Palo Alto, California, June 17-19, 1974.
9. Rich, J.W., Lordi, J.A., Gibson, R.A., and Kang, S.W., "Supersonic Electrically Excited Laser Development", Calspan Report No. WG-5164-A-3, June 1974.
10. Lacina, W.B., et al., IEE J. Quant. Elec. QE-9, 120 (1973).
11. Smith, N.S., Hassan, H.A., McDuville, R.M., "Analysis of High-Flow Electric Discharge CO Laser Systems", AIAA Paper No. 74-180, AIAA 12th Aerospace Sciences Meeting, Washington, D.C., January 30 - February 1, 1974.
12. Center, R.E. and Caledonia, G.E., Appl. Phys. Lett. 19, 211 (1971).
13. Rich, J.W., J. Appl. Phys. 42, 2719 (1971).
14. Suchkov, A.F., and Shebeko, Yu. N., Sov. J. Quant. Electron. 9, 565 (1979).

accurate knowledge of these upper state energy transfer rates. Finally, upper state kinetic data of this type is required for the analysis of much recent work in laser isotope separation and laser induced chemistry experiments.¹⁵⁻¹⁹

In this report, we describe measurements of energy transfer from high-quantum-number vibrational levels of the ground electronic state of carbon monoxide during molecular collisions. Measurements have been made of the specific rates of vibration-to-translation (V-T) energy transfer in CO-Ar and CO-He collisions, for CO vibrational energy levels from $V = 20$ to $V = 40$. The highest vibrational energy levels involved in these measurements are within $3/4$ of the carbon monoxide dissociation energy; indeed, evidence of dissociation is observed.

Until quite recently, the 1971 measurements of Hancock and Smith²⁰ for some of the CO-He V-T rates at 300°K remained the only data for relatively high-lying, anharmonic states of a diatomic molecule. In 1977, some additional CO-He V-T rates were measured by Fisher, Rabitz, and Lam²¹ at 150°K in an

-
15. Letokhov, V.S., Ann. Rev. Phys. Chem. 28, 133 (1977).
 16. Gordiets, B.F., and Mamedov, Sh. S., Sov. J. Quant. Electronics 5, 1082 (1976).
 17. Basov, N.G., Belenov, E.M., Gavrilina, L.K., Isakov, V.A., Markin, E.P., Oraevskii, A.N., Romanenko, V.I., and Ferapontov, N.B., JETP Lett. 20, 277 (1974); 19, 190 (1974); Basov, N.G., Belenov, E.M., Isakov, V.A., Markin, E.P., Oraevskii, A.N., Romanenko, V.I., and Ferapontov, N.B., Sov. J. Quant. Electron. 5, 510 (1975); JETP 41, 1017 (1976).
 18. Manuccia, T.J., and Goesling, C.E., Appl. Phys. Lett. 31, 575 (1977).
 19. Manuccia, T.J., and Clark, M.D., Appl. Phys. Lett. 28, 372 (1976).
 20. Hancock, G., and Smith, I.W.M., Chem. Phys. Lett. 8, 41 (1971).
 21. Fisher, E.R., Rabitz, H., and Lam, S.H., "CO-He V-T Rates at High Quantum Numbers", Paper presented at 5th Conference on Chemical and Molecular Lasers, St. Louis, Mo. 1977.

electric discharge. In the present experiments, additional CO-He V-T rates over an extended range of vibrational quantum numbers, and also, upper-state CO-Ar V-T rates have been obtained. In contrast to previous measurements in reaction vessels^{20,22} or electric discharges,²¹ the present study is in an experimental environment relatively free from extraneous modes of energy transfer.

In addition to the measurement of state resolved V-T rates, a separate series of experiments were conducted which examined transfer of energy from the vibrational mode of CO to the electronic mode of various molecular collision partners (V-E transfer). Evidence of electronic excitation of electronic states of NO, C₂, and CN molecules by this mechanism has been obtained.

The following section, 2, describes the apparatus and experimental technique used in this study. Section 3 presents the details of the V-T rate measurements. Section 4 gives the results of computer modeling of the experiment, and a further discussion of the V-T rate data.

As mentioned above, vibrational excitation of CO to high quantum levels has resulted in observable dissociation and in the formation of gas phase C₂ dimers. These aspects of the present program are reported in Section 5. Finally, the results of the program on energy transfer from vibrationally excited CO to the electronic mode of collision partners are given in the concluding Section, 6.

22. Hancock, G., and Smith, I.W.M., Appl. Opt. 10, 1827 (1971).

Section 2 EXPERIMENTAL METHOD

2.1 APPARATUS

The apparatus used in the present experiments is basically a flowing gas absorption cell, in which a nonequilibrium distribution of vibrational energy is created in CO gas. This type of nonequilibrium vibrational population distribution is created by vibration-vibration (V-V) inelastic collisions between the diatomic molecules, in which a quantum of vibrational energy is exchanged by the vibrational modes of the collision partners. Such an inelastic collision is not typically an exact resonance energy transfer event, due to energy mismatch caused by the anharmonicity of the vibrational quantum states. This resonance defect must be supplied by energy exchange with the translational and rotational modes. At low translational temperature, collisions between molecules in anharmonic vibrational states m and n ($m > n$) have greater probability for producing V-V transitions to states $m + 1$ and $n - 1$ compared with transitions to $m - 1$ and $n + 1$. This biasing occurs because the former transition results in a net surplus of vibrational energy which is readily fed into the translational mode. In contrast, the latter transition requires energy to be supplied from the translational mode, which, at low temperature, has relatively little available energy. Accordingly, a population inversion tends to be created among the upper anharmonic vibrational states. Theoretical treatment of the kinetic equations governing these processes by Treanor, Rich and Rehm²³ has shown that under the stated conditions of high vibrational energy and low translational temperature, the vibrational population distribution created by this exchange mechanism will be non-Boltzmann, and characterized by relative overpopulation of the higher anharmonic vibrational quantum states with respect to the lowest vibrational states. This kinetic effect has been found to be the major inversion mechanism in carbon monoxide lasers. In the present apparatus, the nonequilibrium distribution is produced in steady state by direct optical pumping.

23. Treanor, C.E., Rich, J.W., and Rehm, R.G., J. Chem. Phys. 48, 1798 (1968).

The experimental apparatus, as presently set up, is shown schematically in Figure 1. Premixed carbon monoxide, helium and argon gases flow through the 25-cm-long absorption cell. Radiation from an electrically excited supersonic flow cw carbon monoxide laser is admitted along the axis of the cell through a calcium fluoride window; the beam diameter nearly fills the 0.95-cm cell diameter. The pump radiation is absorbed into the vibrational energy mode of the CO component of the cell gas mixture. The degree of absorption of the laser beam by the gases is determined by measuring the power incident upon and transmitted through the cell using thermopiles. The cell is equipped with calcium fluoride windows along its length to permit spectroscopic monitoring of the carbon monoxide vibrational excitation.

A 3/4 meter Spex scanning monochromator is used as the basic spectroscopic monitoring instrument. To record spontaneous infrared emission from the side windows of the cell, the monochromator is equipped with a 300 line/m.m. optical grating, blazed at $4\ \mu\text{m}$, and an InSb liquid-nitrogen-cooled photovoltaic detector. The radiative signal into the monochromator is interrupted with a synchronous-motor-driven chopper, driven at 800 hertz. Chopped output from the detector is amplified by a Princeton Applied Research Corporation Model 124 phase-sensitive amplifier; the amplified signal is recorded on a Varian Corporation Model 2400 chart recorder.

The monochromator is evacuated. The relative amplitude response of the system is determined in standard fashion by scanning a calibrated black body source. Details of the instrument response determination are given in Reference 24.

With this optical pumping technique, measurements using the monochromator system described above have shown that vibrational energy of the carbon monoxide in the cell can be made quite high, typically 0.3 - 0.4 eV per

24. Rich, J.W., Bergman, R.C., and Williams, M.J., "Measurement of Kinetic Rates for Carbon Monoxide Laser Systems", Calspan Report No. WG-6021-A-1, November 1977.

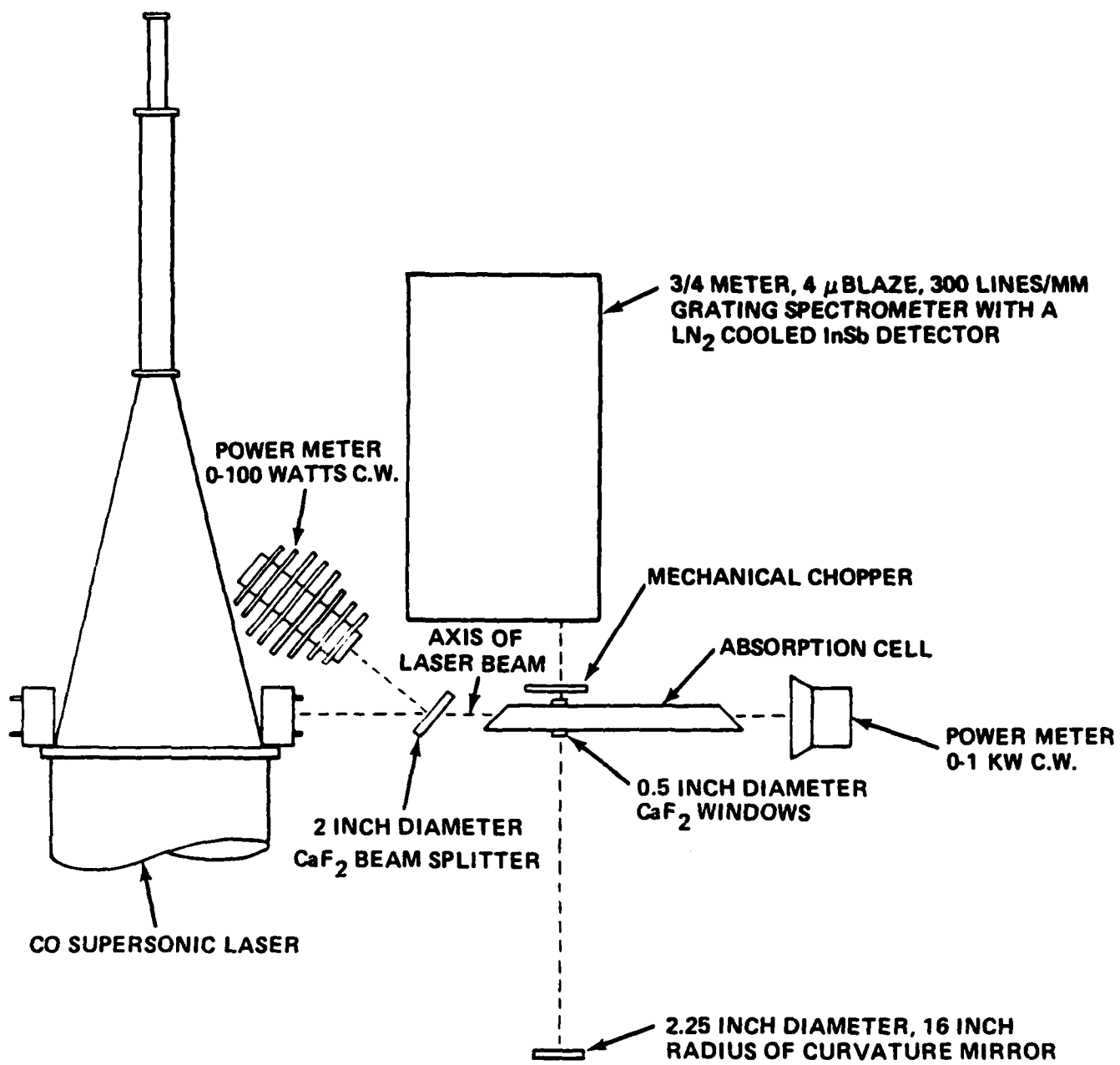


Figure 1 SCHEMATIC OF OPTICAL PUMPING APPARATUS

CO molecule, while the translational-rotational temperature can be kept relatively low ($0[300^{\circ}\text{K}]$). This nonequilibrium condition is maintained in the steady state in the cell by the flow.

There are several advantages of this method of vibrational excitation for the study of kinetic rates, in contrast to the usual methods involving direct electric-discharge excitation or thermal excitation. The principle advantages are:

- (1) Vibrational excitation is achieved in an environment free from the kinetic complications of ionized gas processes.
- (2) Higher levels of vibrational excitation can be achieved than are typically obtained in either electric discharge or by thermal excitation.
- (3) Pressures and gas mixtures can be varied over a large range. Conditions can be achieved that would be totally incompatible with electric discharge stability.

2.2 OPERATING CHARACTERISTICS

2.2.1 Conditions of Measurement

Table 1 lists typical operating parameters of the pump laser and absorption cell for the rate measurements reported here. The c.w. pump laser output is broad-band, distributed over more than thirty CO vibrational-rotational lines ranging in wavelength from 4.8 to 5.5 μm . These lines are from vibrational transitions $v=3 \rightarrow 2$ up to $v=15 \rightarrow 14$. With the addition of argon in the amount listed in the table, the heat capacity of the gas flow is quite high; the maximum temperature rise that could occur if all the absorbed laser power were relaxed into the translational and rotational gas modes at equilibrium is 71°K . In practice, the actual translational-rotational temperature rise throughout the region of measurement in the cell is far less than this. Spectroscopic measurement of the relative rotational line intensity of CO and other molecular

TABLE 1

TYPICAL OPERATING CONDITIONS FOR V-T
RATE MEASUREMENT EXPERIMENTS

Laser Power	205 Watts
Laser Power Absorbed	39 Watts
Cell Pressure	760 Torr
Cell Gas Inlet Temperature	300°K
Cell Flow Velocity	907 cm/sec
Cell Gas Concentrations:	
Carbon Monoxide	$2.10 \times 10^{17} \text{ cm}^{-3}$
Helium	$1.30 \times 10^{18} \text{ cm}^{-3}$
Argon	$2.30 \times 10^{19} \text{ cm}^{-3}$

emitters (see Section 3.1.3 below) in the flow allows a rotational temperature of $\sim 300^\circ\text{K} \pm 10^\circ\text{K}$ to be inferred. Accordingly, the rate measurements given in subsequent sections are reported for a temperature of 300°K .

2.2.2 Test Gases

The gases used in the cell were Air Products Co. UHP grade CO, nominal purity 99.8%; Linde Corporation H.P. grade Ar, nominal purity 99.996%; Linde Corporation H.P. grade He, nominal purity 99.995%. Before entering the cell, the CO and Ar gases pass through a system of double traps. The first traps consist of a 10' long helical coil of 3/8" tubing, filled with alumina pellets. These coils are wall-cooled by a dry ice/methanol bath. The second set of traps consist of 10' long coils filled with copper wool; these coils are wall-cooled by baths of freezing propanol slush. This system is a development of the method originally proposed by Milliken.²⁵ The system is designed to reduce the concentrations of condensable impurities, most especially water vapor and hydrocarbons other than CH_4 , to less than 0.5 ppm. The details of the gas purification system used, and an assessment of the influence of residual impurities, have been given in Reference 24.

2.2.3 Absorption Process

It can be seen from Table 1 that, for the conditions listed there, 19% of the pump laser power is absorbed. The details of the mechanism by which the pump laser beam is absorbed at the relatively low cell pressure and temperature of Table 1 remain to be clarified. As noted previously, the output from the pump laser beam is distributed among approximately 30 P-branch rotation-vibration lines from the $v=3 \rightarrow 2$ to the $v=15 \rightarrow 14$ vibrational transition, the most intense lines being on the lower vibrational transitions. After transmission through

25. Milliken, R.C., J. Chem. Phys. 38, 2855 (1963).

the CO in the cell, it is observed that the lowest level transitions, beginning with $v=3 \rightarrow 2$, are the most strongly absorbed. The extent of absorption decreases with increasing vibrational band quantum number, with transitions above $v=11$ being only slightly attenuated. The total amount of absorption increases with decreasing total gas pressure; while approximately 19% of the pump beam is absorbed at the one atmosphere conditions of Table 1, more than 70% of the pump beam is absorbed in 40 torr of pure CO, without any diluent. Figure 2 shows the spectral dependence of the absorption of the pump laser radiation for such a low pressure case. The output of the pump laser is displayed on the lower trace; the upper trace shows what is transmitted through 40 torr of CO in the cell. The variation of absorption with vibrational quantum level is qualitatively similar to the higher pressure cases; however, at the lower pressure, it can be seen that all lines on the $v=3 \rightarrow 2$, $4 \rightarrow 3$, and $5 \rightarrow 4$ bands have been entirely absorbed, and the other lower bands are greatly attenuated. The higher vibrational bands transitions are absorbed to a lesser extent. It appears that the absorbing transitions occurring in the pumped gas are identical to those of the laser emission; given the nature of the V-V pumped distribution in the cell, it is predictable that the lower level transitions will be more readily absorbed, due to the higher populations of these states. The major unknown effect at this time, however, is the mechanism by which the $V = 2$ level of the CO in the cell is initially populated. Since the laser does not emit on the $V = 1 \rightarrow 0$ or $V = 2 \rightarrow 1$ bands, calculation shows absorption of pump radiation would be very slow, level $V = 2$ of the cell CO gas being very slightly populated at the initial cell kinetic temperature of approximately 300°K . However, it is observed that there is some initial local absorption near the cell end window which provides for beam exit. This cell volume undoubtedly contains small regions of slow moving or recirculating gas that remains in the beam for long periods of time. Since the gas is optically thick on the fundamental vibrational transitions, such local absorption regions can transfer energy to the body of the gas, and can provide $V = 2$ level population in the small amount necessary to cause significant $V = 2 \rightarrow 3$ absorption. After this triggering occurs, V-V pumping insures an exponentially increasing number of molecules capable of resonance absorption of the pump radiation.

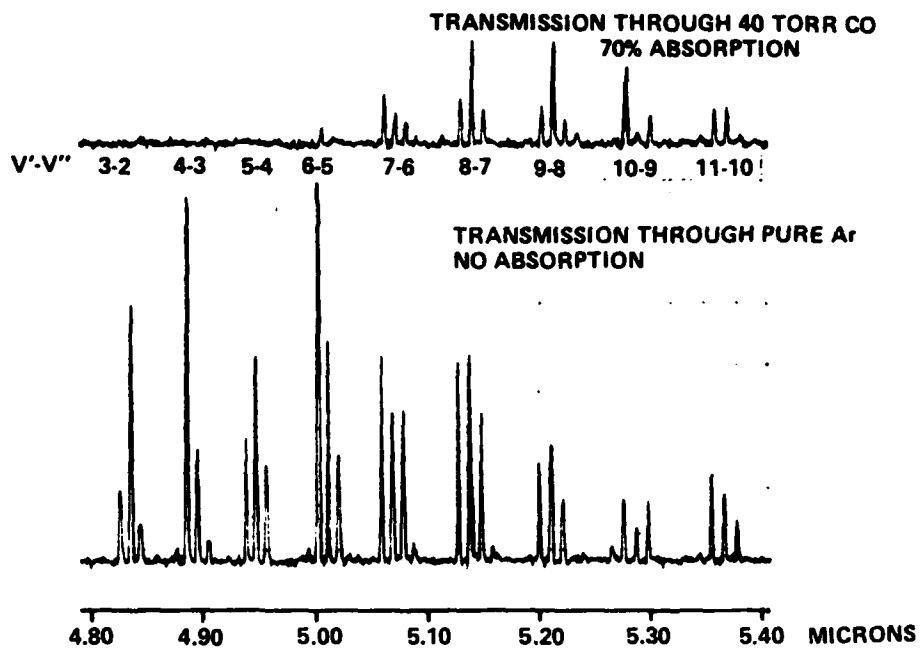


Figure 2 ABSORPTION OF PUMP LASER RADIATION. SPECTRAL DEPENDENCE

We note that the relatively short wavelength output of the supersonic flow pump laser, which provides transitions on the $V = 3 \rightarrow 2$ band, appears essential for the large absorptions observed. We have attempted to pump the cell with a more conventional, wall-cooled CO laser, having its shortest-wavelength output on the $V = 6 \rightarrow 5$ band. No absorption was observed, even when cell gases were preheated to $\sim 600^\circ\text{K}$.

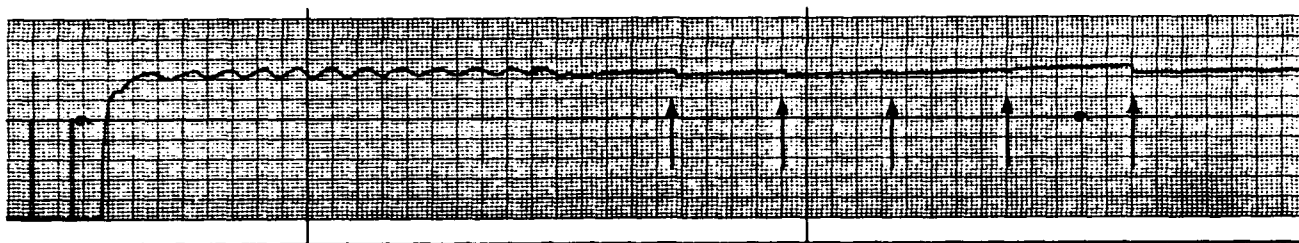
2.2.4 Laser Stabilization

The supersonic flow CO laser used for an optical pump in the present experiments has good amplitude stability; short term stability (millisecond-time scale) is well within $\pm 10\%$; long term stability is within $\pm 3\%$. However, the laser does exhibit rotational line jumping; while the laser output power per vibrational band is roughly constant, the oscillation is usually on three or four rotational lines in each band, and peak power in each band varies among these lines. An individual rotational line may actually cease oscillation entirely, and an adjacent line, having comparable gain, may turn on. This phenomenon causes a long-term amplitude oscillation of $\pm 3\%$. The period of this oscillation is rather long, being of several seconds duration when the laser is just turned on, and increasing to almost a minute after several minutes of operation. It is apparent that this behavior is caused by the cooling of the laser mirror mounts. The in-cavity gas temperature is near 45°K , and the mirror mounts are initially at room temperature. As they are cooled by the cold gas flow, they begin to move in one direction, causing the observed rotational line shifting. The movement is most rapid in the initial moments of laser operation, when thermal gradients are largest. As the laser cools, mirror movements slows, causing the observed increase in the period of the oscillation due to line jumping.

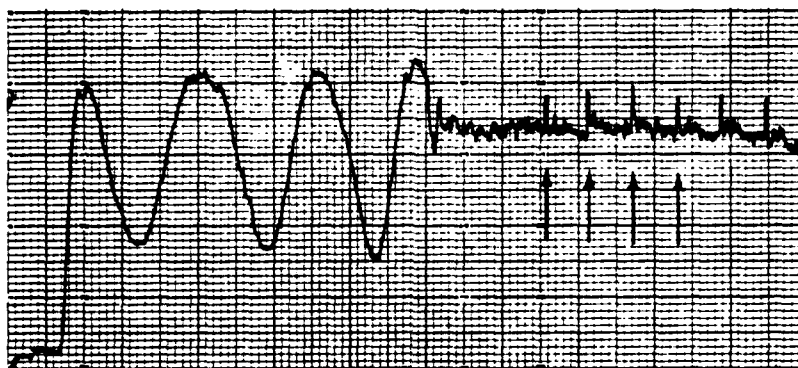
For experimental conditions for which the energy absorbed per CO molecule in the cell is high, the gas rapidly becomes fully vibrationally excited and the detected sidelight emission is not significantly perturbed by the pump laser

oscillations. Thus, the inferred V-T and radiative rates based on this emission also are not significantly affected. However, in experiments where the energy absorbed is low and the gas is not fully vibrationally excited, the IR sidelight radiation is observed to oscillate in phase with the oscillations of the pump radiation. Furthermore, instead of exhibiting the $\pm 3\%$ oscillation of the pump radiation, the emitted radiation in this upstream, initial absorption region may oscillate by $\pm 50\%$ or more. It is clear that this amplifying effect is caused by the oscillations of the shortest-wavelength pump laser lines; these are the only lines that are significantly absorbed in the initial absorption region of the cell, and any fluctuations in these lines can cause large variations in IR emission from this region.

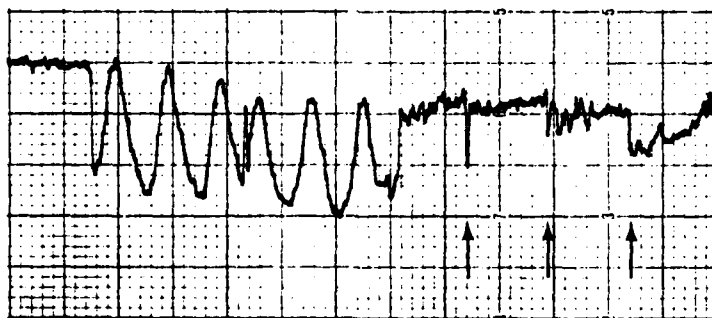
In order to stabilize the pump laser, the totally reflecting mirror in the optical cavity was mounted on a piezoelectric translator. This translator is part of a feedback loop which senses a change in laser output power and adjusts the cavity length to maximize that laser power. Initially the total laser output power was monitored to adjust the translator. This resulted in fairly good stabilization as can be seen in Figure 3 which shows the total laser output power (a), the output power of one laser line (b), and the cell sidelight emission at a given wavelength (c), initially without laser stabilization and then with stabilization. The arrows on the stabilized portions of the curves indicate the points at which the feedback loop performed a "mode jump". This mode jump occurs when the translator reaches its maximum extension. The translator then "jumps" back to a preset position which ideally results in maximum laser output. It can be seen from Figure 3 that these mode jumps occur frequently and that they do have an effect on the observed powers and sidelight emission. The effect is relatively small in Figure 3; however, in other experimental runs the effect was not tolerable. The basic problem was in finding the preset position for the translator to jump to; the position appeared to change from run to run. Between the mode jumps, the pump laser appears to be very well stabilized. However, for some experimental conditions, all the necessary data can not be recorded in this time interval.



a) LASER OUTPUT, TOTAL POWER



b) LASER OUTPUT, SINGLE LINE

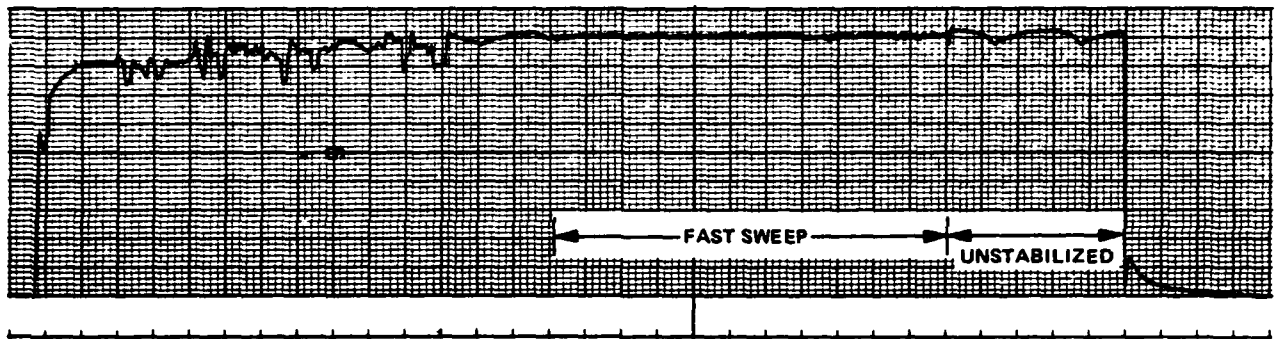


c) CELL SIDELIGHT EMISSION

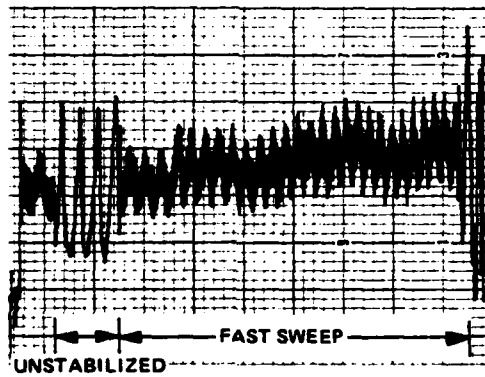
Figure 3 LASER STABILIZATION; BROADBAND POWER LOCK-ON

A second stabilization procedure utilized the power output of one laser line instead of the total laser power to signal adjustment of the translator. However, this method also exhibited mode jump effects, with no significant improvement over broad-band lock-on.

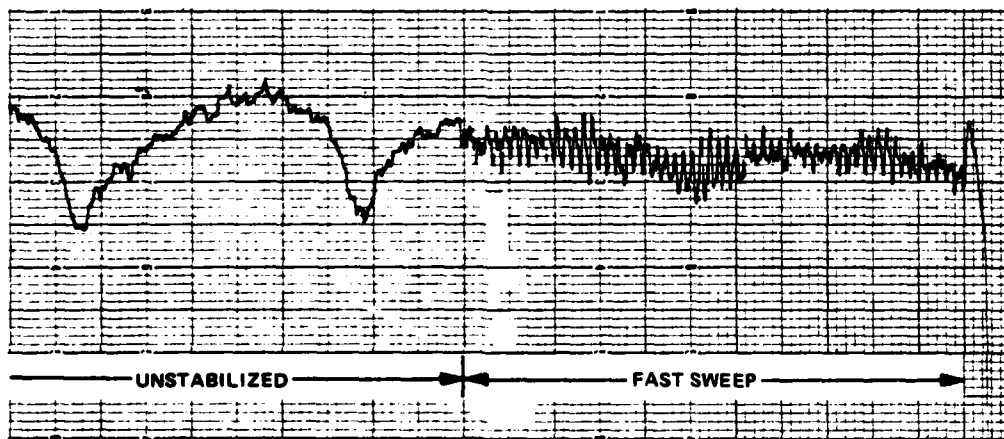
The final solution was to operate the translator in the "fast sweep" manner. In the fast sweep, the translator moves through its full extension at a frequency of 5 Hz. In this way the observed data is seen to have an averaged stability. Figure 4 shows the total laser output power (a), the output power of one laser line (b), and the cell sidelight emission at a given wavelength (c), with and without the translator operated in the fast sweep manner.



a) LASER OUTPUT, TOTAL POWER



b) LASER OUTPUT, SINGLE LINE



c) CELL SIDELIGHT EMISSION

Figure 4 LASER STABILIZATION; FAST SWEEP MODE

Section 3
MEASUREMENT OF V-T RATES

3.1 MEASUREMENTS OF VIBRATIONAL POPULATION DISTRIBUTIONS

3.1.1 CO-He Measurements

A series of runs for three gas mixtures was performed at one atmosphere total pressure in the cell. Table 2 lists the operating conditions for these three cases. It will be noted that Case I is a CO/Ar mixture, and that Cases II and III have added amounts of helium. For these three cases, spectra of the CO 1st overtone bands were recorded from emission at a side window in the cell 6 cm downstream from the gas injection port. The optical instrumentation discussed in Section 2.1 was used. Figure 5 shows these spectra. The lowest trace is for Case I, and is the emission from a mixture of CO in argon alone. The approximate center of selected vibrational band components is indicated on the figure. Measurable emission is obtained from the lowest forty vibrational quantum states of CO. The topmost state detected, $V=42$, corresponds to an energy of approximately 8 eV, an energy level equal to approximately 75% of the CO dissociation energy. This large number of populated states is characteristic of the V-V pumped "plateau" under conditions of very small rates of vibration-to-translation (V-T) deactivation. The upper two traces of Figure 5 illustrate the effect of helium addition to the CO/Ar gas mixture. CO-He V-T rates provide much faster collisional deactivation of the upper vibrational quantum states, and this feature is evident in the spectra. In the middle trace, with 5% He, (Case II), levels above approximately $V=38$ are quenched; in the top trace, with 12% He, (Case III), levels above $V=33$ are quenched.

3.1.2 CO-Ar Measurements

While a CO-Ar V-T rate can be inferred from the spectrum of Case I of Table 2 and Figure 5, CO-Ar V-T rate data over a wider range of vibrational quantum numbers can be inferred by varying Ar pressure in the cell. For this purpose, cell pressure was varied from 1.0 to 23.5 atmospheres. A set of four experimental conditions spanning this range was chosen. To accomplish the

TABLE 2
OPERATING CONDITIONS FOR SERIES OF CO - He V-T RATE MEASUREMENTS

Run No.	<u>I</u>	<u>II</u>	<u>III</u>
Cell Pressure, atm.	1	1	1
CO Concentration, cm ⁻³	2.10x10 ¹⁷	2.10x10 ¹⁷	1.93x10 ¹⁷
Ar Concentration, cm ⁻³	2.43x10 ¹⁹	2.30x10 ¹⁹	2.15x10 ¹⁹
He Concentration, cm ⁻³	0	1.30x10 ¹⁸	3.03x10 ¹⁸
Cell Gas Flow Velocity, cm sec ⁻¹	905	907	980
Laser Power, Watts	200	205	205
Laser Power Absorbed, Watts	40	39	39

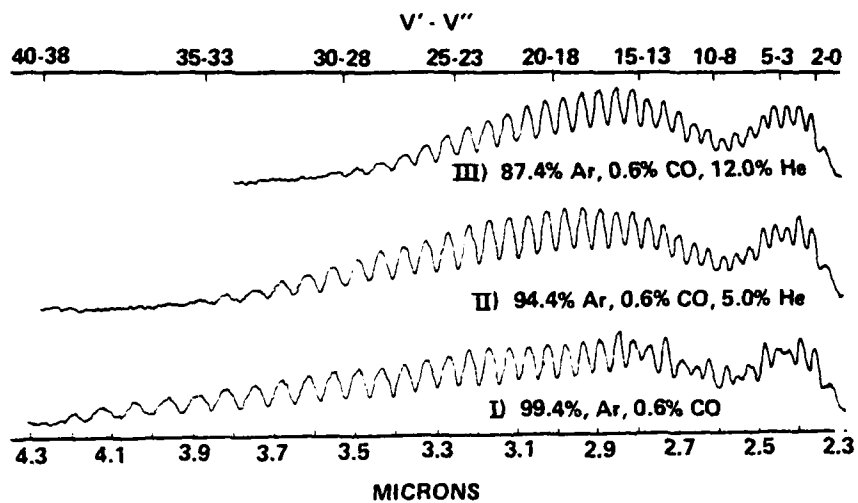


Figure 5 CO 1st OVERTONE SPECTRA FOR SELECTED PRESSURES OF He ADDITIVE

pressure change an orifice downstream of the cell was restricted until the desired pressure was achieved. With the mass flows of CO and Ar fixed, the gas flow velocity changed to accommodate this pressure change. Table 3 lists the pump laser operating conditions and cell conditions for the four cases. In each case the CO 1st overtone infrared sidelight emission was again recorded at the station 6 cm from the gas inlet port. Figure 6 shows these spectra with Case I the lowest pressure run and Case IV the highest pressure run. The approximate center of selected vibrational band components is indicated on the figure.

3.1.3 Rotational Temperature Measurements

It is possible to make direct measurements of the rotational temperature of the CO in the cell by using highly resolved emission spectra from the $V = 1 \rightarrow 0$ R branch component of the CO fundamental IR radiation. As noted previously, the cell operating conditions are such that the fundamental CO band is optically thick in the streamwise direction. However, for a 1 cm path across the cell, the higher rotational lines of the $V = 1 \rightarrow 0$ R branch are thin, permitting an unambiguous temperature measurement.

Figures 7 and 8 show typical resolved $V = 1 \rightarrow 0$ R branch spectra, from which rotational temperature was determined. These spectra were measured at the same station (6 cm downstream) as the 1st overtone band spectra of Figures 5 and 6 which are used to determine vibrational state population distribution; the rotational line scans were typically made immediately before the scans of the overtone vibrational bands. Figure 7 is a spectrum taken with precooling of cell gases; Figure 8 is a spectrum from uncooled gases. Rotational temperature is inferred from the slope of a plot of $\ln [I/(J' + J'' + 1)]$ vs. $J'(J' + 1)$, in the standard fashion. Such plots for the spectra of Figures 7 and 8 are shown in Figure 9 and 10. It can be seen that a rotational temperature of 350°K is inferred for the uncooled case, and 260°K for the cooled case. The effect of self-absorption can be noted on these plots. At low rotational quantum numbers, $\ln [I/(J' + J'' + 1)]$ becomes nonlinear in $J'(J' + 1)$, falling below a straight line extrapolation. Only the higher rotational level lines can be used to infer T_{ROT} .

TABLE 3
OPERATING CONDITIONS FOR SERIES OF CO-AR V-T RATE MEASUREMENTS

<u>Case No.</u>	<u>I</u>	<u>II</u>	<u>III</u>	<u>IV</u>
Cell Pressure, atm	1.0	5.2	10.7	23.5
CO Concentration, cm^{-3}	1.97×10^{17}	1.02×10^{18}	2.10×10^{18}	4.62×10^{18}
Ar Concentration, cm^{-3}	2.28×10^{19}	1.17×10^{20}	2.43×10^{20}	5.34×10^{20}
Cell Gas Flow Velocity, cm sec^{-1}	965	187	90.5	41.1
Laser Power, watts	220	220	220	220
Laser Power Absorbed, watts	50	43	48	55
Rotational Temperature, $^{\circ}\text{K}$	320	340	365	400

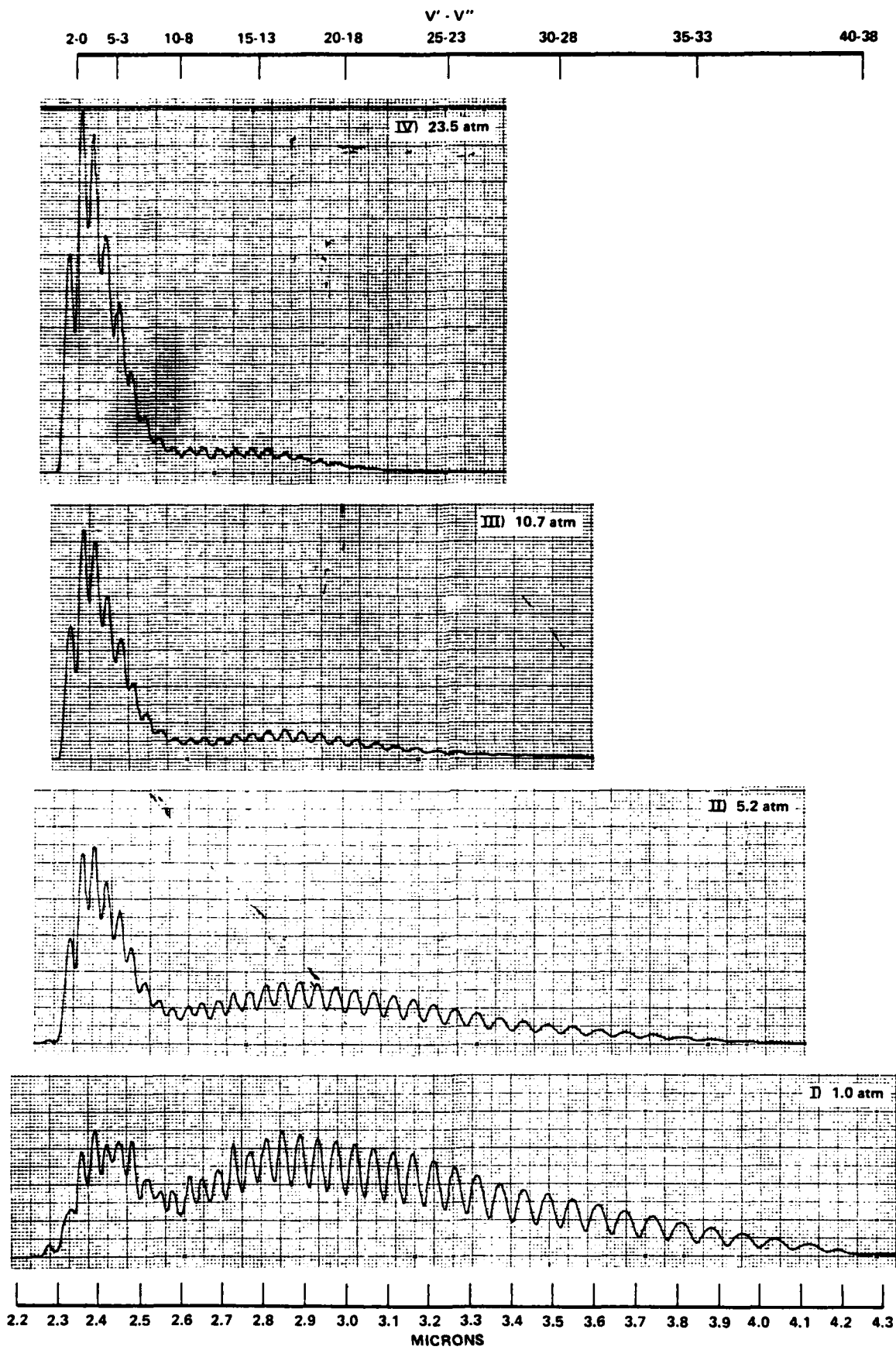


Figure 6 CO 1st OVERTONE SPECTRA FOR SELECTED PRESSURES OF Ar DILUENT

$T_{\text{ROT}} = 260^{\circ}\text{K}$

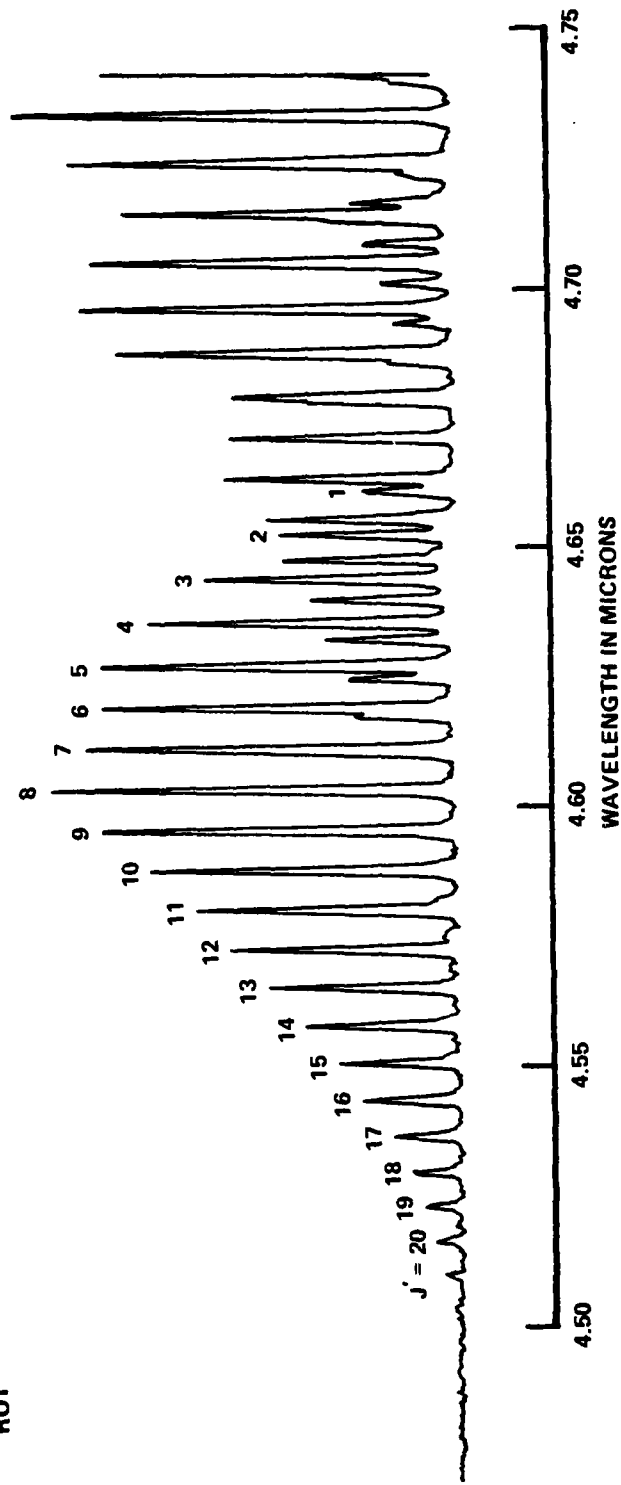


Figure 7 ROTATIONAL-LINE RESOLVED $V = 1 \rightarrow 0$ R-BRANCH SPECTRUM,
PRECOOLED GASES

$T_{ROT} = 353^{\circ}K$

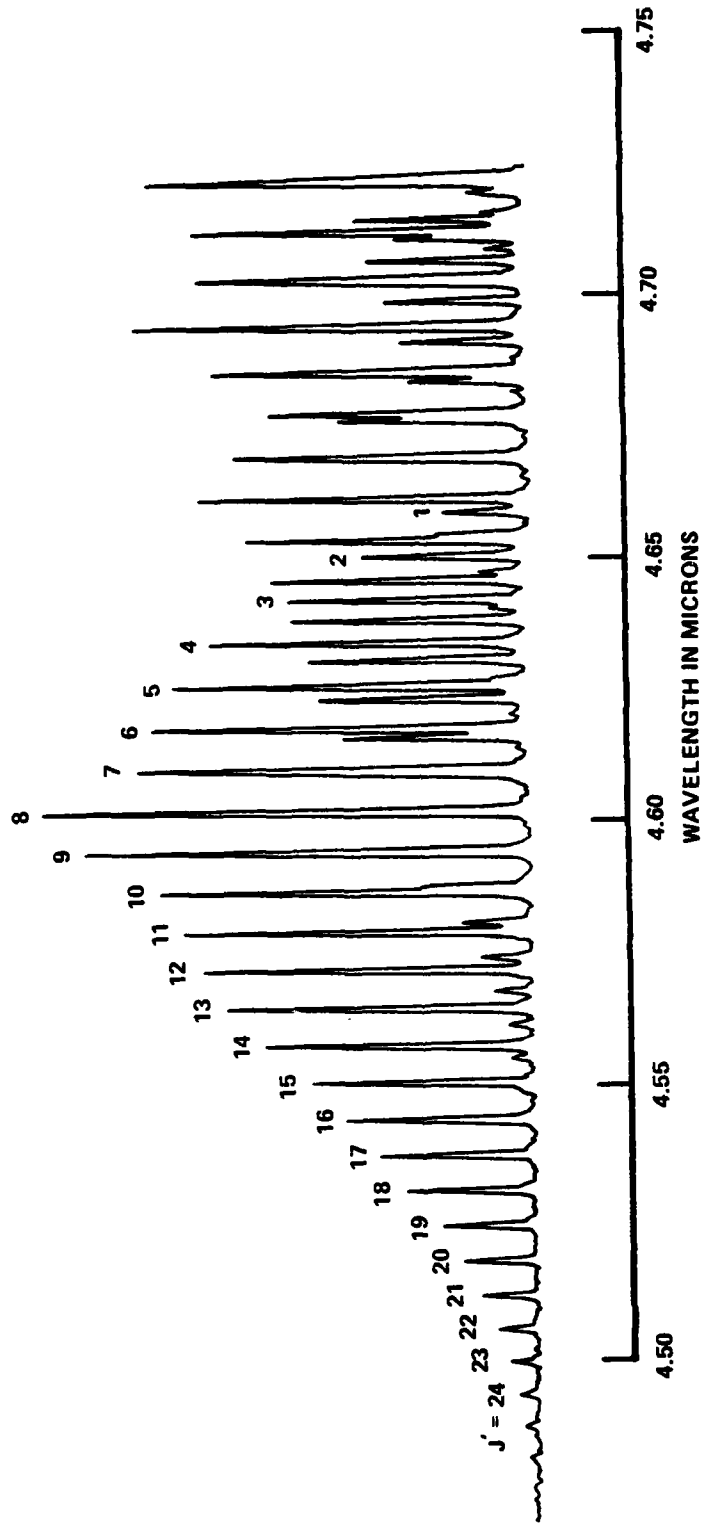


Figure 8 ROTATIONAL-LINE RESOLVED V = 1-0 R-BRANCH SPECTRUM,
UNCOOLED GASES

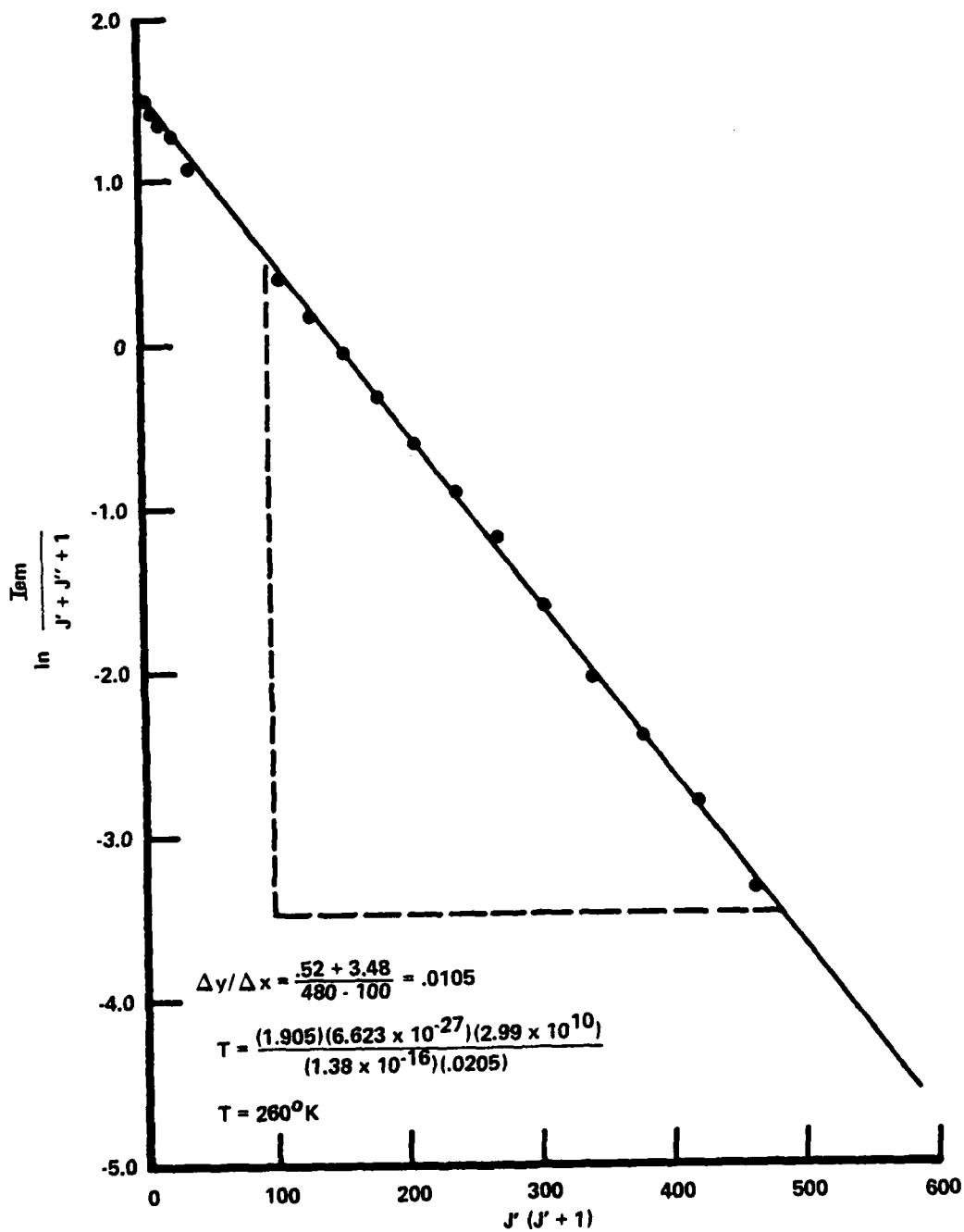


Figure 9 DETERMINATION OF ROTATIONAL TEMPERATURE, PRECOOLED GASES

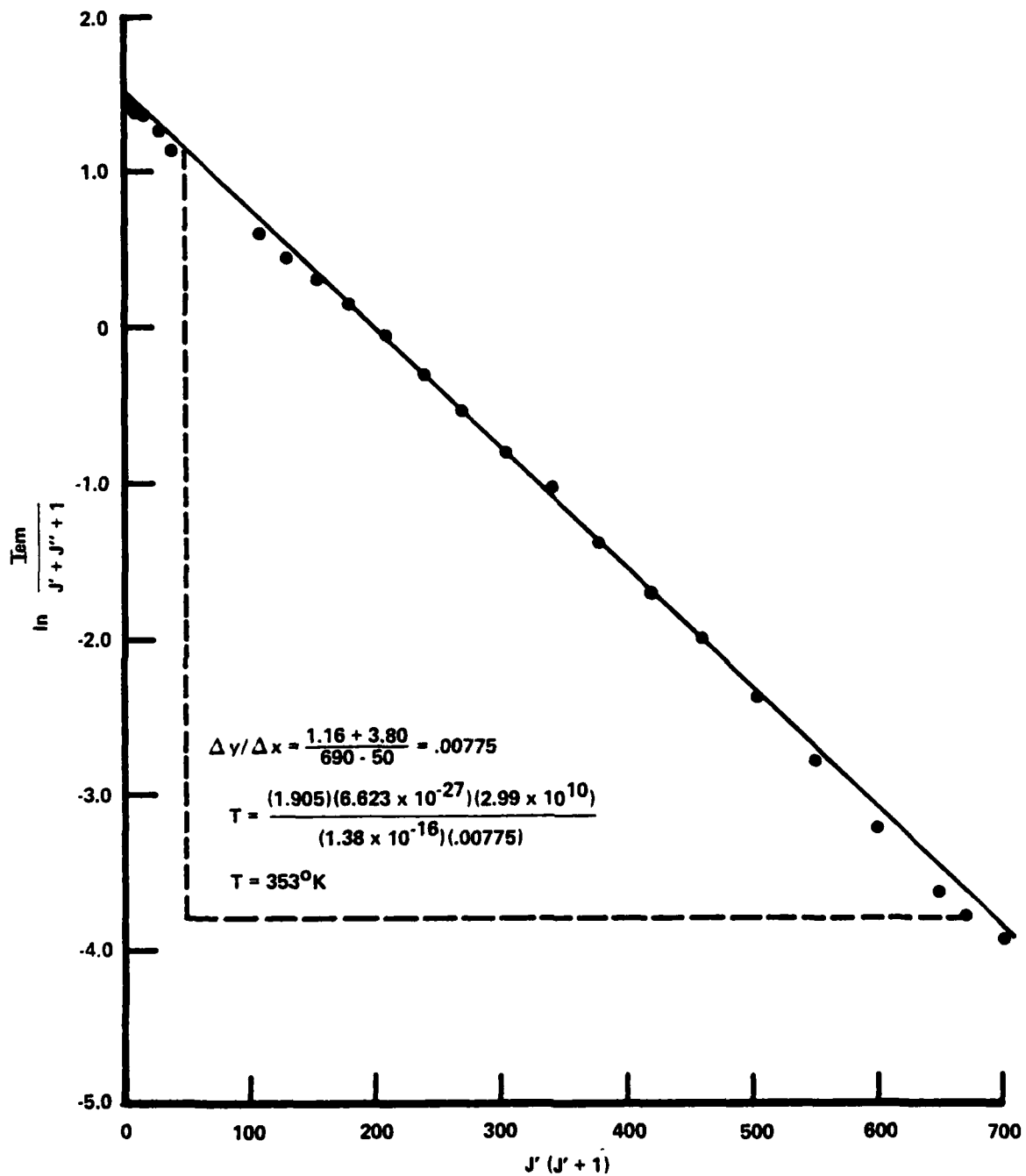


Figure 10 DETERMINATION OF ROTATIONAL TEMPERATURE, UNCOOLED GASES

At the pressures and residence times of our experiments, rotational and translational modes are in equilibrium. Accordingly, the translational temperature is taken as equal to the measured T_{ROT} in all data reduction. We estimate a probable error in this method of T_{ROT} measurement of $\pm 10^\circ K$. For the four cases in Figure 6, the measured rotational temperatures are $320^\circ K$, $340^\circ K$, $365^\circ K$, and $400^\circ K$ for Cases I thru IV respectively. The temperature rise with increased pressure in these cases is a result of the decreased gas flow velocity decreasing the convective gas cooling. For the three cases in Figure 5 no direct measurement of rotational temperature was made. However, Case I in Figure 5 and the cases of Figure 5 have similar operating conditions, so a rotational temperature of $320^\circ K$ is assigned to the cases of Figure 5 and used in the rate reduction.

3.1.4 Synthetic Spectrum Code

Vibrational population distributions are inferred by comparison of the experimental spectra of Figures 5 and 6 with computer-generated spectra, calculated using the same instrument response as the laboratory equipment. This spectrum is calculated for the experimental rotational-translational temperature, and for a vibrational quantum state population distribution chosen for the best fit to the experimental spectrum. A detailed description of this by-now-standard method of inferring vibrational populations from partially resolved spectra is given by Oettinger and Horn.²⁶ We will only note that the relative total emission intensity, $I(\lambda)$, at any wavelength, λ , is given by:

$$I(\lambda) = \frac{D_\lambda}{\lambda^4} \sum_{\substack{\text{CONTRIBUTING} \\ \text{PROGRESSIONS}}} \sum_{\substack{\text{CONTRIBUTING} \\ \text{BANDS}}} \left\{ |R_{v',v''}|^2 N_{v'} \frac{1}{(Q_{ROT})_{v'}} \right. \\ \cdot \left[\sum_{\substack{\text{CONTRIBUTING} \\ \text{P-BRANCH LINES}}} S_{\lambda_{LC} - \lambda} (J'_p + 1) e^{-J'_p(J'_p + 1) h c B_{v'} / k T_{rot}} \right. \\ \left. \left. + \sum_{\substack{\text{CONTRIBUTING} \\ \text{R-BRANCH LINES}}} S_{\lambda_{LC} - \lambda} (J'_R) e^{-J'_R(J'_R + 1) h c B_{v'} / k T_{rot}} \right] \right\}$$

26. Horn, K.P., and Oettinger, P.E., J. Chem. Phys. 54, 3040 (1971).

where

- D_λ = arbitrarily normalized detector response function
- $|R_{V'V''}|^2$ = squared transition moments for the vibrational transition $V' \rightarrow V''$ obtained from "A" coefficient data
- V', V'' = vibration quantum numbers for the upper and lower levels respectively for a given transition
- J'_P, J'_R = rotational quantum numbers for the upper and lower levels for transition of the P branch and R branch respectively. (The corresponding lower level quantum numbers are $J''_P = J'_P + 1$ and $J''_R = J'_R - 1$)
- $(Q_{ROT})_V$ = approximate rotational partition function for vibrational level $V = \frac{h T_{ROT}}{h c B_V}$
- $N_{V'}$ = number density (molecules per unit volume of radiating species in vibrational level $V = V'$)
- h = Planck's constant
- c = speed of light
- k = Boltzmann's constant
- B_V, D_V = rotational constants for vibrational level V
 $B_V = B_e - \alpha_e (V + \frac{1}{2}) + \gamma_e (V + \frac{1}{2})^2$
 $D_V = D_e - \beta_e (V + \frac{1}{2})$
- T_{ROT} = rotational temperature
- $S_{|\lambda_{LC} - \lambda|}$ = triangular scanning function
 $= \frac{\Delta \lambda_{CUT} - |\lambda_{LC} - \lambda|}{\Delta \lambda_{CUT}^2}$

where

$$\Delta \lambda_{CUT} = \text{half the base of the scanning function triangle}$$

$$\begin{aligned}\lambda_{Lc} &= \text{wavelength at line center} \\ &= 10^4 / (E_V' - E_V'' + (E_{J'}')_{V'} - (E_{J''})_{V''})\end{aligned}$$

where

$$\begin{aligned}E_V &= \omega_e (v + \frac{1}{2}) - \omega_e x_e (v + \frac{1}{2})^2 + \omega_e y_e (v + \frac{1}{2})^3 \\ &\quad - \omega_e z_e (v + \frac{1}{2})^4 + \omega_e a_e (v + \frac{1}{2})^5 - \omega_e b_e (v + \frac{1}{2})^6 \\ (E_{J'})_{V'} &= [J(J+1)] B_V - [J(J+1)]^2 D_V\end{aligned}$$

It will be noted that inputs to the computed spectra, in addition to the vibrational populations N_V and the translational-rotational temperature T , include the usual molecular spectroscopic constants for the CO molecule, and the spontaneous emission "A" coefficients for all significantly intense transitions in the spectral range of interest. In the present work, the CO molecular spectroscopic constants of Mantz²⁷ and Roh and Rao²⁸ are used; these are listed in Table 4. The "A" coefficients used are based on the model calculations of Young and Eachus,²⁹ as extended by Fisher;³⁰ these are tabulated in Table 5.

Figure 11 shows a comparison of an experimental spectrum and a computer-generated spectrum with the vibrational population distribution chosen for optimal matching. (The experimental spectrum is Case I of Figure 5). It can be seen that the fit is quite good. It should be noted that with significant

-
27. Mantz, A.W., Nichols, E.R., Alpert, B.D. and Rao, K.N., *Journal of Molecular Spectroscopy* 35, 325-328, (1970).
28. Roh, W. B. and Rao, K.N., *J. Mol. Spectrosc.* 49, 317 (1974).
29. Young, L.A. and Eachus, W.J., *J. Chem. Phys.* 44, 4195 (1966).
30. Lightman, A.J. and Fisher, E.R., *Appl. Phys. Lett.* 29, 593 (1976); Fisher, E.R., Private Communication (1977).

TABLE 4
CO MOLECULAR SPECTROSCOPIC CONSTANTS

Values of Mantz (Ref. 45)

ω_e	=	2.1698196 (3) cm^{-1}
$\omega_e x_e$	=	1.329180 (1) cm^{-1}
$\omega_e y_e$	=	1.1229 (-2) cm^{-1}
$\omega_e z_e$	=	-4.7 (-7) cm^{-1}
$\omega_e a_e$	=	2.94 (-6) cm^{-1}
$\omega_e b_e$	=	5.65 (-8) cm^{-1}
B_e	=	1.9312649 cm^{-1}
α_e	=	1.7505337 (-2) cm^{-1}
β_e	=	1.38 (-7) cm^{-1}
D_e	=	6.1025 (-6)
γ_e	=	1.39 (-9)

TABLE 5
EINSTEIN A COEFFICIENTS FOR CARBON MONOXIDE

$$\frac{A_{v', v'-q}}{A_{q,0}}$$

v'	First Overtone	Second Overtone
	($q = 2$)	($q = 3$)
2	1.0000	_____
3	2.9763	1.000
4	5.8985	4.1217
5	9.7298	1.0569 (1)
6	1.4557 (1)	2.1768 (1)
7	2.0120 (1)	3.8746 (1)
8	2.6457 (1)	6.3506 (1)
9	3.3786 (1)	9.6598 (1)
10	4.1556 (1)	1.3990 (2)
11	5.0314 (1)	1.9560 (2)
12	5.9282 (1)	2.6271 (2)
13	6.9251 (1)	3.4504 (2)
14	7.9709 (1)	4.4471 (2)
15	9.0023 (1)	5.6109 (2)
16	1.0130 (2)	6.9496 (2)
17	1.1290 (2)	8.5077 (2)
18	1.2476 (2)	1.0262 (3)
19	1.3765 (2)	1.2516 (3)
20	1.4986 (2)	1.4595 (3)
21	1.6212 (2)	1.7099 (3)
22	1.7536 (2)	1.9825 (3)
23	1.8754 (2)	2.2921 (3)
24	1.9956 (2)	2.6256 (3)
25	2.1249 (2)	2.9909 (3)

TABLE 5 (Cont'd)

EINSTEIN A COEFFICIENTS FOR CARBON MONOXIDE

V'	First Overtone ($q = 2$)	Second Overtone ($q = 3$)
26	2.2520 (2)	3.3793 (3)
27	2.3642 (2)	3.8206 (3)
28	2.4846 (2)	4.2747 (3)
29	2.6134 (2)	4.8679 (3)
30	2.7249 (2)	5.5296 (3)
31	2.8310 (2)	5.8685 (3)
32	2.9310 (2)	6.4639 (3)
33	3.0510 (2)	7.0745 (3)
34	3.1573 (2)	7.7563 (3)
35	3.2292 (2)	8.4187 (3)
36	3.3129 (2)	9.1178 (3)
37	3.3881 (2)	9.8685 (3)
38	3.4536 (2)	1.0567 (4)
39	3.5085 (2)	1.1358 (4)
40	3.5538 (2)	1.2121 (4)
41	3.6022 (2)	1.2883 (4)
42	3.6382 (2)	1.3657 (4)
43	3.6625 (2)	1.4488 (4)
44	3.6751 (2)	1.5281 (4)
45	3.6745 (2)	1.6027 (4)
46	3.6607 (2)	1.6715 (4)
47	3.6453 (2)	1.7428 (4)
48	3.6161 (2)	1.8245 (4)
49	3.5721 (2)	1.8707 (4)
50	3.55 (2)	1.9424 (4)
51	3.50 (2)	2.00 (4)
52	3.43 (2)	2.06 (4)
53	3.37 (2)	2.11 (4)

TABLE 5 (Cont'd)
EINSTEIN A COEFFICIENTS FOR CARBON MONOXIDE

V'	First Overtone ($q = 2$)	Second Overtone ($q = 3$)
54	3.30 (2)	2.17 (4)
55	3.21 (2)	2.21 (4)
56	3.13 (2)	2.25 (4)
57	3.04 (2)	2.30 (4)
58	2.97 (2)	2.32 (4)
59	2.88 (2)	2.36 (4)
60	2.78 (2)	2.39 (4)

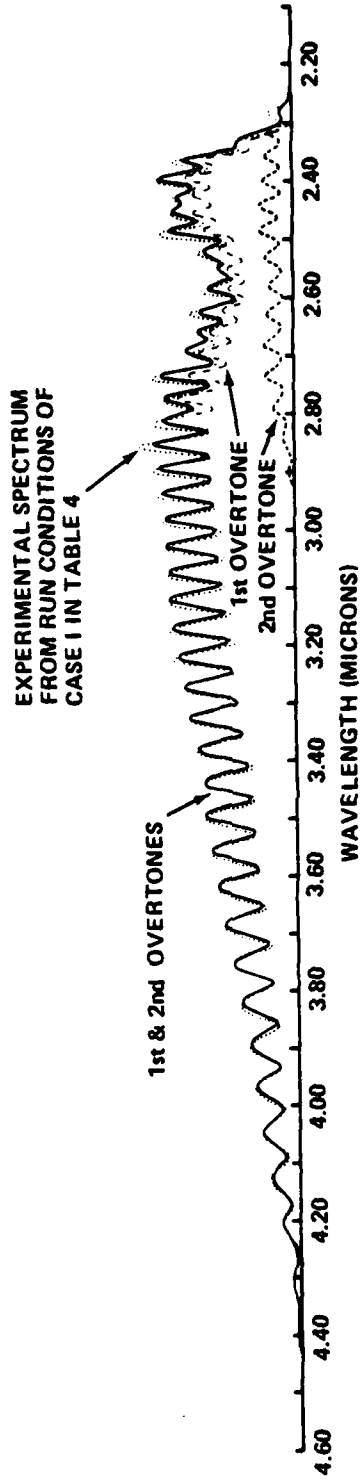


Figure 11 COMPARISON OF EXPERIMENTAL AND COMPUTER-GENERATED SPECTRA

population of vibrational quantum states up to $V \approx 40$, there is a substantial contribution of the 2nd overtone ($\Delta V = 3$) transitions to the total spectrum in the 2.3 to 2.9 micron region. The second overtone transitions involved in this region are $V=29 \rightarrow 27$ up to $V=41 \rightarrow 39$. This redundancy on the measurement of emission from levels $V=29$ to $V=41$ provides a verification of the correctness of the extended Young and Eachus model of the overtone A coefficients for CO, as given in Table 5.

Figure 12 and Figure 13 show the vibrational population distributions inferred, using the synthetic spectrum method, from the spectra of Figure 5 and Figure 6, respectively. Figure 12 are distributions for a total cell gas pressure of ~ 1 atm., showing the effect of adding helium. Figure 13 are distributions measured for various argon diluent pressures, showing the effect of argon quenching.

Referring to these figures, it will be noted that the distribution functions can be characterized by three regions of radically differing slopes. In the first region, below $V \approx 10$, the distribution initially falls rapidly from $V = 0$. From the initial slope of the distribution in this region, a vibrational "temperature" can be inferred which is of the order of 2500°K . The initial slope decreases, entering a second, or "plateau" region, for $V \geq 10$. In the plateau region, the slope is relatively small, the decrease in population with increasing vibrational quantum number being slight. The quantum number at the end of the plateau region is a function of the partial pressures of the gas mixture. Beyond the plateau region, there is again a region of rapid falloff. The slope of the distribution in this region asymptotes to a value for which the inferred vibrational "temperature" is near the gas translational-rotational temperature, a Boltzmann distribution.

The kinetic processes governing the establishment of such "V-V pumped" distributions as those of Figures 12 and 13 are now well understood. The most recent systematic analysis is that of Lam;³¹ the results of this work are used in the

31. Lam, S.H., J. Chem. Phys. 67, 2577 (1977).

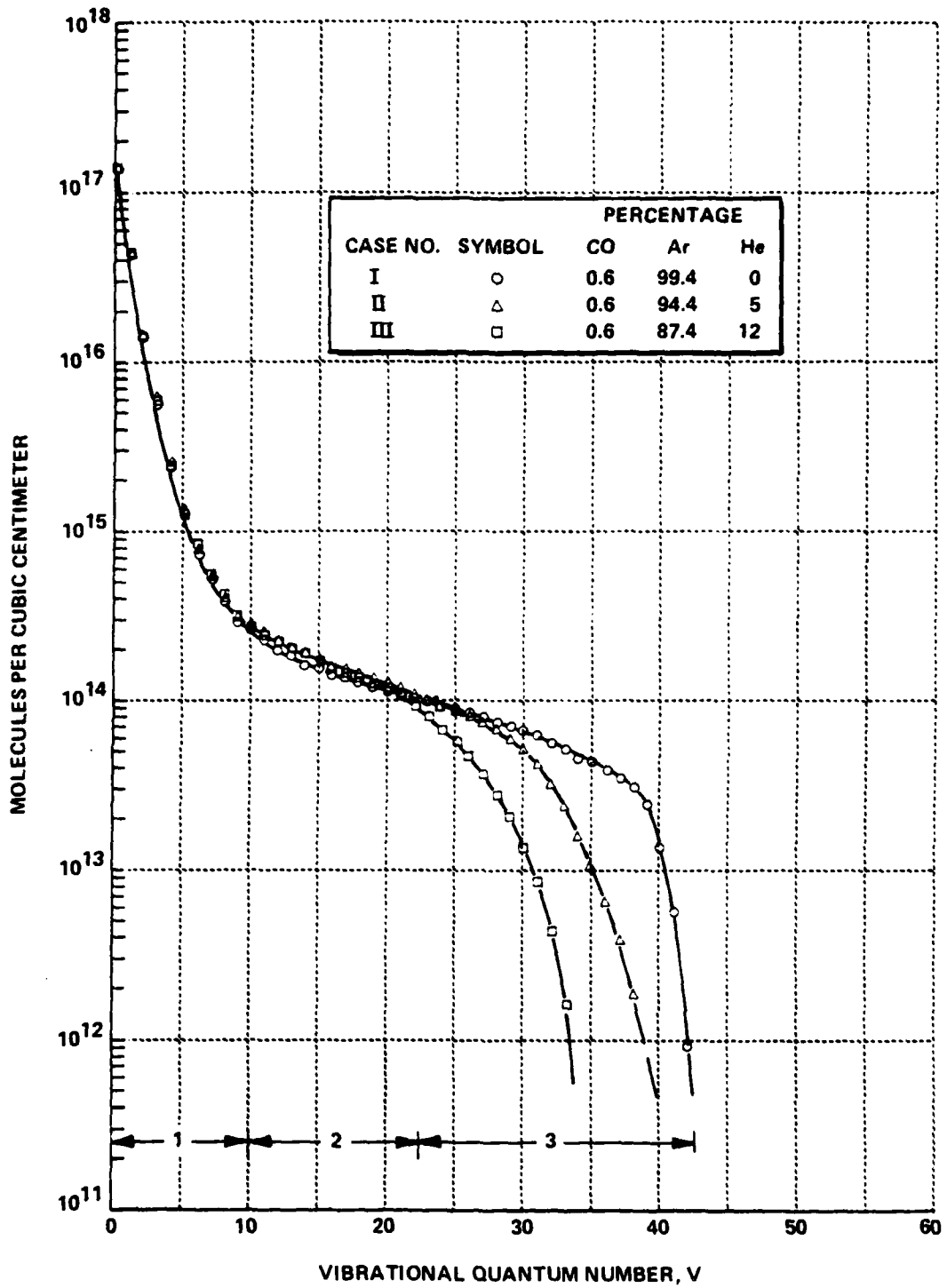


Figure 12 MEASURED VIBRATIONAL POPULATION DISTRIBUTIONS FOR VARIOUS He CONCENTRATIONS

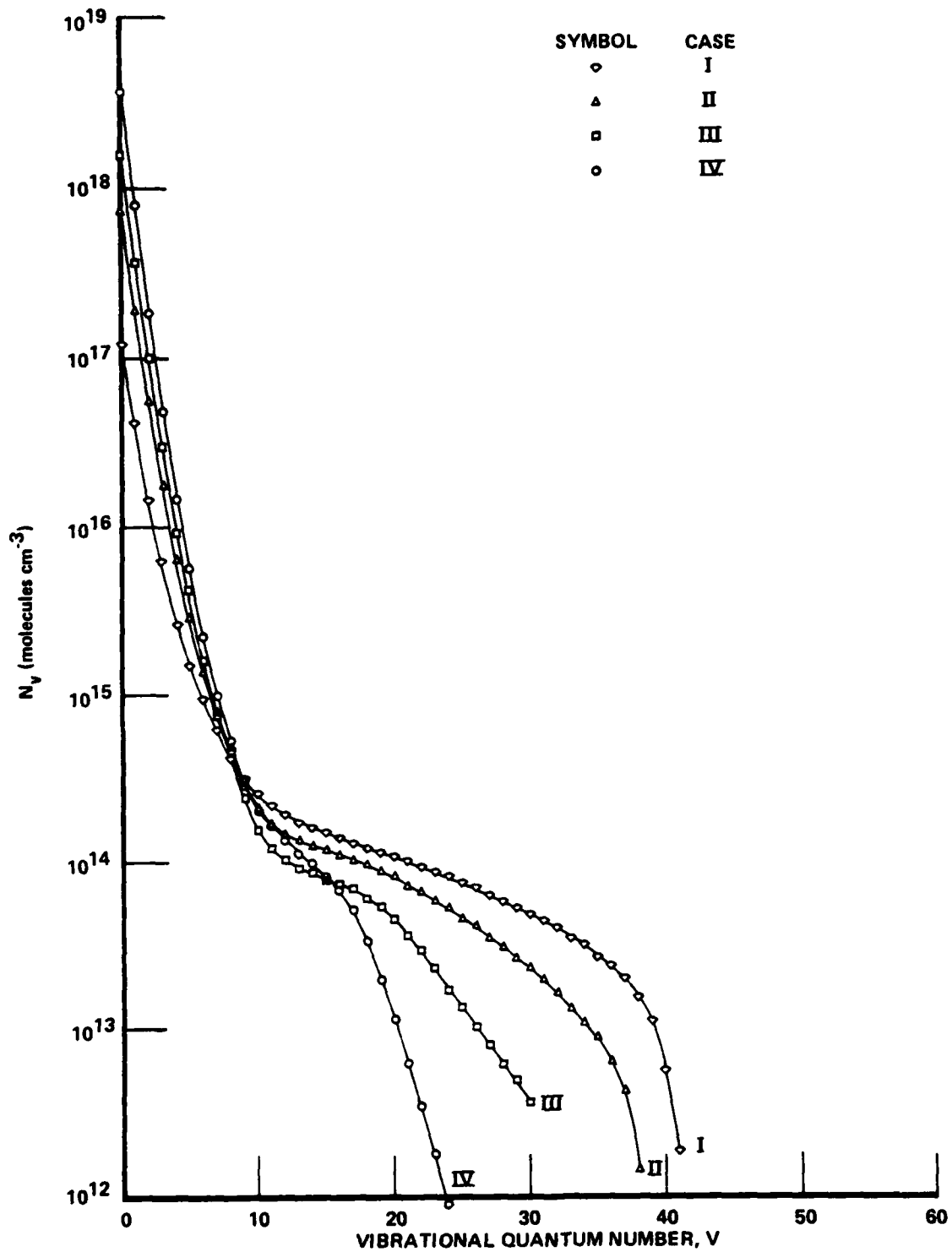


Figure 13 MEASURED VIBRATIONAL POPULATION DISTRIBUTIONS FOR VARIOUS Ar PRESSURES

reduction of the present data. It has been shown that V-V pumped population distributions are created among the vibrational quantum levels of a diatomic gas whenever: (1) the rate of vibration-to-vibration (V-V) energy exchange upon collision of the diatomic molecules greatly exceeds the rate of energy addition into the vibrational mode, and (2) the specific internal energy in the rotational and translational modes is much less than the specific internal energy of the vibrational mode. With such a distribution established, it is shown in Reference 20 that the shape of the distribution in Region 1 is entirely determined by nonresonant V-V processes involving collisions of CO molecules in an excited vibrational state v with ground state molecules, i.e., inelastic processes between $v=0$ and $v=n$ molecules causing simultaneous $v=n \rightarrow n-1$ and $v=n \rightarrow n+1$ transitions. In the plateau region, 2, the distribution is largely determined by resonant V-V processes, i.e., inelastic collisions involving simultaneous $v=n \rightarrow n-1$ and $v=n-1 \rightarrow n$ transitions. Finally, the steep-slope Region 3 is controlled by V-T processes, i.e., direct collisional quenching of CO molecules in transition $v = n \rightarrow n-1$, not involving exchange of energy with other diatomic molecules. At the low concentrations of CO used in the present experiments, such V-T processes are controlled by collisions with the Ar and He diluents, V-T self-quenching by CO itself being negligible.

3.2 REDUCTION OF CO-He AND CO-Ar V-T RATES AS FUNCTIONS OF VIBRATIONAL QUANTUM NUMBER

The distribution functions of Figures 12 and 13 can be predicted analytically as functions of the specific reaction rates for the V-V and V-T processes involved. Following Reference 31, the specific single-quantum-jump VT rate of $i+1 \rightarrow i$ collisions between CO and a diluent molecule M (M = Ar or He) can be written as:

$$k^{VT}(i+1 \rightarrow i) = \omega_{CO-M}^{VT}(T) L_i^{VT}(A_i^{VT})_M, \quad (3-1)$$

and the specific single-quantum jump V-V rate of $i \rightarrow i+1$, $j+1 \rightarrow j$ collisions between two CO molecules is:

$$k^{VV}(i \rightarrow i+1, j+1 \rightarrow j) = \omega^{VV}(T) l_i^{VV} l_j^{VV} A_{ij}^{VV}(T) \quad (3-2)$$

Here,

l_i^{VT} , l_i^{VV} are proportional to the square of the appropriate matrix elements and A_i^{VT} and A_i^{VV} are the "adiabaticity" factors, terms having an exponential dependence on the quantum numbers involved in the transition.

We assume

$$l_i^{VT} = \frac{1+i}{1-(.00598)i} \quad (3-3)$$

$$l_i^{VV} = \frac{1+i}{1+(.00897)i} \quad (3-4)$$

Still following the results of Lam et al., if one writes the V-T adiabaticity factors as

$$(A_i^{VT})_{Ar} \equiv B_r^{Ar} \exp \beta_{Ar} (i-r) \quad (3-5a)$$

and

$$(A_i^{VT})_{He} \equiv B_r^{He} \exp \beta_{He} (i-r) \quad (3-5b)$$

it can be shown that the distribution function in Regions 2 and 3 is expressed as

$$N_i = \frac{1}{l_i^{VV}} \left\{ N_r l_r^{VV} - N_{Ar} (C_{Ar})_r \left[\frac{e^{\beta_{Ar}(i-r)} - 1}{1 - e^{-\beta_{Ar}}} \right] - N_{He} (C_{He})_r \left[\frac{e^{\beta_{He}(i-r)} - 1}{1 - e^{-\beta_{He}}} \right] \right\} \quad (3-6)$$

Here,

N_i = population of the i^{th} vibrational quantum level, [molecules cm^{-3}].

N_r = population of a selected reference vibrational quantum level, r , [molecules cm^{-3}].

$$C_{Ar} \equiv \frac{B_r^{Ar} T \omega_{\text{CO-Ar}}^{VT} l_r^{VT}}{2 b g \omega^{VV} l_r^{VV}} \quad (3-7a)$$

$$C_{He} \equiv \frac{B_r^{He} T \omega_{\text{CO-He}}^{VT} l_r^{VT}}{2 b g \omega^{VV} l_r^{VV}} \quad (3-7b)$$

$$b \equiv \frac{1}{2} \sum_{j=0}^{\infty} (i-j)^2 A_{ij}^{VV}(T) \exp [(\Delta E_i - \Delta E_j) / 2kT] \quad (3-8)$$

b is essentially the second moment of the V-V rate adiabaticity factors. It is shown in Reference 31 that this parameter is essentially independent of i . Using recent data of Brechignac,³² it is shown that this parameter can be scaled as a simple function of temperature:

$$b \cong 6.6 \left(\frac{T}{150} \right)^{3/2} \quad (3-9)$$

$$g = 2\omega_e x_e / k, \text{ where } \omega_e x_e \text{ is the CO anharmonicity} \\ = 37^\circ\text{K.}$$

$$\omega_{VV} = 1.26 \times 10^{-12} \text{ cm}^5 \text{ sec}^{-1} \text{ molecule}^{-1}, \text{ as determined by matching } 300^\circ\text{K} \\ \text{ data of Reference 33, using procedure of Reference 32.}$$

32. Brechignac, Ph., Chem. Phys. 34, 119 (1978).

33. Powell, H.T., J. Chem. Phys. 59, 4937 (1973).

From Equations (3-1), (3-5) and (3-7), it can be shown that the V-T rates can be rewritten as

$$k^{VT}(i+1 \rightarrow i) = \frac{2bq\omega^{VV}l_r^{VV}}{T l_r^{VT}} (C_M)_r l_i^{VT} \exp \beta_M(i-r) \quad (3-10)$$

If the reference level $V=r$ were chosen at the beginning of the plateau region, it can be shown that only the last two terms in the distribution function, Equation (3-6), are dependent on the V-T rates. Then for states $v=i$ in the beginning of the plateau region, these V-T dependent terms are negligible, and $N_i \approx \frac{l_r^{VV}}{l_i^{VV}} N_r$; This distribution can be considered the zeroeth approximation to the shape of the V-V pumped plateau, and, noting the quantum number dependence of l_i^{VV} , shows the product iN_i is approximately constant in this region, a result first noted by Center and Caledonia.³⁴ Farther into the plateau, the V-T quenching terms in Equation (3-6) begin to be significant, resulting in a steeper slope, and finally, creating a "knee" in the distribution which ends the plateau.

Fitting the predicted distribution function, Equation (3-6), to the measured distributions permits the V-T rates of the form (3-10) to be inferred.

The distributions for CO in pure Ar (Figure 13) are reduced first. The fitting procedure is as follows. A reference level r is selected, and N_r chosen to equal the experimentally measured population for this quantum level.* The remaining undetermined constants C_{Ar} and β_{Ar} in the rate expression, Equation (3-10), are then chosen by trial and error to give the best fit of Equation (3-6) to the measured distribution in Region 2. The results of this procedure are shown in Figures 14 - 17 for each of the four cases. The measured

34. Caledonia, G.E. and Center, R., J. Chem. Phys. 55, 552 (1971).

*The reference level chosen in the actual fitting procedure is not at the beginning of the plateau region, but well into the region of the distribution where V-T effects are significant.

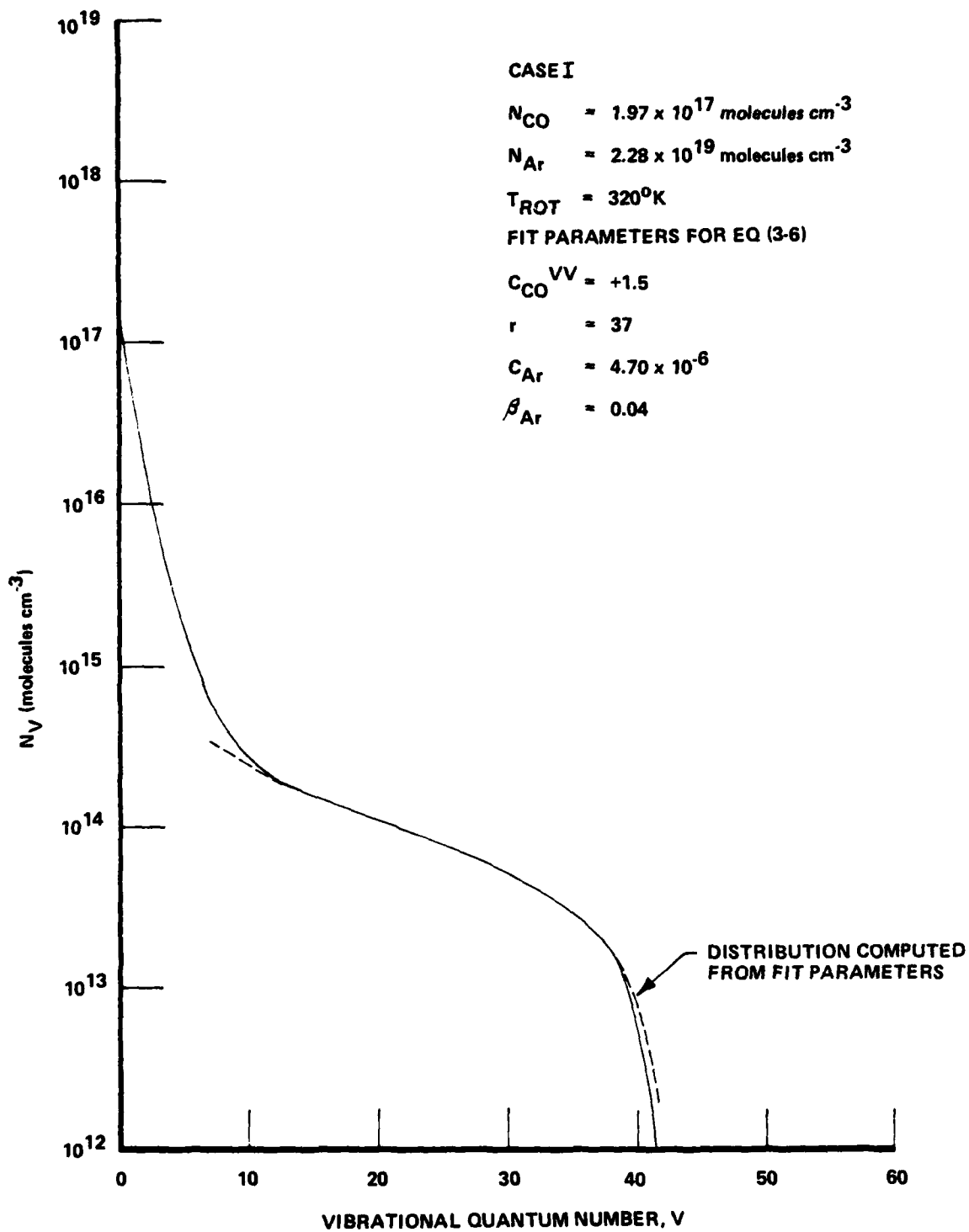


Figure 14 REDUCTION OF MEASURED DISTRIBUTION FOR CO-AR MIXTURE, CASE I

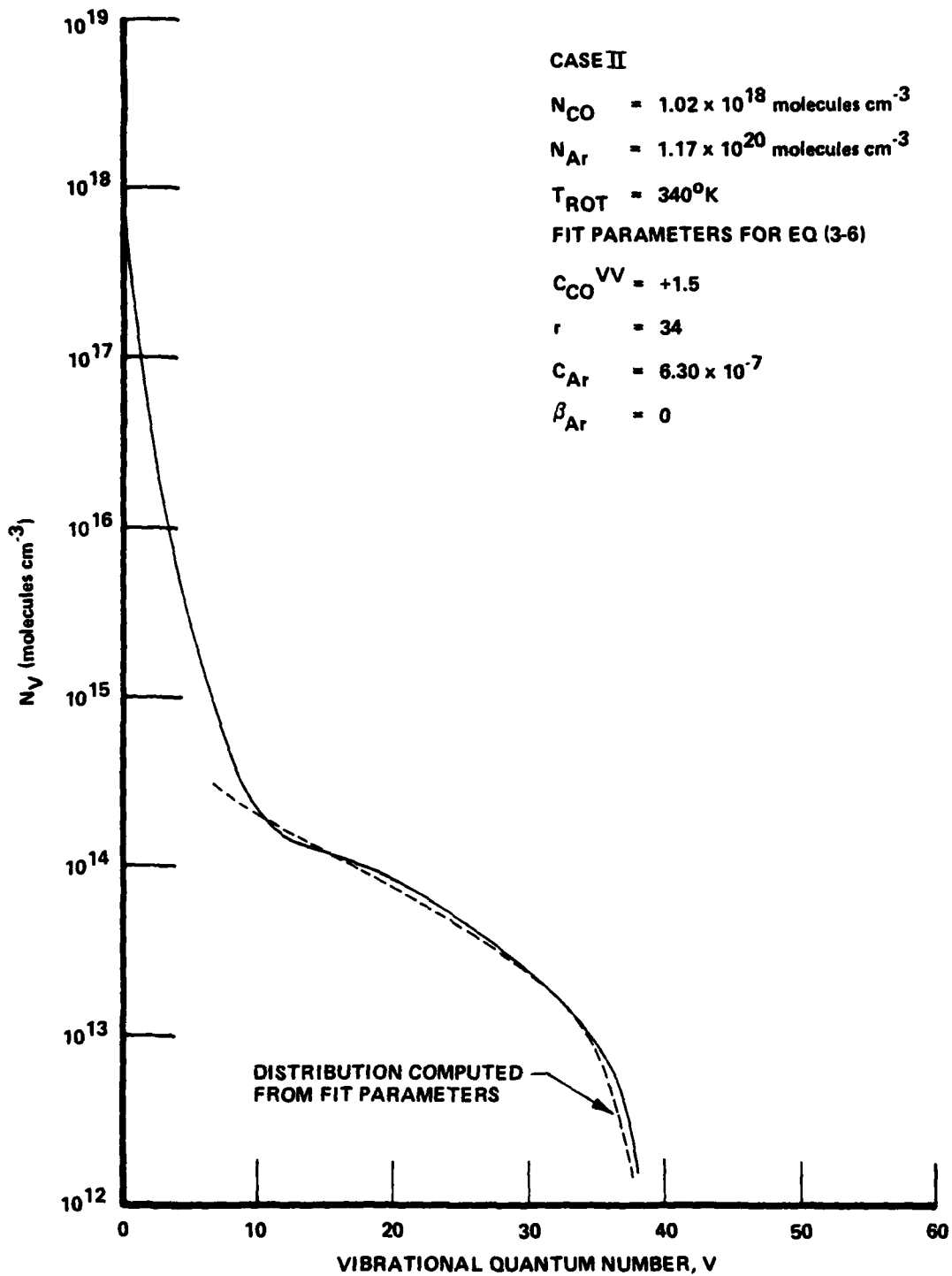


Figure 15 REDUCTION OF MEASURED DISTRIBUTION FOR CO-Ar MIXTURE, CASE II

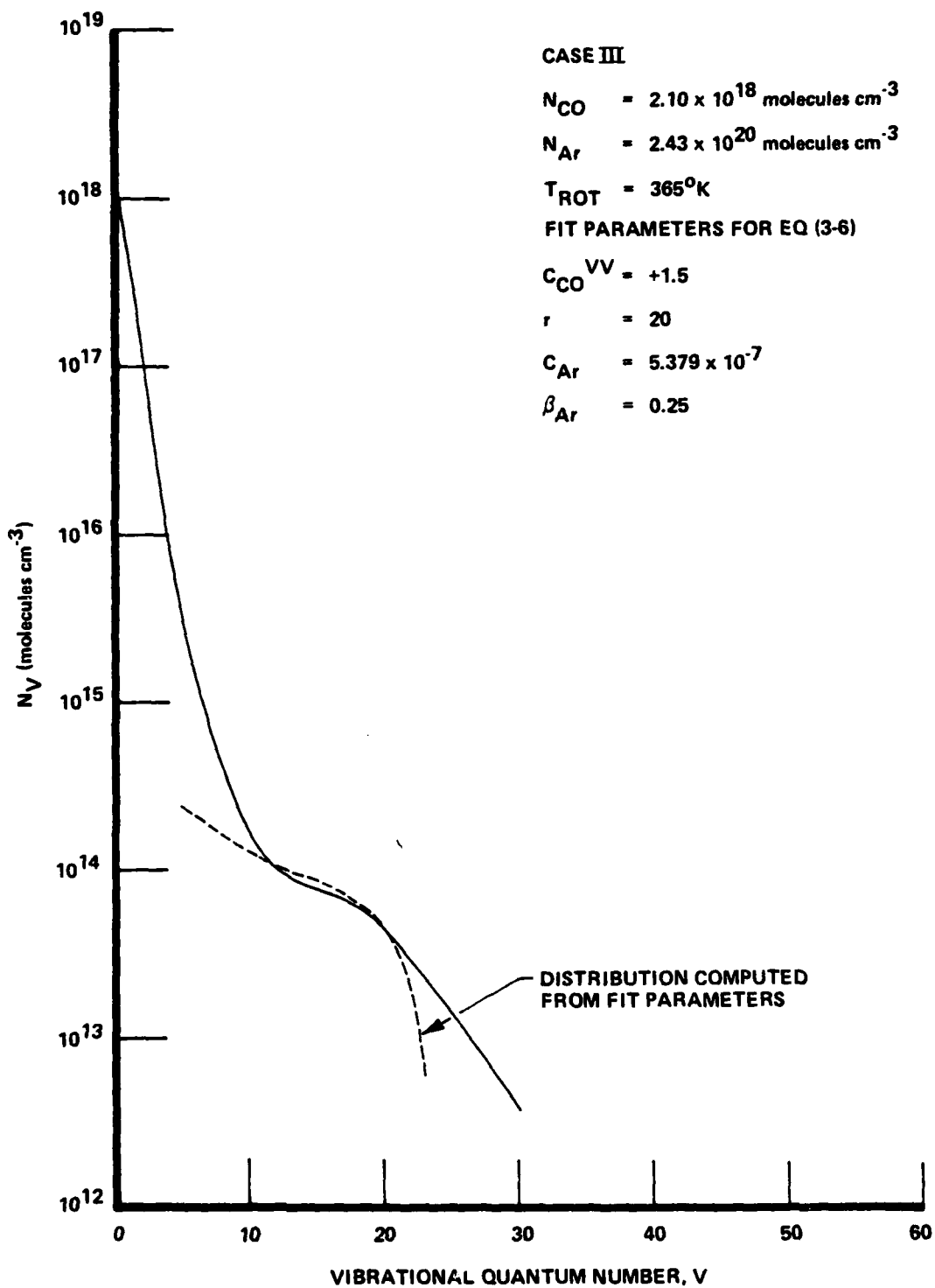


Figure 16 REDUCTION OF MEASURED DISTRIBUTION FOR CO-Ar MIXTURE, CASE III

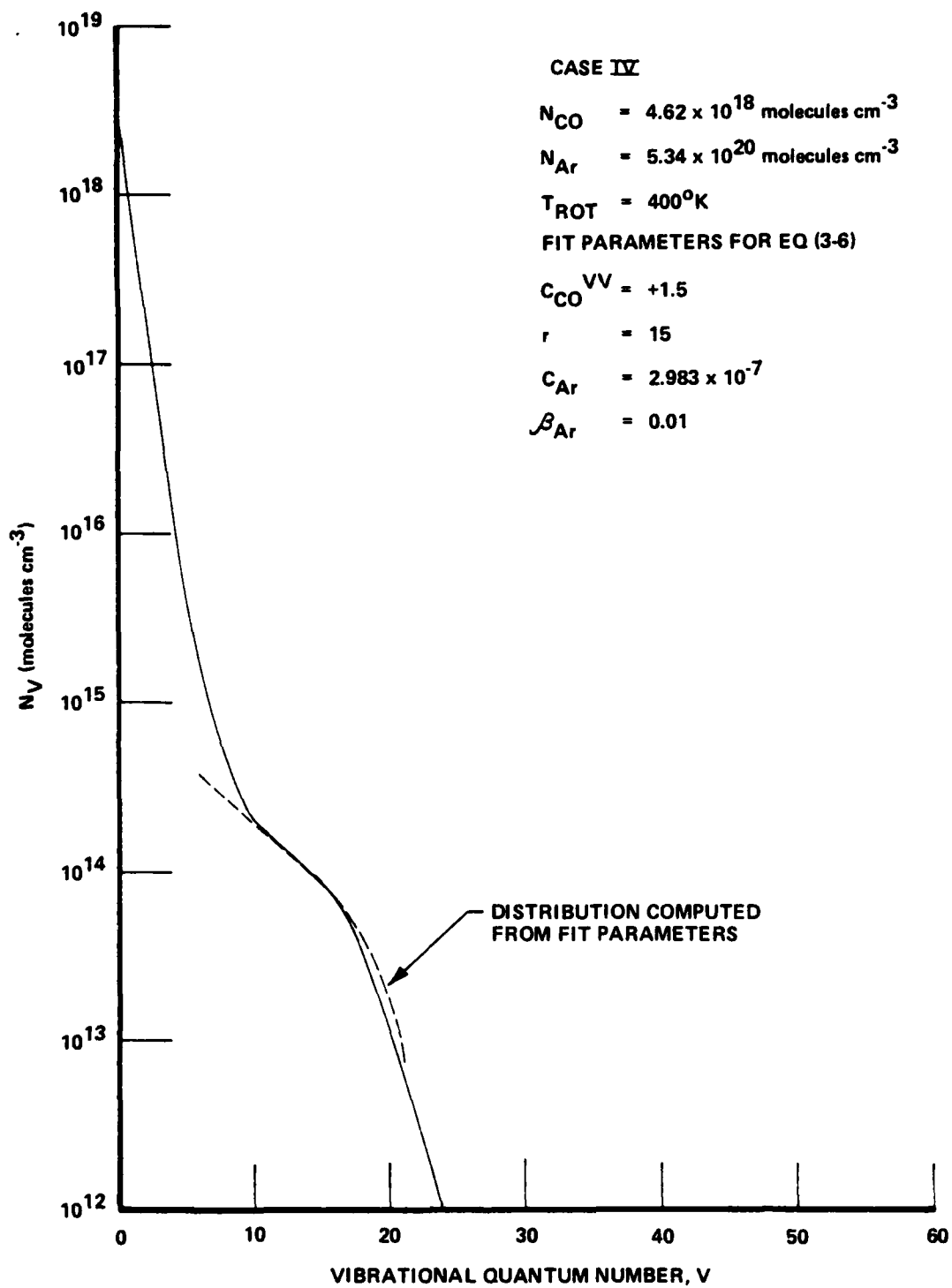


Figure 17 REDUCTION OF MEASURED DISTRIBUTION FOR CO-Ar MIXTURE, CASE IV

distribution is plotted, together with the best fit of the analytical distribution Equation (3-6). It can be seen that the fit to the experimental distribution in the plateau region, Region 2, is quite good. Since Equation (3-6) applies only to Region 2, the fit in Regions 1 and 3 is not critical to the rate reduction. The experimental distribution in Case III shows an anomalously slow fall off in Region 3, whereas the other cases show fair agreement even in this region.

In each case, the rate expression reduced has maximum sensitivity to the fit parameters at the boundary of Regions 2 and 3. Thus in the vibrational quantum number range about this boundary is where each case will yield an accurate V-T rate measurement. Figure 18 shows the rates reduced for five vibrational levels from each case that lie near the boundary of Regions 2 and 3. The reduced rates are shown as points; the solid curve is an exponential fit to these reduced rates. It must be emphasized that the exponential fit has an experimental basis only in the range $V \approx 10$ to $V \approx 42$. The rate is plotted as a dimensionless transition probability, $P_{v,v-1}$, for the $v \rightarrow v-1$ transition, versus vibrational quantum number, V . The "transition probability", $P_{v,v-1}$, is related to the specific V-T rate $k^{VT}(v+1 \rightarrow v)$ of Equation (3-10) by the collision frequency Ξ ,

$$k^{VT}(v \rightarrow v-1) = \Xi P_{v,v-1}$$

where

$$\Xi = \text{collision frequency in units of cm}^3 \text{ sec}^{-1} \text{ molecule}^{-1}$$

$$\Xi = 4 \sigma^2 \sqrt{\frac{\pi kT}{2\mu}}$$

$$\sigma = \text{molecular hard sphere diameter}$$

$$\mu = \text{reduced mass of collision partners}$$

In this report

$$\Xi \text{ CO-Ar (300}^\circ\text{K)} = 2.664 \times 10^{-10} \text{ cm}^3 \text{ sec}^{-1} \text{ molecule}^{-1}$$

The inferred CO-Ar V-T rate expression, as plotted as the solid curve in Figure 18, is given by

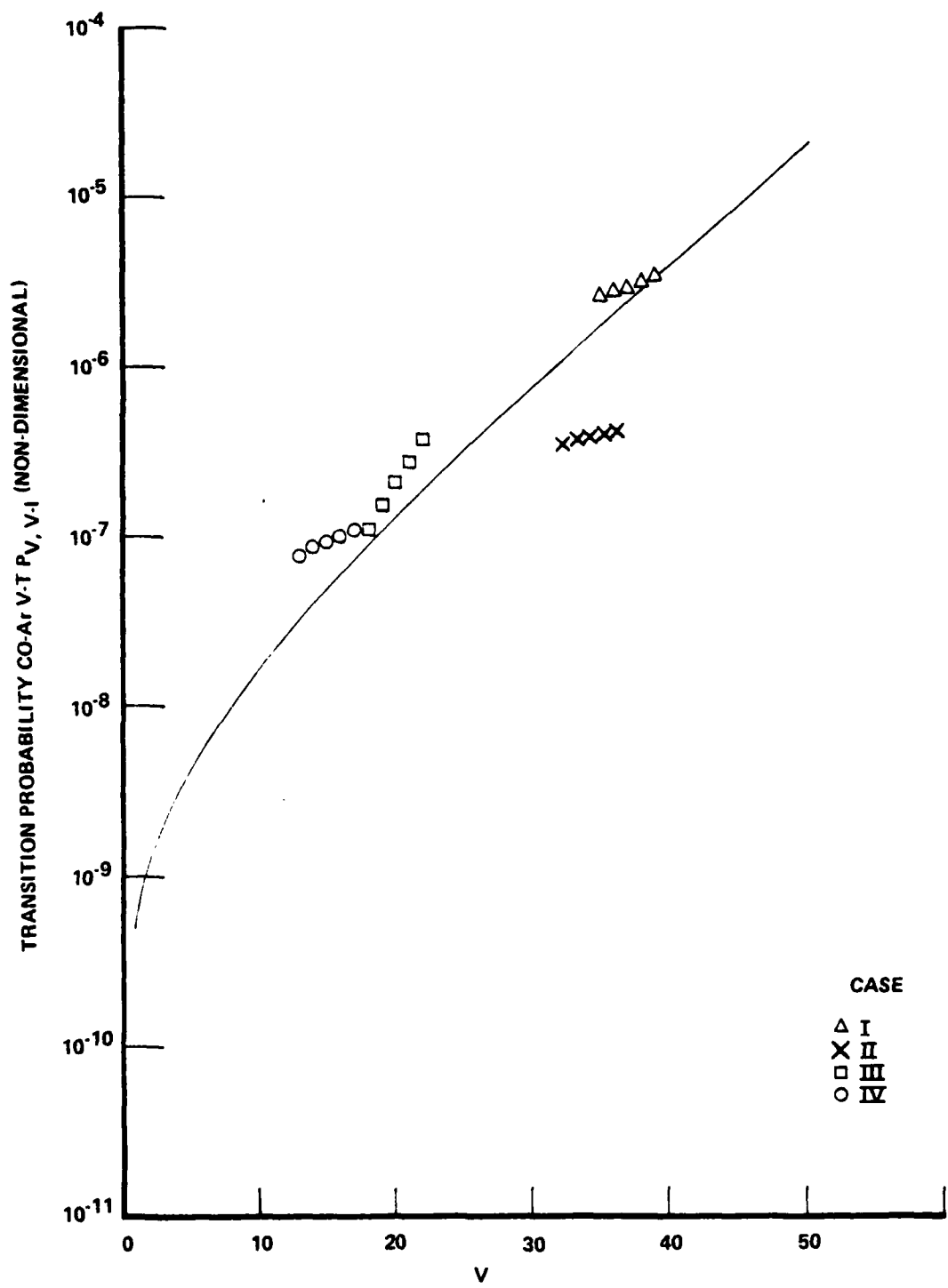


Figure 18 CO-Ar V-T TRANSITION PROBABILITY

$$k_{\text{CO-Ar}}^{\text{VT}}(V+1 \rightarrow V) = 1.34 \times 10^{-19} l_v^{\text{VT}} e^{0.13V} \text{ cm}^3 \text{ sec}^{-1} \text{ molecule}^{-1}$$

The values for $P_{v \rightarrow v-1}$ for CO-Ar collisions presented in Figure 18 are the only data at present available for the room temperature vibrational relaxation of CO in Ar. There are shock-tube measurements of the CO-Ar relaxation time for temperatures above $T \cong 2000^\circ\text{K}$; these data are essentially a measurement of $P_{1 \rightarrow 0}$ only. This paucity of data is due to the very large room temperature relaxation time of CO-Ar mixtures; the CO-Ar collisional deactivation rate of the $v = 1$ level, $k_{\text{Ar}}^{\text{VT}}(1 \rightarrow 0)$, is undoubtedly slower at room temperature and atmospheric pressure than the rate of spontaneous radiative decay of CO ($v = 1$), which has a lifetime of 33 milliseconds.

Having reduced the measured distribution for the CO in pure Ar case, Equation (3-6) can now be applied to the distributions of Figure 12 to infer a CO-He V-T rate. In this case, the previously experimentally-determined CO-Ar constants, C_{Ar} and β_{Ar} , are used in Equation (3-6), and C_{He} and β_{He} are determined by fitting. The distribution of Case III of Figure 12 is used for this fit. The results of this procedure are shown in Figure 19. As in the previous case, a reasonable fit can be obtained. Finally, as a cross-check on the values of the CO-He V-T rate constants inferred, these same values of C_{He} and β_{He} can be used in Equation (3-6) to predict the distribution for the lower helium concentration case, II. The results of this check are shown in Figure 20. It can be seen that there is fair agreement with the measured extent of the "plateau region" for this helium concentration.

Figure 21 is a plot of the CO in He V-T rates inferred from the data reduction. Again, the rate is plotted in the form of a dimensionless transition probability. Unlike the CO in Ar case, there are some rate data and theory available for comparison. Shown on the figure are the 300°K measurements of

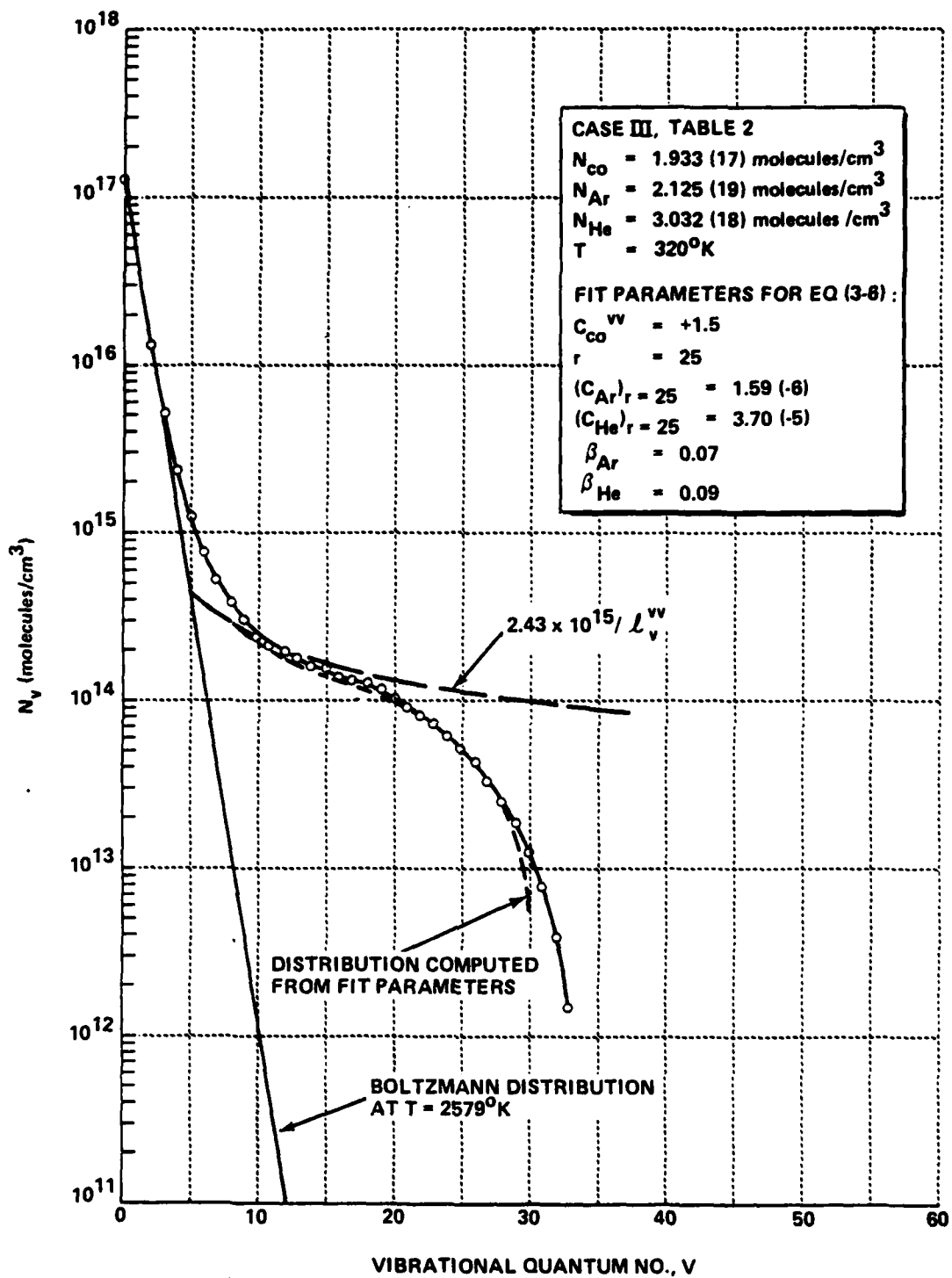


Figure 19 REDUCTION OF MEASURED DISTRIBUTION FOR CO-Ar-He MIXTURE, CASE III

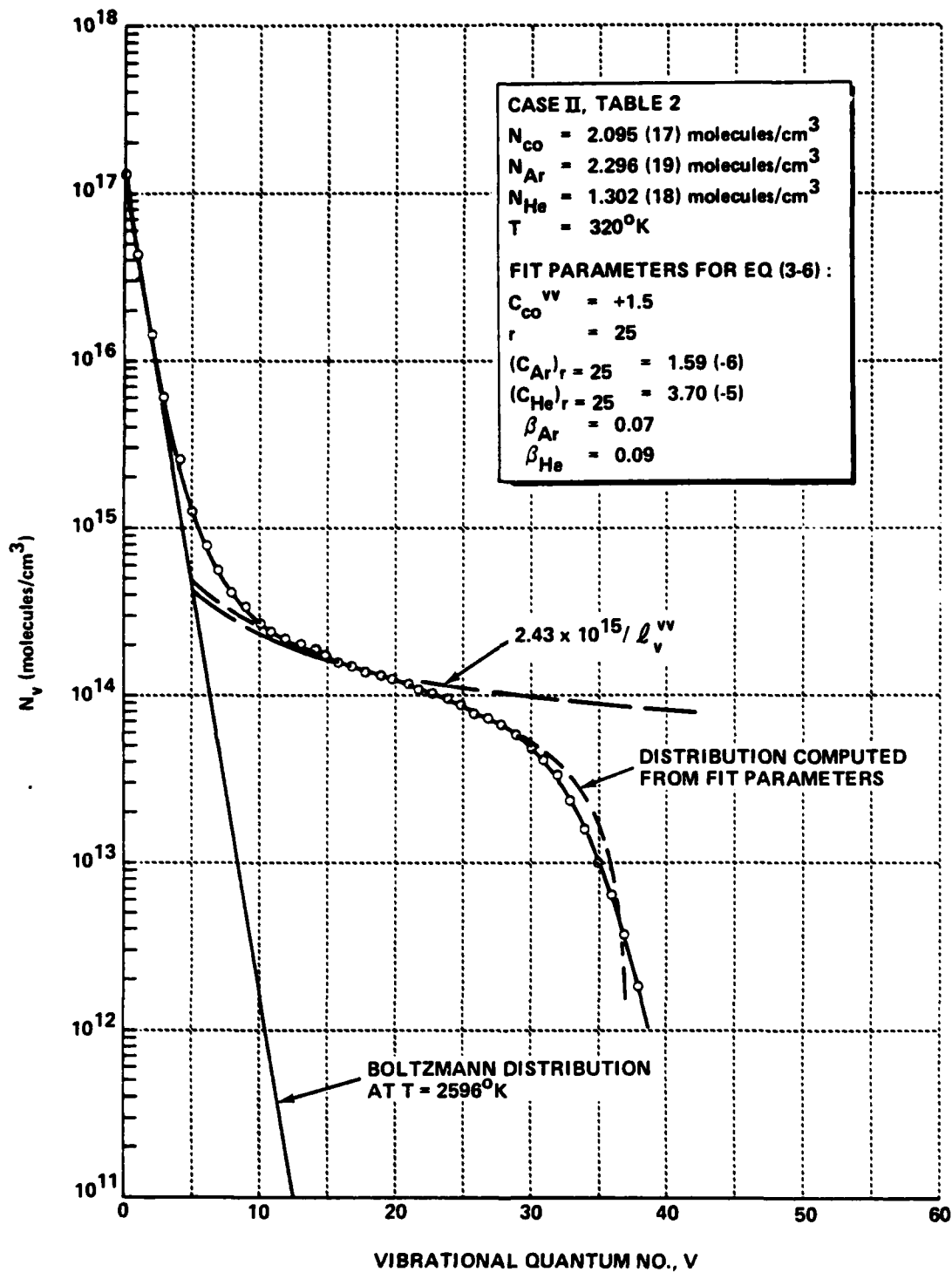


Figure 20 REDUCTION OF MEASURED DISTRIBUTION FOR CO-Ar-He MIXTURE, CASE II

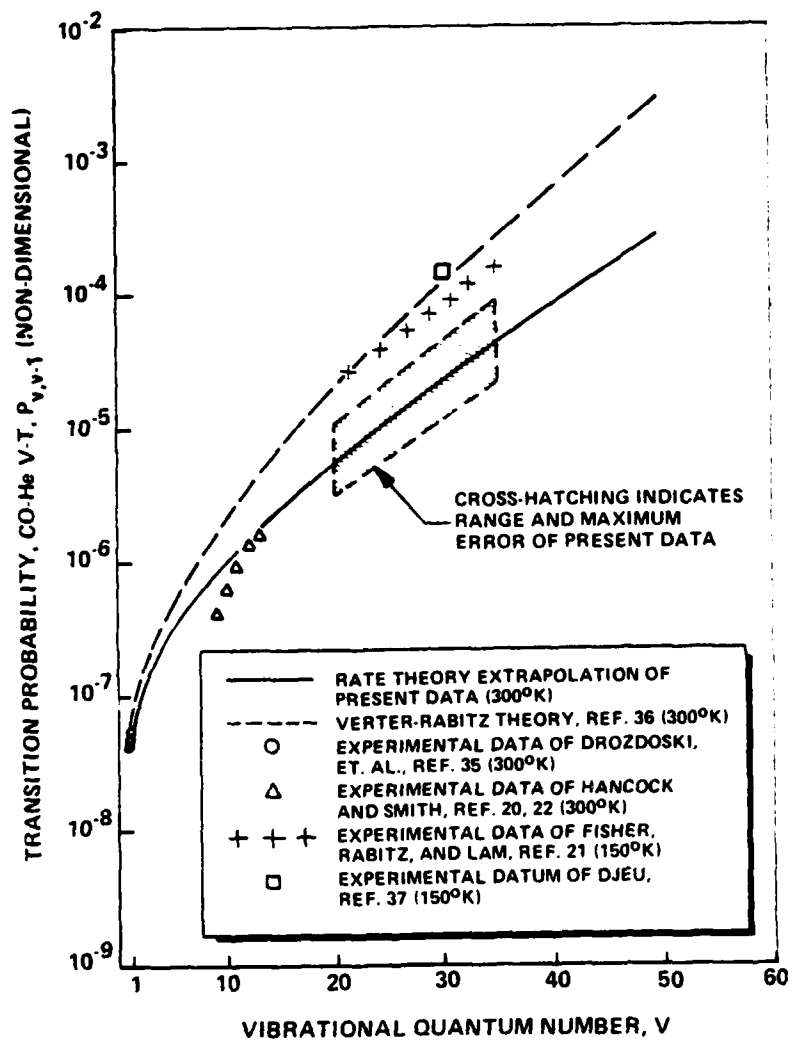


Figure 21 CO-He V-T TRANSITION PROBABILITY

Hancock and Smith for $P_{v, v-1}$, $v = 9$ to 13 . Also shown is the 300°K $P_{1,0}$ measurement of Drozdowski,³⁵ which is in general agreement with earlier measurements of room temperature CO-He relaxation rates. There is also an isolated data point for $P_{30,29}$ (150°K) which represents an estimate made several years ago by Djeu.³⁷ Finally, the theoretical curve of Verter and Rabitz³⁶ is plotted. The range of actual measurement and the estimated experimental error are indicated by a dotted parallelogram.

The inferred CO-He V-T rate expression, as plotted in the figure, is

$$k_{\text{CO-He}}^{VT} (V+1 \rightarrow V) = 4.6 \times 10^{-15} \left(\frac{l_v^{VT}}{l_{25}^{VT}} \right) e^{0.09(V-25)}$$

[$\text{cm}^3 \cdot \text{sec}^{-1} \cdot \text{MOLECULE}^{-1}$]

It is seen that the present data show significantly slower CO-He V-T upper-state rates than the prediction of Verter and Rabitz. It is interesting that the probability curve Equation (3-1) when matched to the upper-state measurements and extrapolated to $v = 1$, passes through the data of Hancock and Smith and of Drozdowski. As discussed previously, in connection with the CO-Ar data, however, this agreement is to some extent fortuitous; our measurements are not sensitive to the CO-He V-T rates for states below $v \approx 20$.

-
35. Drozdowski, W.S., Young, R.M., Bates, R.D., Jr., and Hancock, J.K., J. Chem. Phys. 65, 1542 (1976).
36. Verter, M. and Rabitz, H., J. Chem. Phys. 64, 2939 (1976).
37. Djeu, N., Chem. Phys. Lett. 15, 392 (1972).

Section 4
COMPUTER MODELING OF CELL KINETICS

The methods of the previous section, leading to the inference of the upper state V-T rates given in Figures 18 and 21, are dependent on the rapid establishment of a quasi-steady state vibrational population distribution. It is assumed that the measured distributions of Figures 12 and 13 are a result of a balance between radiative absorption, V-V pumping, and V-T deactivation of the upper states. In such a quasi-steady state, the vibrational population distributions will remain similar along the length of the absorption cell, until some pump laser lines are totally absorbed (bleached out), or unless substantial translational-rotational temperature rise significantly alters the kinetic rates. In particular, the data reduction procedure is only valid if V-V equilibration is established upstream of the measurement station in the cell. The experiment was designed on the basis of previous measurements of CO V-V rates;^(20,33) using these rates, it was estimated that quasi-steady distributions would be established in the first 1-2 cm of cell length. Check measurements made at several stations along the cell length support this quasi-steady model assumption made in the data reduction. We have however, made modeling calculations to check further into the validity of the data reduction procedure; these calculations are described in the present section.

Under a related USAF contract, a kinetic model and computer code has been developed^(38,39) which can be used for analysis of the optically-pumped-cell experiments of the present program. A full description of the model and code is given in Reference 28; its major features are briefly summarized here for completeness.

-
38. Lordi, J.A., and Rich, J.W., "A Theoretical Study of a High-Pressure, Tunable CO Laser", Report No. AFAL-TR-75-184, USAF Avionics Laboratory, December 1975.
 39. Rich, J.W., Lordi, J.A., Gibson, R.A. and Kang, S.W., "Supersonic Electrically Excited Laser Development", Calspan Report No. WG-5164-A-3, June 1974.

The model describes the optical pumping of the vibrational distribution by the absorption of the incident laser radiation, collisional pumping by vibration-vibration (V-V) energy exchange collisions, and losses due to vibration-translation (V-T) energy exchange collisions and to spontaneous radiative transitions. The incident laser beam is directed along the axis of the high-pressure cell, which is also the flow direction of the gases in the cell. The primary assumptions made in the model are:

- (1) The flow in the cell and the radiative absorption process are one-dimensional, i.e., the flow properties, population distributions, and radiative intensities are constant over a cross-section normal to the beam/flow direction.
- (2) The incident laser lines have a much smaller linewidth than the absorption lines in the cell.
- (3) The individual vibrational-level populations depart from equilibrium due to the radiative and collisional processes, but the rotational state populations within each vibrational level remain in equilibrium with the translational temperature.

First, the radiative transport equations are given for the variation through the cell of the intensities of the pumping laser lines. If at axial position x , the spectrally integrated intensity of the j^{th} laser line (in watts/cm²) is $I_{\nu_j}(x)$, the radiative transport equation for each line intensity is written

$$\frac{dI_{\nu_j}}{dx} = \alpha_{\nu_j} I_{\nu_j} \quad (4-1)$$

where α_{ν_j} is the net gain coefficient in cm⁻¹ (α_{ν_j} is defined to be negative when the gas is in absorption at ν_j). The gain coefficient expression is used which accounts for the overlapping of the pressure-broadened vibration-rotation lines. The spontaneous emission or source term has been dropped from this equation because spontaneous emission, which is isotropic, is not expected to be important in the specific direction of I_{ν_j} .

In addition to the equations for the radiative intensities, the kinetics equations for the vibrational level populations are required. Since the cell kinetics computer program has been based on the Calspan CO flow-laser kinetics code,^{39,40} the master equations for the vibrational level populations have been written in the same form as used there, with suitable modification of the stimulated emission and absorption terms. The concentration of molecules in the v^{th} level, in moles per gram of mixture, δ_v , satisfies

$$\begin{aligned} u \frac{d\delta_v}{dx} = & C_v^{v-T} + C_v^{v-v} + \psi_{v+1,v} - \psi_{v,v-1} \\ & + A_{v+2,v} \delta_{v+2} + A_{v+1,v} \delta_{v+1} - (A_{v,v-2} + A_{v,v-1}) \delta_v \end{aligned} \quad (4-2)$$

where u is the flow velocity, C_v^{v-T} and C_v^{v-v} are the rates of production of molecules in level v due to $v-T$ and $v-v$ collisions, $A_{v',v} \delta_{v'}$ represents the spontaneous emission terms, and $\psi_{v',v}$ is the net production rate for level v by stimulated emission and absorption transitions between levels v and v' . The stimulated emission and absorption rates are written in terms of the intensities and the absorption coefficients for individual vibrational-rotational transitions. The detailed descriptions of the $v-T$ and $v-v$ rate models are given in References 39 and 40.

These coupled equations for the line intensities and vibrational level populations are integrated together with the gasdynamics equations for one-dimensional flow. The form of the equations for the gasdynamic variables are as given in References 39 and 40, specialized to a constant cross-sectional area of the flow channel; the method of numerically integrating the equations is presented there also.

-
40. Lordi, J.A., Falk, T.J., and Rich, J.W., "Analytical Studies of the Kinetics of Electrically Excited, Continuously Operating CO Flow Lasers", AIAA Paper No. 74-563, AIAA 7th Fluid and Plasma Dynamics Conference, Palo Alto, California, June 17-19, 1974.

Given initial gas properties, an initial vibrational population distribution, the initial intensities and the frequencies of the incident laser lines, the above equations can be integrated to find the variation of these quantities along the cell. The V-V, V-T, and radiative rates that are used in the calculation are all-important in determining the vibrational distribution function at various axial positions. Previous calculations using this code did not have available the CO-He and CO-Ar rates measured in the present program. These previous calculations accordingly used the sparse earlier CO-He data,²⁰ and used very crude approximations for the CO-Ar rates, since no experimental values were available.

Using the newly-determined CO-Ar rates as given in Figure 18, we have performed a series of calculations with the modeling code. These new calculations verify that vibrational distribution functions are produced that are similar to those determined by experiment, thus providing a cross-check on the analytical theory of Reference 31 used in the data reduction. In addition, the validity of certain key assumptions made in the data reduction process can be examined in detail.

One of the limitations of the computer code, as presently set up, is that it does not model the "triggering" process, which establishes the initial absorption of pump radiation. (This triggering process is briefly discussed in Section 2 above.) Without incorporation of this triggering feature, absorption of pump radiation is slow, and an unrealistically long length of the cell is required before pumped distributions comparable to those of Figure 13 are produced. In the actual experiments, the triggering processes discussed in Section 2 combined with streamwise radiative coupling on the optically thick CO fundamental band IR transitions, result in production of vibrationally excited CO within two centimeters of cell length. For the range of flow velocities and concentrations of the experiments summarized in Figure 13 and Table 3, V-V pumping is sufficiently rapid to create a fully developed plateau-pumped distribution within this same ~ 2 cm of cell length. Experimental monitoring of the IR emission from various axial stations confirms that these

quasi-steady state distributions are maintained along the subsequent length of the cell. In order to simulate this triggering effect, all computer runs were started, at the upstream $x = 0$ axial station, with an initial vibrational distribution equal to Case I of Figure 13. As will be shown, for all cases run, the vibrational population distribution adjusted to a quasi-steady value determined by the particular run parameters selected.

Figures 22 to 24 show the results of these model calculations, using the new CO-Ar rates of Figure 18. Three runs were made using the parameters of the CO-Ar experimental Cases I through III of Table 3. Note that the basic parameter varied among these three cases is the total gas pressure, going from 1.0 atm in Case I to 10.7 atm in Case III. The CO/Ar mole fraction remains approximately constant. As noted above, all three runs commenced with an initial vibrational population distribution given by the plot of Case I, Figure 13. Initial cell temperature was 300°K, and the pump laser spectral distribution was as given in Table 6.

Figure 22 is a plot of the calculated vibrational energy as a function of distance along the cell axis for the three cases. Initial vibrational energy is 0.508 eV per CO molecule; since the calculation commenced with a population distribution determined experimentally to be the quasi-steady state for the parameters of Case I, the vibrational energy remains very nearly constant for this case. For the two higher pressure cases, II and III, the vibrational energy quickly falls, establishing new, lower, quasi-steady values within 2 cm. The quasi-steady values are maintained by the balance between energy input via absorption of pump laser radiation, and losses via radiative, V-V, and V-T processes. As the gas pressure increases, the V-T loss rate increases, resulting in the lowering of the quasi-steady vibrational energy shown in Figure 22.

Figure 23 shows the quasi-steady distribution functions at the $x = 4.0$ cm station in the cell, for the same three cases. These distributions are established

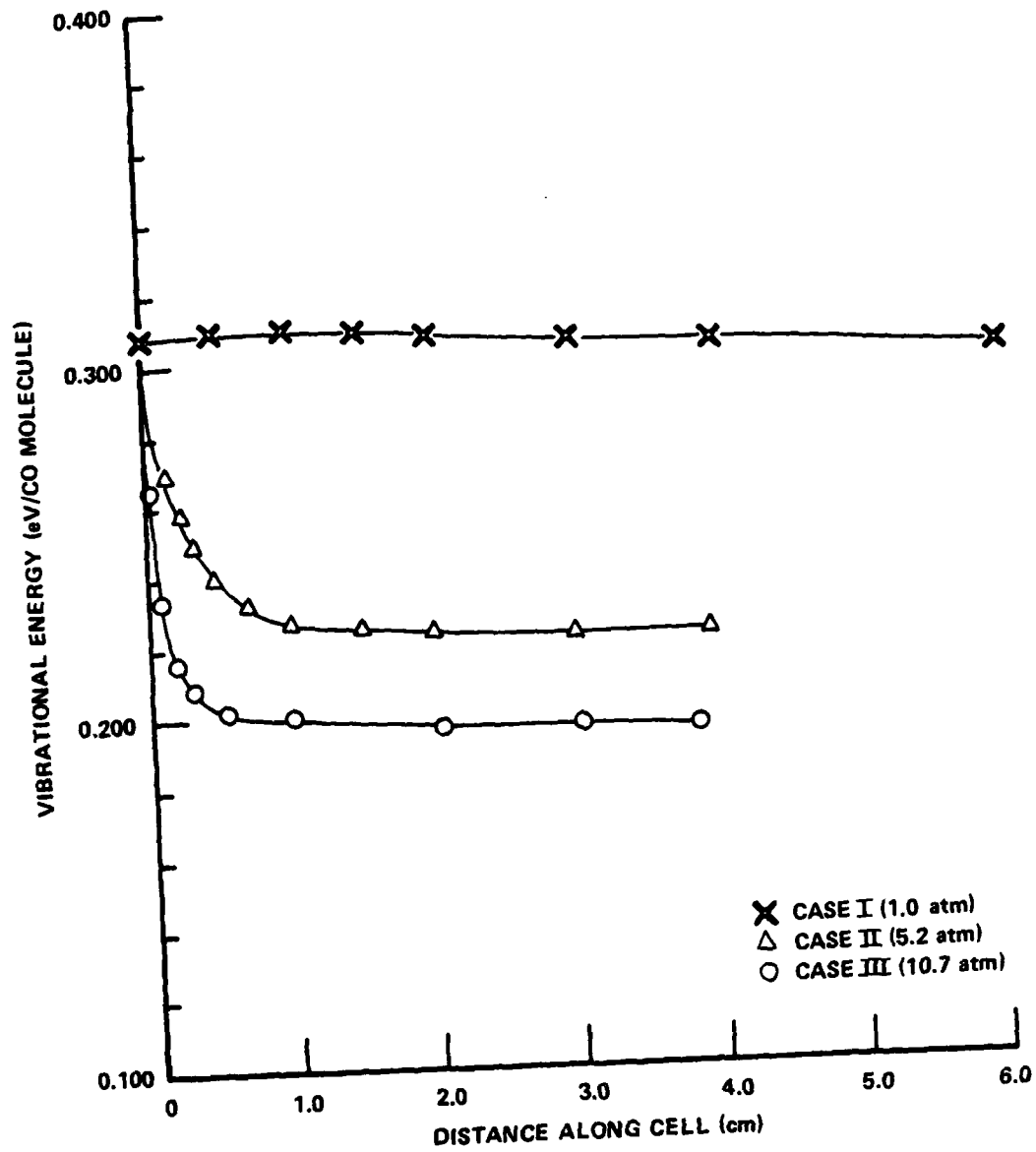


Figure 22 CALCULATED VIBRATIONAL ENERGY FOR SELECTED PRESSURES OF Ar DILUENT

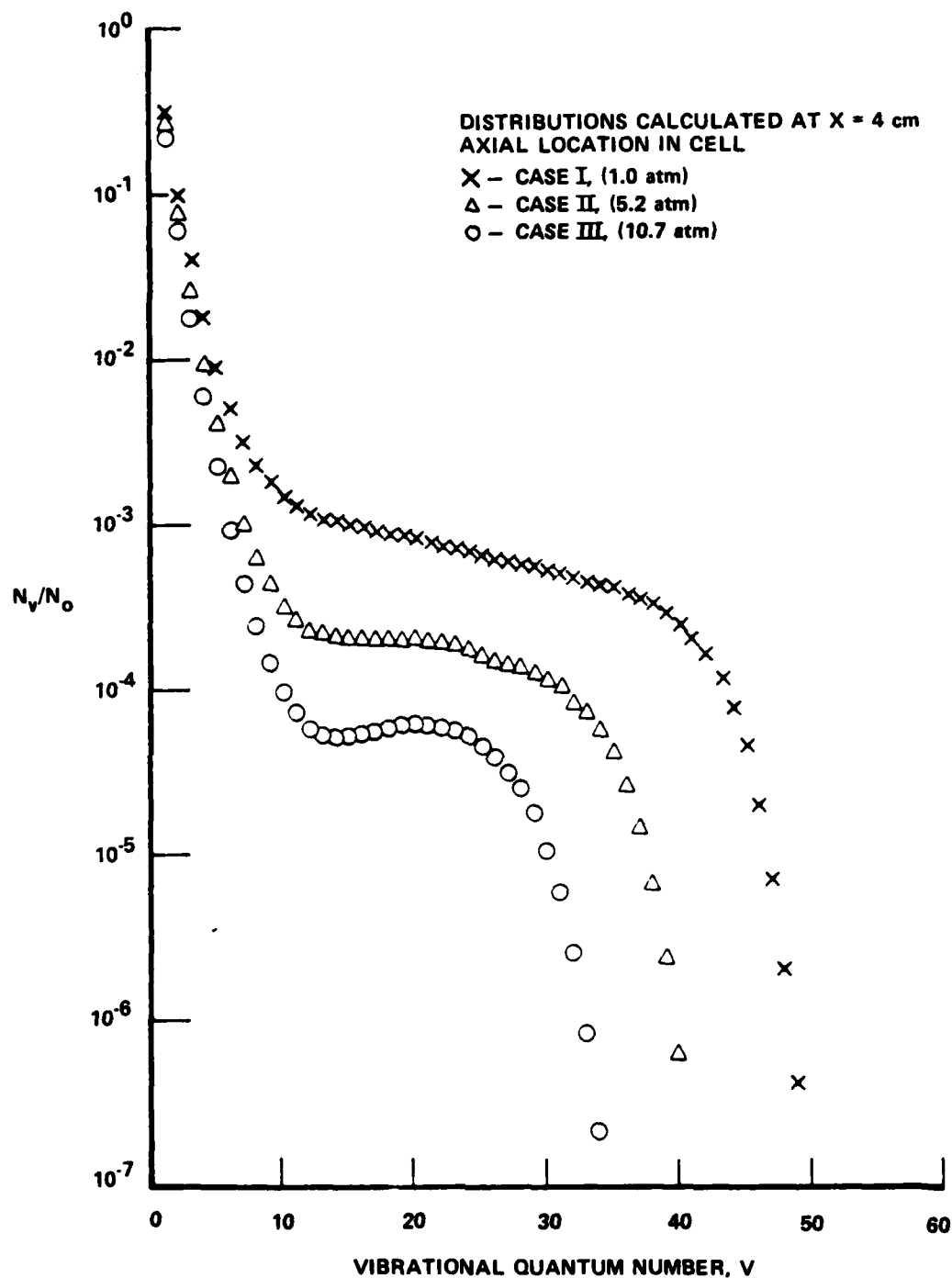


Figure 23 CALCULATED CO VIBRATIONAL POPULATION DISTRIBUTIONS FOR SELECTED PRESSURES OF Ar DILUENT

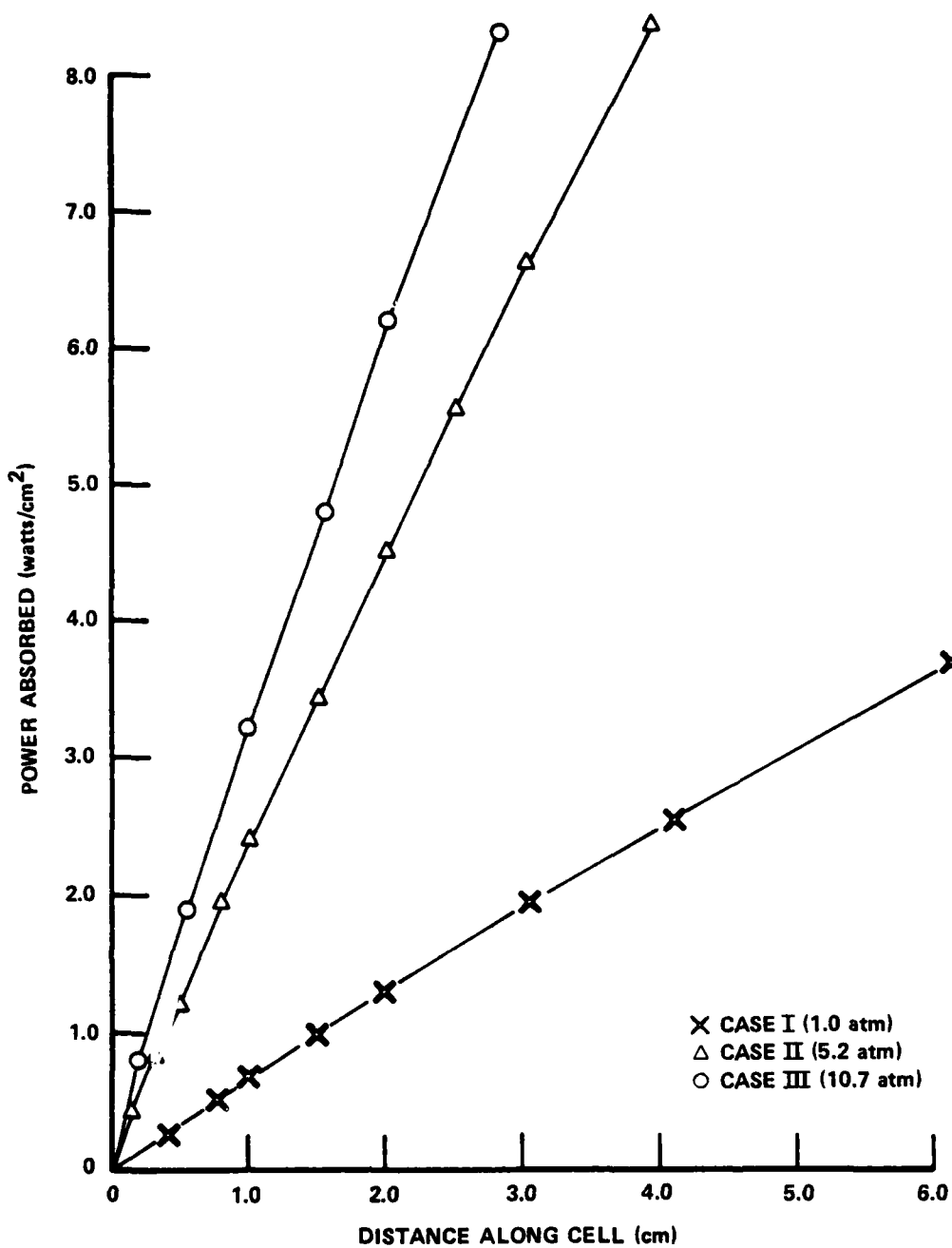


Figure 24 CALCULATED LASER PUMP POWER ABSORBED FOR SELECTED PRESSURES OF Ar DILUENT

TABLE 6

PUMP LASER OUTPUT SPECTRAL DISTRIBUTION USED IN MODELING CALCULATIONS

Vibrational Band	Rotational Line	Wavelength, μ	% Total Power
V = 3 - 2	P(7)	4.84679	2.90
	P(8)	4.85624	1.88
V = 4 - 3	P(5)	4.89001	0.84
	P(6)	4.89939	6.42
	P(7)	4.90888	6.04
	P(8)	4.91849	1.01
V = 5 - 4	P(5)	4.95323	1.76
	P(6)	4.96277	5.63
	P(7)	4.97242	5.10
V = 6 - 5	P(5)	5.01793	6.30
	P(6)	5.02763	9.05
	P(7)	5.03745	5.13
V = 7 - 6	P(4)	5.07441	0.59
	P(5)	5.08415	3.25
	P(6)	5.09401	4.53
	P(7)	5.10400	1.48
V = 8 - 7	P(4)	5.14205	1.19
	P(5)	5.15195	7.25
	P(6)	5.16198	2.88
	P(7)	5.17214	0.34
V = 9 - 8	P(4)	5.21129	4.31
	P(5)	5.22137	4.26
	P(6)	5.23158	1.07
	P(7)	5.24192	0.40

TABLE 6 (Cont'd)
 PUMP LASER OUTPUT SPECTRAL DISTRIBUTION USED IN MODELING CALCULATIONS

Vibrational Band	Rotational Line	Wavelength, μ	% Total Power
V = 10 - 9	P(3)	5.27209	2.80
	P(4)	5.28222	1.34
	P(5)	5.29247	1.94
V = 11 - 10	P(4)	5.35489	1.72
	P(5)	5.36533	4.35
	P(6)	5.37591	0.36
V = 12 - 11	P(4)	5.42933	1.37
	P(5)	5.43996	1.90
	P(6)	5.45073	0.66
V = 13 - 12	P(3)	5.49496	1.54
	P(4)	5.50565	0.53
	P(5)	5.51647	0.95
	P(6)	5.52744	0.39
V = 14 - 13	P(5)	5.59488	0.81
V = 15 - 14	P(4)	5.66407	0.60

before $x = 2.0$ cm, and persist downstream in the cell unless laser pump power is exhausted. As total gas pressure decreases, the V-V pumped plateau extends to higher quantum numbers. Figure 22 should be compared with the experimentally measured distributions of Figure 13, inferred for the same operating conditions. It can be seen that the relative populations of the plateau regions and their extent are quite similar. The details of the shape of the plateaus and high-quantum-number fall-off regions differ; however, the agreement among the measured distributions, the machine-code calculation of Figure 23, and the analytic results of Reference 31, as plotted in Figures 14 to 18, is sufficiently good to create confidence in the inferred CO-Ar V-T rates of Figure 18.

Finally, Figure 24 is a plot of the total pump laser power absorbed as a function of distance along the cell. For all cases, power is absorbed linearly with distance. Absorption is primarily by the lowest vibrational quantum states of the CO, below the plateau; since populations of these states do not change, even in the first 1-2 cm of the cell, the absorption rate remains constant. The total power that is absorbed in the 25 cm total cell length is of the order of the total absorptions observed experimentally for these conditions.

Section 5
CO DISSOCIATION AND C₂, CN FORMATION

5.1 C₂ FORMATION

It is observed that the energy per CO molecule stored in the vibrational mode increases with decreasing total gas pressure in the absorption cell. At total gas pressures below approximately 6 atmospheres in CO/Ar mixtures, a visible blue emission is seen in the pumped gas, the intensity increasing as the pressure decreases. This glow is created by emission from the Swan bands of the C₂ molecule. Figures 25-27 show typical spectra of these Swan bands, obtained in a flowing mixture of 0.5% CO in Ar, at a total cell pressure of 1.0 atm. Flow velocity was 105 cm/sec, and 20% of the pump-beam power of 250 watts/cm² was absorbed. In contrast to the typical visible emission from CO/He electric laser discharges, no emission from CO electronic bands has been observed.

Figure 25 shows the $\Delta V = 0$ sequence of these bands, Figure 26 the $\Delta V = +1$ sequence, and Figure 27 the $\Delta V = -1$ sequence. Several features of these spectra demonstrate the low rotational temperature of the C₂.

In the $\Delta V = 0$ sequence, Figure 25, for example, separate, well defined P, Q, and R branches can be seen. The P branches are headed, and degrade to the violet, a well-known feature of the C₂ Swan bands. Most interestingly, however, a small, distinct Q-branch spike can be seen close to the origin of each band component. This branch is not observed in typical C₂ Swan spectra, being only weakly allowed for the $^3\Pi - ^3\Pi$ transition. However, due to the low rotational temperature, high quantum-number P-branch lines do not obscure this feature. The rotational spacing of the R branch is sufficiently large to allow considerable rotational structure to be resolved; from the intensity distribution of these bands, a rotational temperature of $340 \pm 10^\circ\text{K}$ is inferred. This rotational temperature is essentially the equilibrium kinetic temperature of the cell gases. The C₂ Swan lifetime, of the order of 1 μsec ,⁴¹ is much longer than the mean time between collisions at the experimental

41. Smith, *Astrophysical J.* 156 791 (1969)

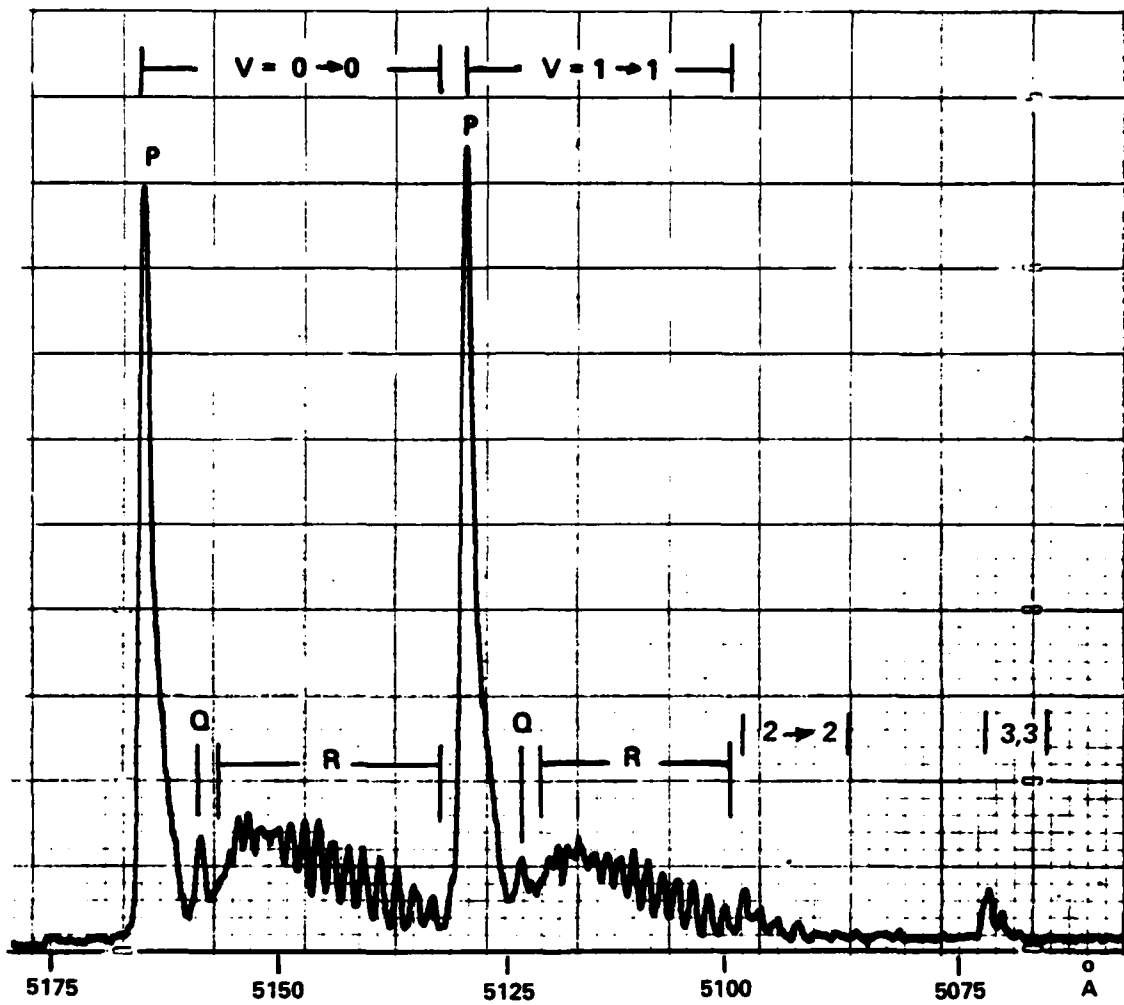


Figure 25 C₂ SWAN BANDS ($A^3 \pi_g - X^3 \pi_u$) $\Delta V = 0$ SEQUENCE

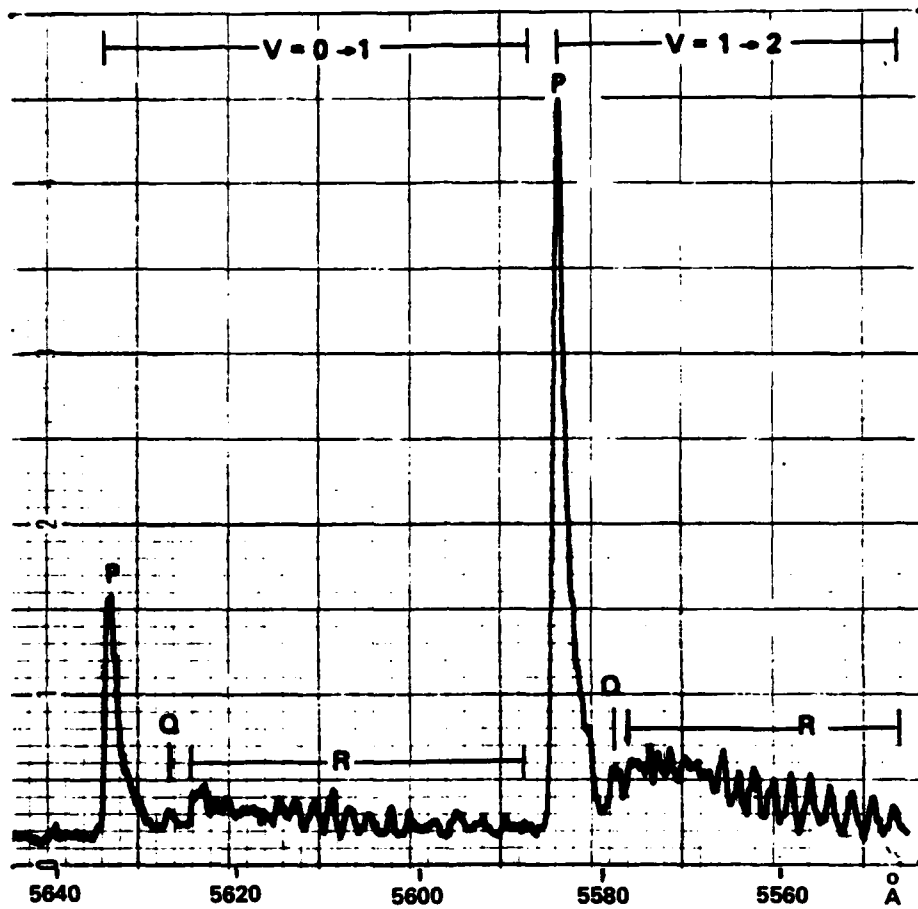


Figure 26 C₂ SWAN BANDS ($A^3 \pi_g - X^3 \pi_u$) $\Delta V = +1$ SEQUENCE

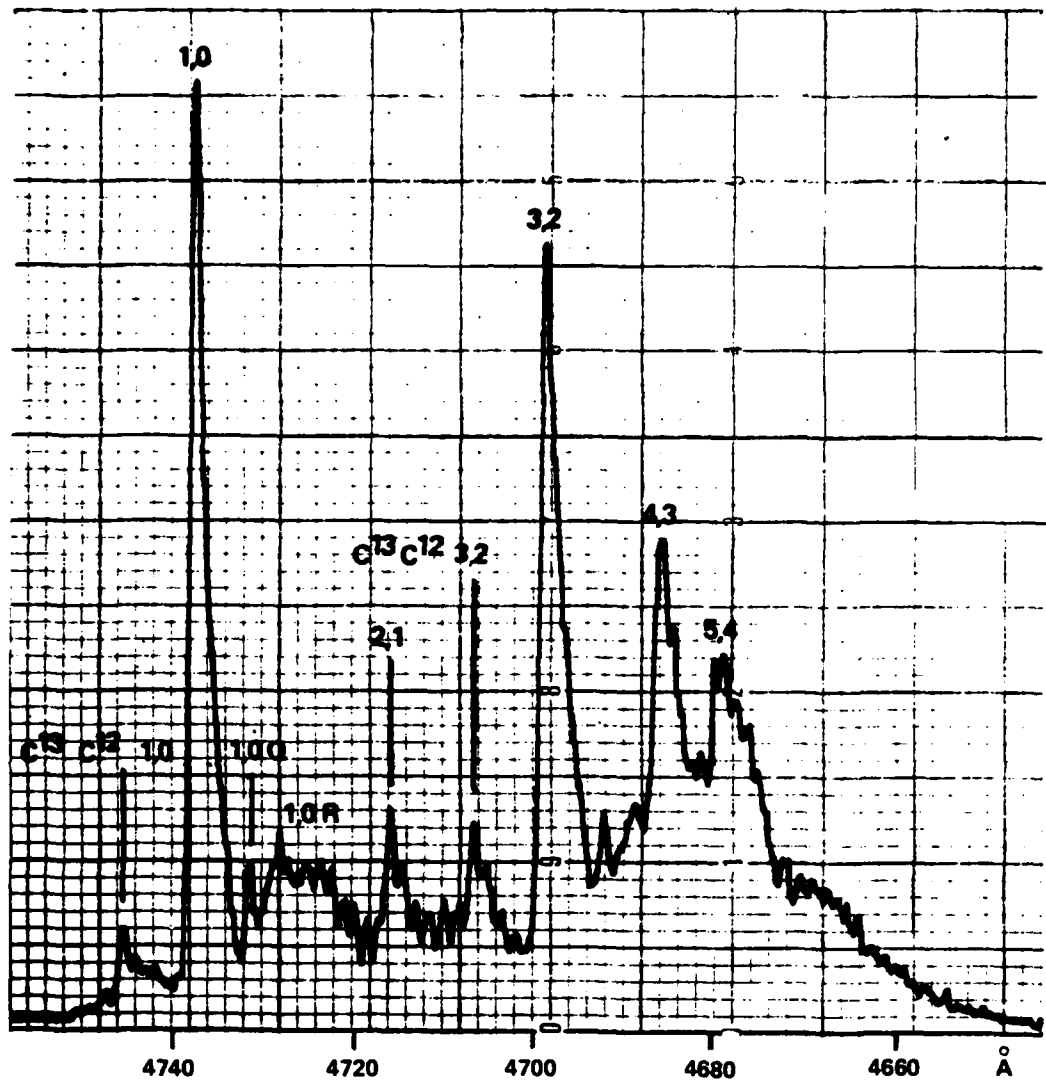


Figure 27 C₂ SWAN BANDS ($A^3 \pi_g - X^3 \pi_u$) $\Delta V = -1$ SEQUENCE

pressures, which are of the order of 1 ns. Since rotational equilibration typically requires of the order of 10 collisions, R-T equilibrium does prevail for all emitting species.

The band structure in the spectral region of the $\Delta V = -1$ sequence, Figure 27, is considerably more complex than the $\Delta V = 0$, $\Delta V = +1$ spectra. This sequence is overlaid by the "tail band" components of the C_2 Swan. However, the $V = 1 \rightarrow 0$, $2 \rightarrow 1$, $3 \rightarrow 2$, $4 \rightarrow 3$, and $5 \rightarrow 4$ band heads are all clearly resolved. In addition, the $V = 1 \rightarrow 0$ and $V = 3 \rightarrow 2$ heads of the $C^{13}C^{12}$ isotope bands are also resolved. In particular, the relative intensities of the $C^{13}C^{12}$ $V = 1 \rightarrow 0$ and $C^{12}C^{12}$ $V = 1 \rightarrow 0$ band heads suggest that the C_2 product is considerably enriched in C^{13} . The normal abundance of C^{13} in carbon is 1.1%; the relative intensities of these $1 \rightarrow 0$ bands suggest enrichments of several hundred per cent. However, sufficient carbon was precipitated on the cell walls during this process to permit accurate mass spectroscopic determination of the C^{13}/C^{12} ratio. Table 7 shows the results of the mass spectroscopic analysis. Samples were taken at three stations along the length of the cell, as indicated. Two samples at each station were taken at diametrically opposite points. It can be seen that enrichments are much less than suggested by the spectrum of Figure 27; maximum enrichment, at the upstream end of the cell, is approximately 20 per cent. At present, the cause of this apparent discrepancy in isotope enrichment ratio has not been resolved.

Finally, it should be noted that only a small amount of the CO flowing through the cell reacts to form C_2 under the conditions generating the spectra of Figures 25-27. Preliminary gas chromatographic monitoring of the CO concentration shows less than 1 per cent of the CO reacts. As total gas pressure is reduced below the one atmosphere level of Figures 25-27, the amount of C_2 produced appears to increase. However, quantitative measurements are not possible at sub-atmospheric pressures, as very rapid carbonization of the cell's optical windows makes them opaque to both the pump laser beam and to the C_2 Swan fluorescence radiation.

TABLE 7

MASS SPECTROGRAPHIC ANALYSIS OF PRECIPITATED CARBON

<u>Sample No.</u>	<u>Axial Position in Cell</u>	<u>Number of Measurements</u>	<u>Ratio, C¹³/C¹²</u>	<u>Relative Standard Deviation, %</u>
Dextrose	Control	5	.01197	1.4
1	4.2 cm	5	.01336	0.7
2	10.8 cm	5	.01262	0.8
3	16.0 cm	5	.01196	0.4
Dextrose	Control	5	.01164	0.7
Dextrose	Control	5	.01175	0.4
4	4.2 cm	5	.01344	0.3
5	10.8 cm	7	.01247	1.0
6	16.0 cm	7	.01196	0.9
Dextrose	Control	6	.01172	0.7

5.2 EXPERIMENTS IN CO/N₂ MIXTURES; CN FORMATION

In a separate series of experiments, mixtures of CO and N₂ in Ar diluent have been optically pumped in the cell. The N₂ vibrational states are in fairly close resonance with those of CO, and the N₂ is vibrationally excited by rapid V-V transfer from the pumped CO. At lower pressures, CN molecules have been observed, strong emission from the CN violet bands being monitored. The CN emission initially increases with added nitrogen, until the diatomic molecule concentration increases to the point where the energy loading of the vibrational modes is substantially lowered. Beyond this point, CN emission decreases as nitrogen is added.

Figures 28 and 29 show the $\Delta V = 0$ sequence of the CN violet bands. The spectrum of Figure 28 was obtained for a 0.4% CO, 1.4% N₂, 98.2% Ar mixture at a total cell pressure of 350 torr and a flow velocity of 943 cm/sec. In addition to the $V = 0 \rightarrow 0$, $1 \rightarrow 1$, $2 \rightarrow 2$, $3 \rightarrow 3$, and $4 \rightarrow 4$ components of the CN $\Delta V = 0$ sequence, the $V = 0 \rightarrow 0$ and $1 \rightarrow 1$ components of the C₂ DesLandres-d'Azambuja bands are also seen. An interesting feature of these CN spectra is that the well known P-branch band heads are not observed. This lack of heading is caused by the low rotational temperature of the CN (approximately 300°K). The P-branch band heads for the CN system occur at rotational quantum level $J = 28$; such high rotational levels are not populated at 300°K, and hence the head does not form. This feature is further illustrated in Figure 29, where the same CN violet $\Delta V = 0$ bands are shown. In the top trace, the unheaded bands are again shown, being created in the cell with a flow velocity of ~ 1000 cm/sec. In the lower trace, the flow velocity has deliberately been slowed down drastically, allowing the translational/rotational temperature of the gas to rise. The band heads become immediately apparent.

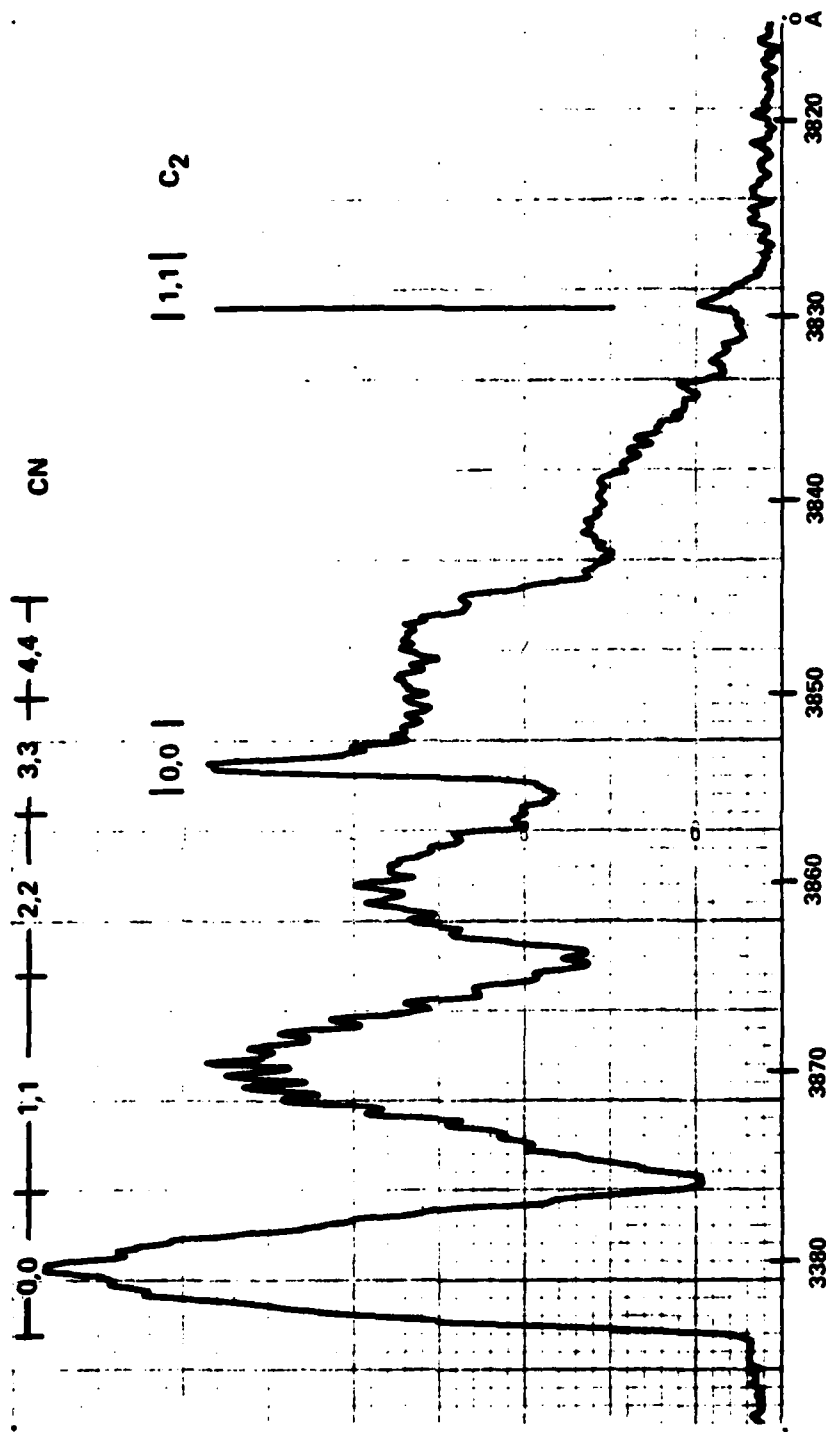
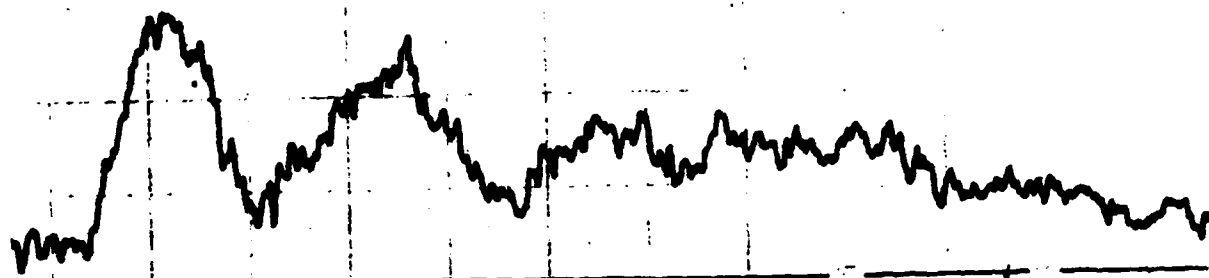
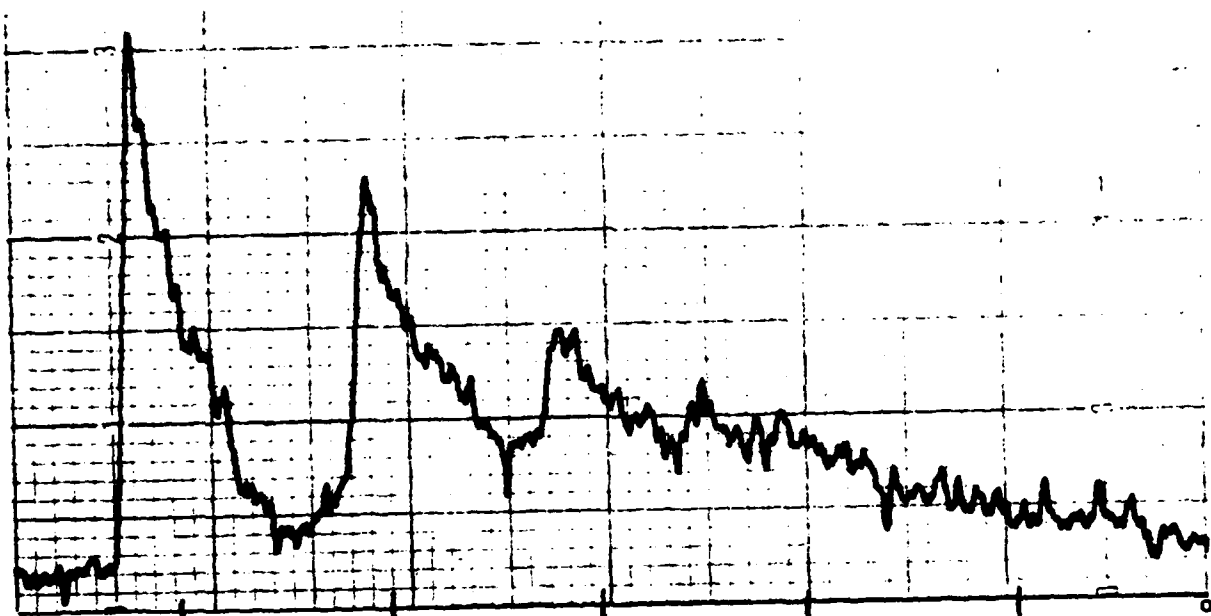


Figure 28 CN VIOLET BANDS ($B^2 \Sigma^+ - X^2 \Sigma^+$), $\Delta V = 0$ SEQUENCE
 C_2 DES LANDRES D'AZAMBUJA ($C' \pi_g - b' \pi_g$) $\Delta V = 0$ SEQUENCE



UNHEADED, FAST FLOW



HEADED, SLOW FLOW

Figure 29 EFFECT OF FLOW VELOCITY ON CN VIOLET BAND HEADING

5.3 DISCUSSION

The evident reaction of CO to form an isotopically enriched C₂ product in the optically pumped cell is a true laser-induced chemical reaction, as opposed to a conventional, thermally induced reaction. The C-O bond in the carbon monoxide diatom is unusually strong, the molecule having a dissociation energy of 11.1 eV. Accordingly, measurements of the rate of thermal dissociation of CO are commonly performed in shock-tube experiments generating equilibrium temperatures of several thousand degrees Kelvin.¹⁻⁴ In contrast, the present results are achieved at translational-rotational temperature near 300°K, as confirmed by quantitative examination of resolved rotational structure of CO and C₂ emission spectra.

The details of the kinetic mechanism of the observed C₂ production have not yet been determined. The simplest hypothesis is that direct CO dissociation is occurring, the dissociation proceeding via collisions involving vibrationally excited CO molecules in the V-V pumped plateaus shown in Figure 13. It should be remarked that such a model implies that the rate-controlling populations are those in the pumped plateau, not those within a few kT of the dissociation energy. Those very uppermost levels would have very small steady-state populations during dissociation. In the present case, two CO molecules, each vibrationally excited to quantum levels in the pumped plateau, could collide and pool sufficient energy to dissociate one partner. Such a model involves a small but finite probability of a collisionally-induced multiquantum transition from a vibrational level in the plateau to the continuum. This model is, of course, related in its basics to the various "vibrational-state ladder-climbing" theories of diatomic molecular dissociation evolved over a period of years.^(2,3,42,43) There are, however, two essential differences between the present

42. McCoy, B.J., and Carbonell, R.G., Chem. Phys. 20, 227 (1977).

43. Hogarth, W.L., and McElwain, D.L.S., Chem. Phys. 19, 429 (1977).

results and these thermal dissociation models. In the present case, it appears that quite small multiquantum V-V transitions may be controlling dissociation. Secondly, there is disequilibrium between the vibrational mode and the modes of rotation and translation; the dissociation models assume essential equilibration among these modes. The influence of vibrational state populations and rotational energy are controlling parameters in the model calculations,²⁻³ and both parameters can be systematically varied and measured in the present experimental setup. Accordingly, further work along these lines is planned.

The details of the demonstrated C¹³ isotopic enrichment are, of course, a part of the general kinetics of the observed C₂ formation. There are two known effects which might cause the C¹³ enrichment, for the operating conditions of our device. These two effects are 1) isotope separation by preferential V-V pumping,¹⁶⁻¹⁷ and 2) the well known "kinetic isotope effect".^{18,44} Effect 1) has been the subject of considerable recent analysis. Theoretical considerations indicate that in a V-V pumped diatomic gas the molecules of the heaviest isotopes will be the most vibrationally excited. Accordingly, for some kinetic mechanisms, the heavier species will react more rapidly. Experiments have been reported on electric-discharge and laser excitation of N₂/O₂ mixtures,¹⁷ leading to NO formation. It was found that the NO product was substantially enriched in the N¹⁵ isotope when the experiments were performed at room temperature or below. However, subsequent attempts to reproduce the result of Reference (17) by Manuccia, and Clark,¹⁹ show N¹⁵ enrichment of the order of 20%, rather than the much larger enrichments previously reported. Accordingly, as pointed out in Reference 19 and in subsequent reviews,¹⁵ it has not been conclusively demonstrated that V-V pumping is responsible for such enrichments; effect 2), i.e., kinetic- and equilibrium-isotope effects may also be contributors. At the low translational temperatures of such experiments, such simple mass effects may be the dominant influence, especially

44. Collins, C.J., and Bowman, N.S., Isotope Effects in Chemical Reactions, ACS Monograph No. 167 (Van Nostrand-Reinhold, NY, 1970), p. 15, p. 15; Lukasik, J., and Ducing, J., Chem. Phys. Lett. 27, 203 (1974).

when only relatively low enrichment ratios are observed. These same conclusions apply to the present observations of C^{13} enrichment; there is as yet no clear demonstration of the precise mechanism for the isotope enrichment.

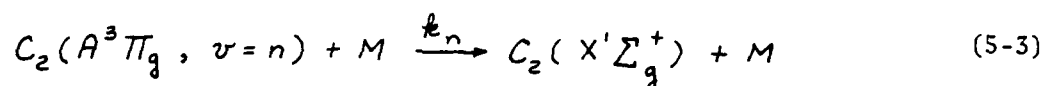
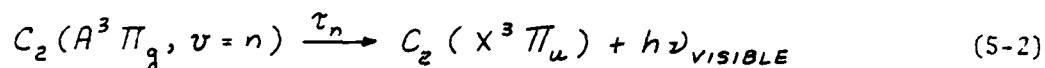
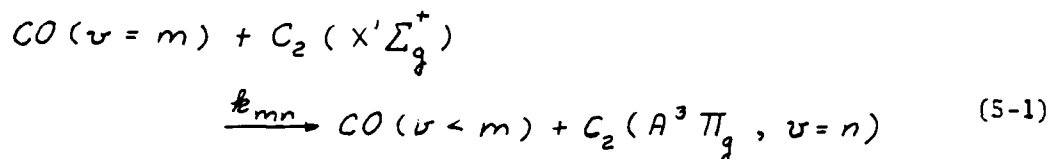
Finally, the cause of the observed electronic fluorescence from C_2 and CN is one of the more interesting questions posed by the present experiments. In forming a working hypothesis, three principal experimental features should be noted:

- i) There is no evidence of electronically excited CO. Unlike the visible emission from a CO laser electric discharge, there appears to be no emission from the CO Angstrom bands or other CO electronic states.
- ii) Two of the observed electronic states of C_2 and CN (the $C_2 C'\pi_g$ and CN $B^2\Sigma^+$) have, respectively an electronically excited C and N atom as one of their dissociation products.
- iii) The C_2 and CN electronic states observed in emission to date have energies below many of the vibrational states observed in the optically pumped CO.

On the basis of these observations, it can be hypothesized that the C_2 and CN are formed in their ground electronic states, and subsequently are electronically excited by energy transfer from the vibrational modes of CO (and N_2) during molecular collisions. It is difficult to see how the electronic excitation of C_2 and CN is accomplished otherwise. Optical pumping is by means of relatively low energy 5μ infrared photons; pump intensities are of the order of a few 100 watts/cm². Accordingly, there is little probability of direct multiphoton excitation of electronic states or multiphoton dissociation. This is supported by the lack of any observed CO excited electronic

states. Further, the direct formation of C_2 and CN in the observed electronic states requires, for some of the transitions noted, the presence of electronically excited C or N atoms; it is difficult to see how these could be formed by direct optical excitation.

This hypothesized mechanism of vibration-to-electronic energy transfer between molecules and subsequent strong visible emission from the excited electronic state can be written for the CO- C_2 system as:



Here, $C_2(A^3\Pi_g, \nu = n)$ and $C_2(X^3\Pi_u)$ are the upper and lower electronic levels of the Swan band emission originating from vibrational level $\nu = n$ of $A^3\Pi_g$; $C_2(X'\Sigma_g^+)$ is the ground electronic state of C_2 ; k_{mn} is the specific rate constant for the V-E transfer; τ_n is the radiative lifetime of the $C_2(A^3\Pi_g, \nu = n)$ state, and k_n is the rate for the collisional quenching of this same state by diluent species M.

This mechanism assumes that the vibrationally excited CO can be regarded as a metastable present in large excess, and that the radiative and quenching steps, Reactions (5-2) and (5-3) are very rapid. These conditions are met by the slow-relaxing vibrational mode of CO and the large f numbers of the Swan transitions. For the C_2 Swan, $\tau_n \sim 10^{-6}$ sec; the quenching rate by diluent also can be significant for pressures above 0.5 atm. For the conditions of our experiment, the average time between collisions of

C_2 with vibrationally excited CO is more than an order of magnitude longer than the radiative (τ_n) or quenching ($\tau_{\text{quenching}} \sim \{k_n [M]\}^{-1}$) times. With such time scales, essentially every $C_2 (A^3\Pi_g)$ formed by Reaction (5-1) undergoes rapid radiative or collisional decay via Reactions (5-2) and (5-3), and pseudo first-order kinetics obtain, with Reaction (5-1) the rate-limiting step. It can be shown that the emitted visible fluorescence intensity on the C_2 Swan is then given by:

$$I_n = \frac{\sum_m k_{mn} [CO (v=m)] [C_2 (X^1\Sigma_g^+)]}{1 + \tau_n k_n [M]} \quad (5-4)$$

Here, I_n is the intensity of Swan band emission from vibrational level n of $C_2 (A^3\Pi_g)$; $[CO (v=m)]$ is the population of vibrational level m of ground electronic state CO. Accordingly, the intensity of emission from the C_2 Swan bands is proportional to the amount of vibrationally excited CO. Strong emission is possible from very small amounts of C_2 , provided large quantities of CO ($v \approx m$) are present.

Section 6

STUDIES OF V-E TRANSFER PROCESSES

6.1 CO-NO V-E EXCHANGE

The electronic mode fluorescence described in the preceding section appears to be caused by vibration-to-electronic (V-E) transfer from the vibrationally excited CO in the optically pumped cell. Reported examples of transfer of energy from vibrationally excited molecules to the electronic mode of other molecules are rare in the literature. However, one such process was reported by Provencher and McKenney in 1971,⁴⁵ in which vibrationally excited nitrogen produced in a flowing gas microwave discharge, was observed to transfer its energy to the $A^2\Pi$ and $B^2\Sigma^+$ excited electronic levels of CN; the latter process appears quite analogous to the presently-observed excitation of CN ($B^2\Sigma^+$) by transfer from vibrationally-excited CO.

The Calspan experiments described in this report have an advantage over microwave excitation in that electronic excitation is occurring in a discharge-free environment; there are no free electrons which might be responsible for some of the observed electronic excitation. However, the electronically excited species, C_2 and CN, are formed by chemical reaction from the CO and N_2 in the cell, and chemiluminescent excitation of the electronic states remains a possibility. While, as discussed in Section 5, there are good kinetic reasons for believing such chemiluminescent processes do not participate in the observed excitation, a more clear-cut demonstration of the molecular V-E transfer effect is to add an electronic mode molecular acceptor to the vibrationally excited CO in the cell. If such a potential acceptor, not being formed by chemical reaction, is observed to be electronically excited, the case for V-E transfer becomes stronger. Accordingly, further experiments were performed in which nitric oxide (NO) was added to serve as an electronic mode acceptor for the vibrationally excited CO in the cell. Two methods of NO addition were

45. Provencher, G.M. and McKenney, D.J., Chem. Phys. Lett. 10, 365 (1971).

investigated. In one case, NO was added to the already vibrationally excited CO at a point several centimeters downstream in the cell. In the second case, NO was premixed with CO before injection of the mixed gases upstream in the cell. In both cases, NO was observed to fluoresce strongly on both the NO γ ($A^2\Sigma^+ - X^2\Pi_r$) and NO β ($B^2\Pi_r - X^2\Pi_r$) electronic bands.

Figure 30 shows a typical emission spectrum of the fluorescence from these NO electronic bands, for one of the premixed cases. The gas concentrations and all operating conditions are listed on the figure. It is important to note that this pumping of NO electronic excitation is occurring at quite high pressures and gas concentrations.

It can be seen from Figure 30, that the $v = 0 \rightarrow n$ and $v = 1 \rightarrow n$ sequences of the NO γ and the $v = 0 \rightarrow n$ sequence of the NO β have been observed. In addition, strong CN violet emission is present. CN formation occurs via the rapid reaction of the added NO with the vapor-phase C_2 formed by CO dissociation. This rapid NO- C_2 reaction has been recently observed by Wittig,⁴⁶ who estimates the reaction cross section for CN formation to be approximately half the gas kinetic cross section for NO - C_2 collisions.

Simultaneously with measurement of the NO emission spectra of Figure 30, the CO vibrational-state infrared emission spectrum is measured at the same position in the absorption cell. Figure 31a shows such a spectrum, being the emission from the first overtone ($\Delta V = 2$) vibrational transitions of the CO ground electronic level. Emission is measured from vibrational levels up to $V = 42$; the energy of this vibrational level is approximately 8 eV, 70% of the CO dissociation energy. The NO electronic levels that have been observed to be excited, NO ($B^2\Pi_r$, $V = 0$) and NO ($A^2\Sigma^+$, $V = 0$, $V = 1$) have energies

46. Reisler, H., Mangir, M. and Wittig, C., "The Kinetics of Free Radicals Generated by IR Laser Photolysis: I. Reactions of C_2 ($a^2\Pi_u$) with NO, Vinyl Cyanide, and Ethylene", Dept. of Elec. Eng., USC, 1979. To be published.

$P_{CELL} = 262 \text{ TORR}$
 $N_{Ar} = 8.37 \times 10^{18} \text{ CM}^{-3}$
 $N_{CO} = 6.32 \times 10^{16} \text{ CM}^{-3}$
 $N_{NO} = 3.12 \times 10^{15} \text{ CM}^{-3}$

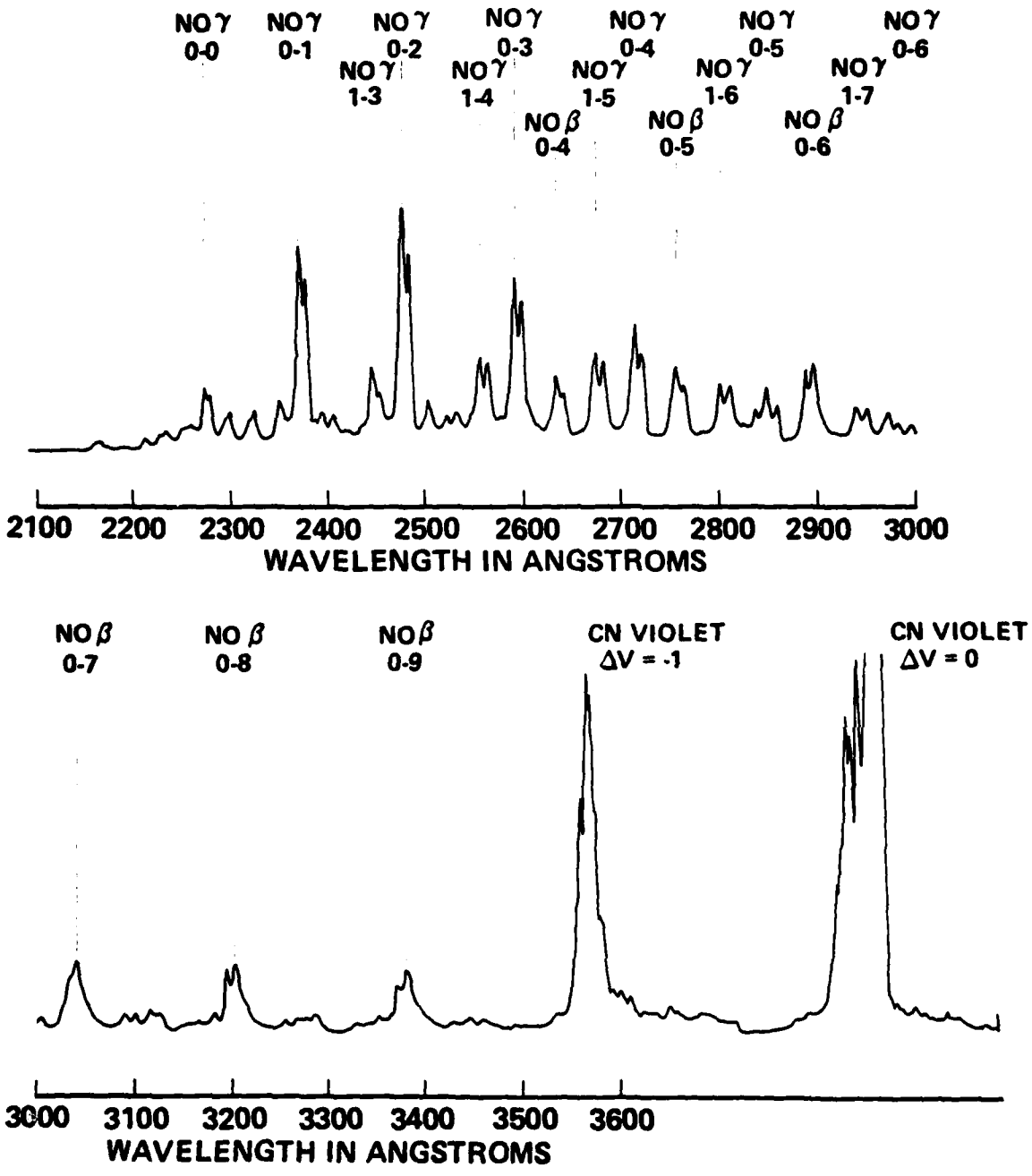


Figure 30 $NO \beta$ AND γ BANDS, EXCITED BY TRANSFER FROM VIBRATIONALLY PUMPED CO

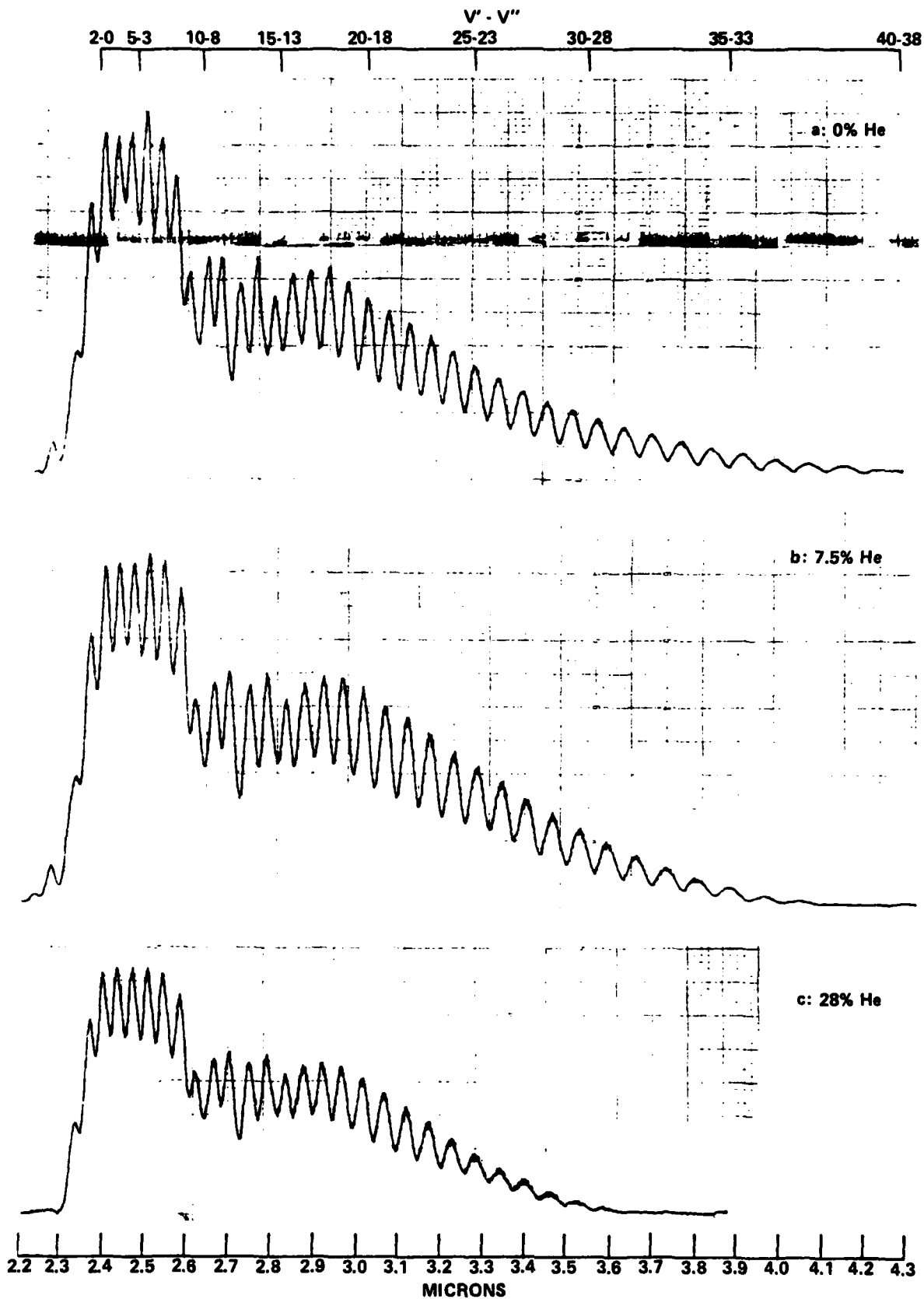


Figure 31 CO $\Delta V = 2$ EMISSION SPECTRA, FOR SEVERAL He CONCENTRATIONS

in the range of 6 - 7 eV, below the energy of the highest excited vibrational levels of the CO.

It is interesting to observe the effect of quenching the population of CO vibrational levels with energies above 6 eV on the observed NO band fluorescence. As shown in Section 3 (Figure 12), helium addition causes rapid depopulation of the high-lying vibrational states of the pumped CO, due to the rapid vibration-to-translation deactivation rates for excited-state-CO collisions with helium. Accordingly, various amounts of helium were added to the CO/NO/Ar mixture in the cell, and the CO vibrational state and NO electronic band fluorescence were monitored simultaneously at the same station in the cell. Figures 31 and 32 show the results of these measurements. Figures 31 and 32 show, respectively, the CO $\Delta V = 2$ vibrational band emission and the NO γ and NO β electronic band emission for the case with no He additive. 31b and 32b are the respective traces for 7.5% He additive, and 31c and 32c are the traces for 28% He additive.

It can be seen from these spectra that with He addition, the topmost detectable populated CO vibrational level decreases from $V \approx 40$ at 0% He, to $V \approx 34$ at 7.5% He, to $V \approx 27$ at 28% He. There is a rapid drop in NO β and NO γ emission. Above 28% He addition, there is no detectable NO electronic band emission, despite the fact that the lower CO vibrational states remain substantially populated.

The preceding observations are correlated with the energy levels of CO and NO in Figure 33. It can be seen from this figure that He concentrations of 28% or lower permit the population of CO vibrational levels having energies greater than those of the NO $A^2\Sigma^+$ and NO $B^2\Pi$ states. It is these vibrational states, above $V \approx 25$, that can transfer energy and result in electronic excitation of NO.

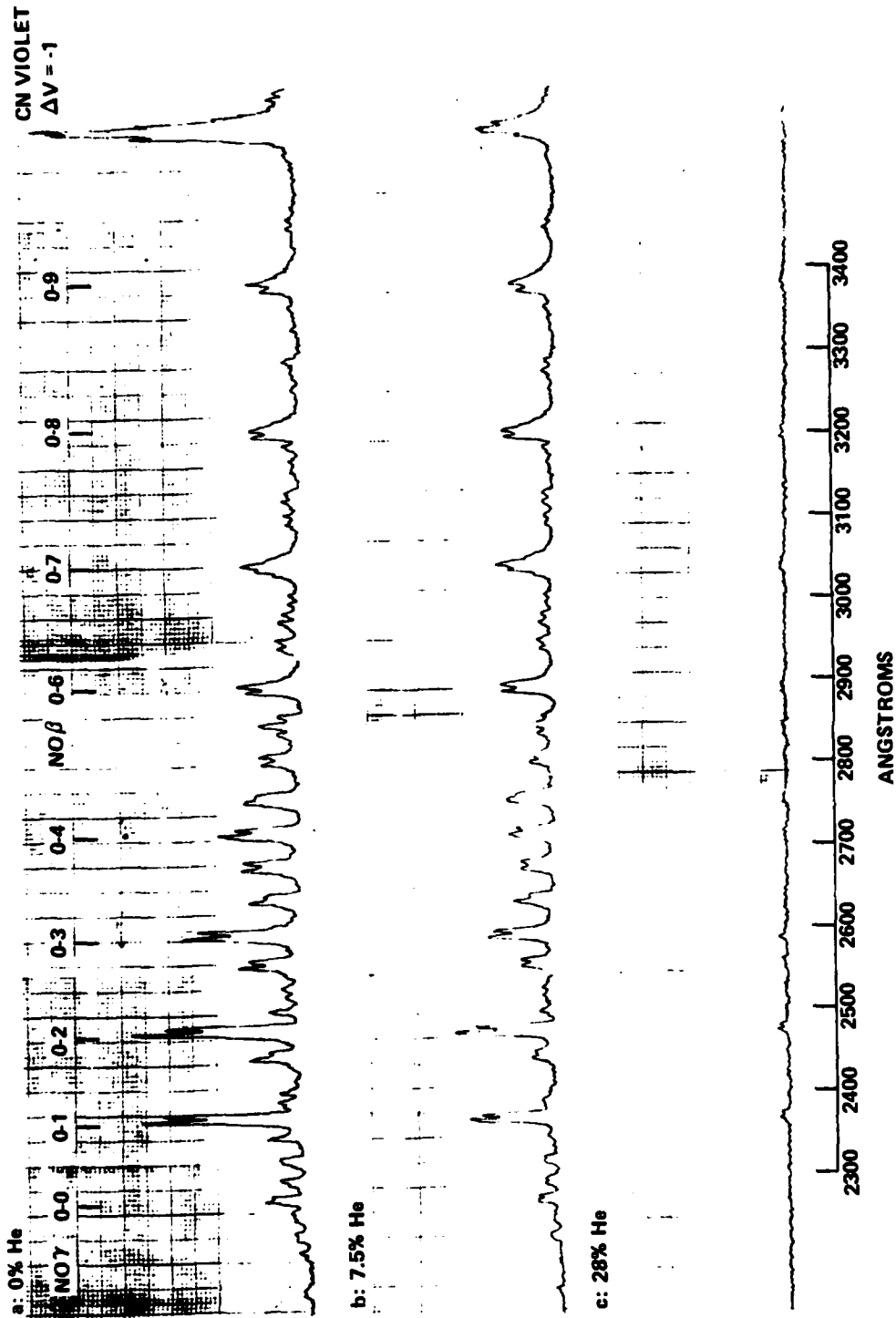


Figure 32 NO β AND γ EMISSION SPECTRA, FOR SEVERAL He CONCENTRATIONS

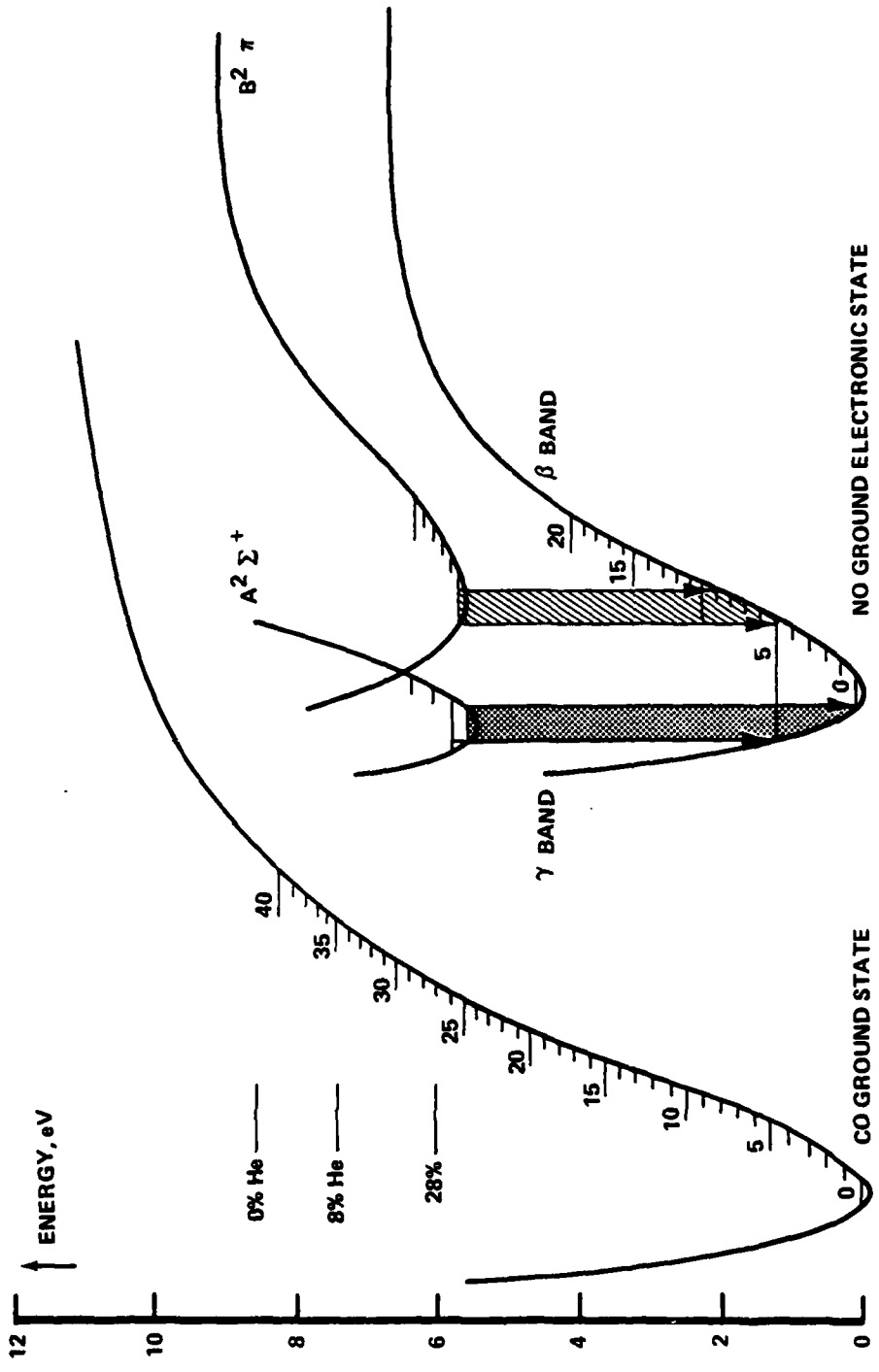


Figure 33 CO AND NO ENERGY LEVELS

The NO electronic emission band spectra, such as those of Figure 30, can readily be used to infer the populations of the emitting NO quantum levels. Due to the low rotational temperature of the experiment, the individual vibrational components of the NO β and NO γ bands do not, in many cases, significantly overlap. For such cases, for optically thin emission, it can be shown that the population of the V' th vibrational quantum level of the emitting electronic state, $N_{V'}$, is given by:

$$N_{V'} = \frac{4\pi \times 10^7 \tau \nu_{00}^2}{hc \nu_{V'V''}^3 f_{FC}} \int I(\lambda)_{exp} d\lambda$$

Here,

- τ = lifetime of the electronic transition in seconds
- $\nu_{V'V''}$ = frequency of the $V' \rightarrow V''$ vibrational band component of the electronic transition, cm^{-1}
- ν_{00} = frequency of the $0 \rightarrow 0$ vibrational band component of the electronic transition, cm^{-1}
- h = Planck's constant, 6.623×10^{-27} erg.sec
- c = speed of light, 2.998×10^{10} cm. sec $^{-1}$
- f_{FC} = Franck-Condon factor
- $I(\lambda)_{exp}$ = intensity of emitted electronic radiation at wavelength λ , watts cm^{-3} micron $^{-1}$ sr $^{-1}$
- λ = wavelength, microns
- $N_{V'}$ = population of V' vibrational level, cm^{-3}

The integral is over the entire $V' \rightarrow V''$ band component.

A standard tungsten filament lamp (Eppley Laboratory) was used to calibrate the emission intensity of the NO bands. The lamp emission was

traceable to NBS standard over a band from $.25\mu$ to $.75\mu$. Since lamp intensity at the short wavelengths is only $\sim 1\%$ of the intensity at longer wavelengths, stray light was a major problem for UV wavelength calibration. Stray light was eliminated by using a series of narrow bandpass filters of known transmission for short wavelength calibration.

Lifetimes for the NO $A^2\Sigma^+$ and $B^2\Pi$ states, the upper states of the γ and β bands, were taken from Reference 47. Franck-Condon factors for these bands were taken from References 47 and 48.

Table 8 lists the measured NO populations, for cell pumping conditions similar to those of Figure 30. As can be seen, it was possible to reduce two components of the $0 \rightarrow n$ sequence of the NO(γ), and to reduce five components of the $0 \rightarrow n$ sequence of the NO(β). Thus there is a fair degree of redundancy in inferring the NO ($A^2\Sigma^+$, $V = 0$) and NO ($B^2\Pi$, $V = 0$) state populations. Measurement deviation is rather high among these redundant measurements; major sources of these deviations are the neglect of partial overlapping of some of the band components, and uncertainties in measurement of filter transmissions used in stray light elimination. The data means of $4.3 \times 10^8 \text{ cm}^{-3}$ for the NO ($A^2\Sigma^+$, $V = 0$) population and $4.2 \times 10^9 \text{ cm}^{-3}$ for the NO ($B^2\Pi$, $V = 0$) population are estimated to be accurate to within a factor of three.

6.3 V-E TRANSFER LASER CONCEPT

The experiments described in the preceding section show that energy can be transferred from the V-V pumped vibrational modes of CO to the

-
47. Suchard, S.N., "Spectroscopic Constants for Selected Heteronuclear Diatomic Molecules" Vol. II. Aerospace Corporation Report No. TR-0074(4641)-6, Vol. II, 1974.
 48. Allen, R.A., "Air Radiation Tables: Spectral Distribution Functions for Molecular Band Systems" Avco Everett Research Lab. Report No. 236, 1966.

TABLE 8
NO EXCITED STATE POPULATIONS

NO ($A^2 \Sigma^+$, $V = 0$)

[Upper State of γ]

Component	Population (cm^{-3})
(0 - 3)	2.38×10^8
(0 - 4)	6.26×10^8
Mean	4.32×10^8

NO ($B^2 \Pi$, $V = 0$)

[Upper State of β]

Component	Population (cm^{-3})
(0 - 5)	8.61×10^9
(0 - 6)	2.91×10^9
(0 - 7)	5.17×10^9
(0 - 8)	1.10×10^9 (Filter ?)
(0 - 9)	3.35×10^9
Mean	4.23×10^9

electronic modes of various molecular collision partners. These results suggest a possible molecular V-E transfer laser, based on highly vibrationally excited CO or N₂ transferring energy to molecular electronic states on which population inversions can be maintained. Accordingly, a simplified model of the laser kinetics was developed, and is described in this subsection.

We consider a vibrationally pumped diatomic molecule "X₂" (in practice, this could be CO or N₂), and a collision partner "A₂" (which could be NO), which will be the lasing molecule. A₂ is assumed to have only two participating electronic states, A₂¹ and A₂², with E₁ > E₂. We are interested in the possibility of creating optical gain on transitions between some rotational substate of the mth vibrational state of A₂¹, and another rotational substate of the nth vibrational state of A₂², i.e., gain on a transition;



The upper state, A₂¹ (v = m), is excited by collisional V → E transfer from the vibrationally excited X₂. In principle, there can be many vibrational states of the lower electronic level of A₂, which can accept vibrational energy from CO and be excited to the A₂¹ (v = m) state. Similarly, there can be many vibrational states of X₂ having sufficient energy to cause such a transition during an inelastic V → E transfer collision. For the purposes of the present discussion, however, it will be assumed that only a single V-E energy transfer channel is open, i.e., only two pairs of states participate in the transfer process. Figure 34 is a sketch of this simplest situation. In the figure, the potential curve on the left is that of the X₂ molecule; on the right are the potential curves for the A₂¹ and A₂² states of the A₂ molecule. The energy exchange channel under consideration is a collision of X₂ in level v = i with A₂² (v = 0) with consequent collision-induced transitions v = i → 0 in X₂ and A₂² (v = 0 → A₂¹ (v = m) in A₂. As sketched in the figure, this V → E exchange transition is nearly a resonant process, with a very small energy defect; in practice, it has been noted that the resonant

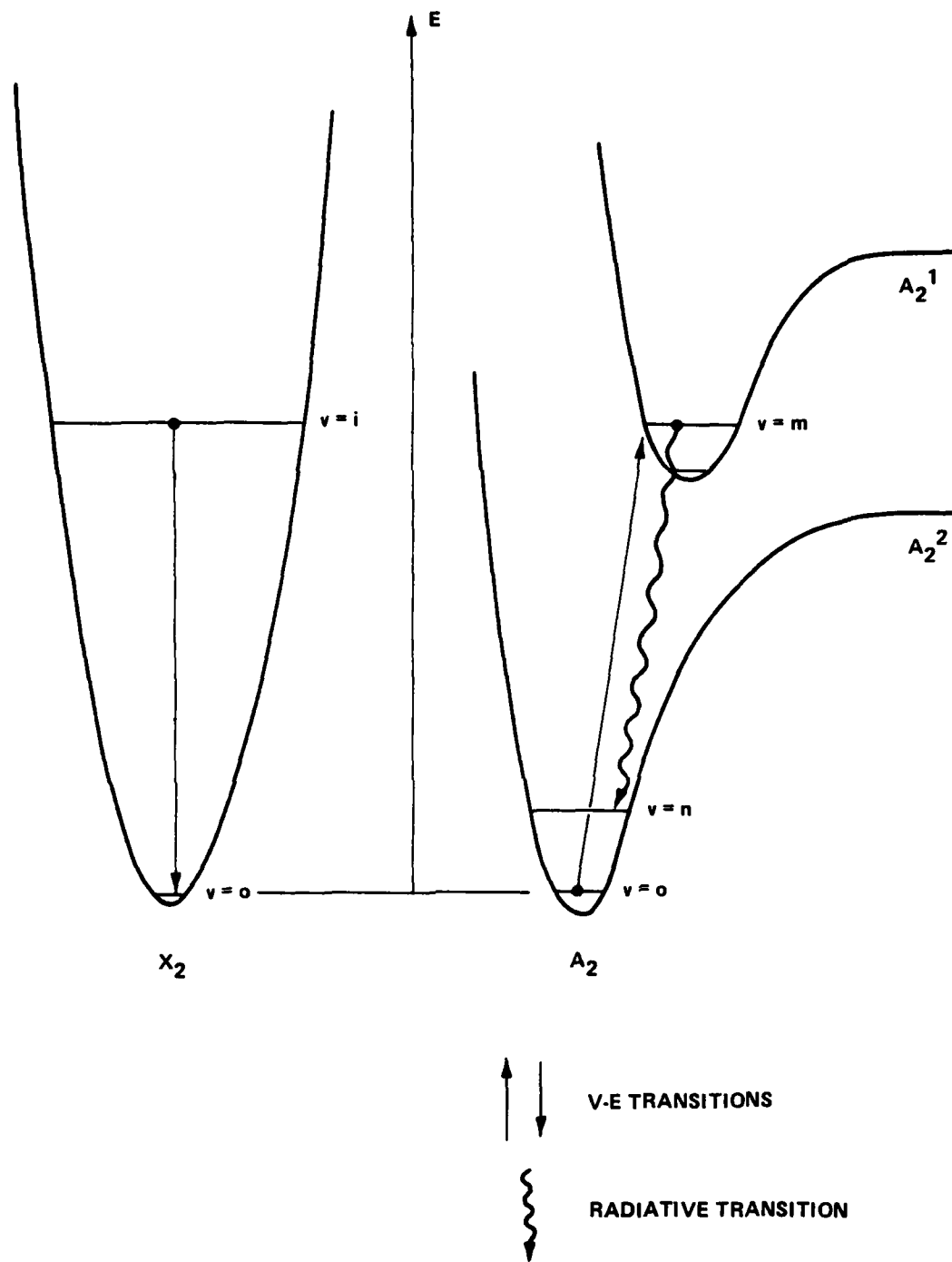


Figure 34 ENERGY LEVELS FOR SIMPLIFIED V-E TRANSFER LASER MODEL

AD-A082 345 CALSPAN ADVANCED TECHNOLOGY CENTER BUFFALO NY AERODYN--ETC F/G 20/10
MEASUREMENT OF KINETIC RATES FOR CARBON MONOXIDE LASER SYSTEMS.(U)
UNCLASSIFIED NOV 79 J W RICH, R C BERGMAN, M J WILLIAMS F49620-77-C-0020
CALSPAN-WG-6021-A-3 AFOSR-TR-80-0207 NL

2 of 2
AD
A082 345

END
DATE
FILMED
4-80
DTIC

channel is not always dominant in all $V \rightarrow E$ exchange processes.⁴⁹ The nature of the argument here, however, is not dependent on near-resonant exchange.

Figure 34 shows these collision-induced V-E transitions, and, in addition, indicates the radiative decay of transition of the upper electronic state, A_2^1 ($v = m$). Again, for simplicity, only one radiative decay transition is shown. Note that this transition need not be to the ground vibrational state of A_2^2 ; as shown, the radiative transition A_2^1 ($v = m$) \rightarrow A_2^2 ($v = n$) terminates in a vibrational level $v = n > 0$.

We will further assume that the electronic acceptor concentration is sufficiently small to insure that the vibrational state populations of the V-V pumped donor molecules are unperturbed by the V-E transfer process, and that the vibrational states of the acceptor molecule are not themselves V-V pumped.

Using the model described above, we consider the processes controlling the populations of A_2^1 ($v = m$) and A_2^2 ($v = n$), namely, $V \rightarrow E$ exchange with X_2 , radiative decay, and direct collisional quenching, and write rate equations governing the populations of these states:

$$\begin{aligned} \frac{d[A_2^1(v=m)]}{dt} &= k_{0 \rightarrow m}^{V \rightarrow E} [X_2(v=i)] [A_2^2(v=0)] \\ &- k_{m \rightarrow 0}^{E \rightarrow V} [X_2(v=0)] [A_2^1(v=m)] \\ &- \frac{1}{\tau_{RAD}} [A_2^1(v=m)] - k'_{QUENCH} [M] [A_2^1(v=m)] \end{aligned} \quad (6-1)$$

$$\frac{d[A_2^2(v=n)]}{dt} = \frac{1}{\tau_{RAD}} [A_2^1(v=m)] - k''_{QUENCH} [M] [A_2^2(v=n)] \quad (6-2)$$

49. Lemont, S., and Flynn, G.W., Ann. Rev. Phys. Chem. 28, 261 (1972).

Here, the brackets indicate concentrations in molecules/cm³. $k_{0 \rightarrow m}^{v \rightarrow E}$ and $k_{m \rightarrow 0}^{E \rightarrow v}$ are the forward and reverse specific V-E constants for the indicated exchange transition, τ_{RAD} is the radiative lifetime of the $A_2^1 (v = m) \rightarrow A_2^2 (v = n)$ transition, k_{QUENCH}^1 and k_{QUENCH}^2 are the specific rates for the quenching of the $A_2^1 (v = m)$ and $A_2^2 (v = n)$ states, respectively, by collision with diluent species M. Naturally, if other V-E channels are open, if there is more than one effective quenching species, or if there are several strong radiative transitions, the single terms in Eqs. (6-1) and (6-2) must be replaced by sums over states and species.

The above equations can be solved for the quasi-steady upper and lower state populations, $[A_2^1 (v = m)]$ and $[A_2^2 (v = n)]$, by setting the time derivatives equal to zero, with the result:

$$[A_2^1 (v = m)] = \frac{k_{0 \rightarrow m}^{v \rightarrow E} [X_2 (v = i)] [A_2^2 (v = 0)]}{k_{m \rightarrow 0}^{E \rightarrow v} [X_2 (v = 0)] + \frac{1}{\tau_{RAD}} + k_{QUENCH}^1 [M]} \quad (6-3)$$

and

$$[A_2^2 (v = n)] = \frac{[A_2^1 (v = m)]}{\tau_{RAD} k_{QUENCH}^2 [M]} \quad (6-4)$$

In the interpretation of our recent experiments, an important limiting case of the above result can be recognized.

For this case,

$$\frac{1}{\tau_{RAD}} \gg k_{m \rightarrow 0}^{E \rightarrow v} [X_2 (v = 0)] \quad (6-5)$$

i.e., every A_2 molecule that is electronically excited by collision with vibrationally excited X_2 is almost immediately deactivated by rapid spontaneous emission (or collisional quenching). In this limit, the emitted spontaneous fluorescence intensity, $I_{\text{FLUORESCENCE}}$ is given by:

$$I_{\text{FLUORESCENCE}} = \frac{1}{\tau_{\text{RAD}}} [A_2'(v=m)]$$

$$\approx \frac{k_{0 \rightarrow m}^{V \rightarrow E} [X_2(v=i)] [A_2(v=0)]}{1 + \tau_{\text{RAD}} / \tau'_{\text{QUENCH}}} \quad (6-6)$$

where

$$\tau'_{\text{QUENCH}} \equiv [k'_{\text{QUENCH}} [M]]$$

This limiting case is an approximation to the actual conditions in our apparatus which create the C₂ Swan band fluorescence discussed in the Section 5 and shown in Figures 25-27. This mechanism requires that the vibrationally excited species be essentially a metastable present in large excess, and that the radiative decay of the electronic acceptor be very rapid. These conditions are met by the slow-relaxing vibrationa' mode of CO and the large f numbers of the C₂ Swan transitions; these transitions have radiative lifetimes of $\sim 1 \times 10^{-6}$ sec. For the typical conditions of our experimental C₂ Swan band spectra of Figures 25-27, the average time between collisions of C₂ with vibrationally excited CO is more than an order of magnitude longer than these radiative lifetimes. With such scales, and in the absence of rapid collisional quenching, essentially every C₂ ($A^3 \Pi_g$) formed by V-E transfer from CO undergoes rapid radiative decay. For this case, using Eq. (7) in the limit $\tau_{\text{RAD}} / \tau_{\text{QUENCH}} \ll 1$, and putting $[A_2^2(v=0)] = [C_2(X^1 \Sigma_g^+)]$, $[X_2(v=i)] = [CO(v=i)]$, one obtains for the emitted visible fluorescence intensity on the C₂ Swan band:

$$I_{\text{FLUORESCENCE}} = k [CO(v=i)] [C_2(X^1 \Sigma_g^+)] \quad (6-7)$$

Accordingly, the intensity of emission from the C_2 Swan bands is proportional to the amount of vibrationally excited CO, $[CO(v=i)]$. Strong emission is possible from very small amounts of C_2 , provided large quantities of CO ($v=i$) are present. It is probable that the fluorescence we have observed on the CN violet bands in pumping of CO/N₂ mixtures also represents a second example of this limiting case of the kinetics.

The limiting case discussed above cannot easily produce a population inversion that would be useful for developing a laser operating on the molecular electronic bands. In the particular cases of the C_2 Swan and CN violet emissions observed in our experiments, the lower levels of the electronic transitions involve vibrational states $V = 0, 1, 2, 3,$ and 4 , i.e., the very lowest vibrational states of the ground electronic level. These states will, of course, be rather highly populated in a steady state situation, making inversion difficult. As is well known, extremely rapid radiative depopulation of the upper level ($C_2(A^3\Pi_g)$ or $CN(B^2\Sigma^+)$), in the absence of any rapid depopulation mechanism for the lower level, precludes population inversion.

The application of the kinetic analysis of Eqs. (6-1) - (6-4) to cases such as observed NO electronic excitation, shows major differences from the preceding case, and offers potential for strong laser action. We specifically consider cases such as the observed NO β fluorescence (Sec. 6.2). This system involves transitions to vibrational states $v = 4, 5, 6, 7, 8$ and 9 of the lower electronic level, i.e., the lower electronic level involves rather high-lying vibrational states, which are not significantly populated at thermal equilibrium. The possibility of obtaining laser action on such transitions is assessed by examining the population expressions for $A_2^1(v=m)$ and $A_2^2(v=n)$, the upper and lower laser levels, Eqs. (6-3) and (6-4), in conjunction with the small signal gain expression:

$$\alpha = \frac{\text{CONSTANT}}{\tau_{RAD}} \left\{ [A_2^1(v=m)] B_{1,m} e^{-E_{J'}/kT} - [A_2^2(v=n)] B_{2,n} e^{-E_{J''}/kT} \right\} \quad (6-8)$$

Here, α is the small signal gain on the $J' \rightarrow J''$ rotational line of the $A_2^1 (v = m) \rightarrow A_2^2 (v = n)$ vibronic transition, $B_{1,m}$, $B_{2,n}$ and $E_{J'}$, $E_{J''}$ are the rotational spectroscopic constants and the rotational energies, respectively, for the indicated states. Eq. (6-8) is for the small signal gain is similar to that originally derived by Patel⁵⁰ for laser transitions on pure vibrational bands. As in the case of such vibrational band lasers, it can be noted from Eq. (6-8) that a total population inversion, $[A_2^1 (v = m)] = [A_2^2 (v = n)]$, is not required to achieve positive gain. The electronic levels can be in a "partial population inversion," wherein gain can be realized on some P-branch rotational lines of the vibronic transitions.

It should first be noted that the largest potential inversions will be obtained on systems in which the laser levels, $A_2^1 (v = m)$ and $A_2^2 (v = n)$, are not coupled by the V-E transfer process itself. This lack of coupling is assumed in the formulation leading to Eqs. (6-1) - (6-4); physically, such coupling is minimized by selecting the lower laser level, $A_2^2 (v = n)$, to be a relatively high-lying state, and one rapidly deactivated by V-T processes. If the lower laser level is a low-lying state which cannot be rapidly V-T deactivated, gain can only be realized in the limit of rapid V-E equilibrium between the donor and acceptor molecules; this will yield rather weak partial inversions comparable to those in the CO V-V pumped "plateaus" of Figure 12; this case is discussed in Reference 51. In the present estimates, we consider the generally more advantageous case of rapid V-T quenching of the lower laser level.

On the basis of Eqs. (6-3), (6-4), and (6-8), and the model assumptions leading to their derivation, we enumerate criteria for a suitable acceptor molecule to be used in an electronic band laser, being excited by V-E transfer from vibrationally excited CO or N₂:

50. Patel, C.K.N., Phys. Rev. Lett. 12, 588 (1964).

51. Rich, J.W., Bergman, R.C., and Williams, M.J., "Measurement of Kinetic Rates for Carbon Monoxide Laser Systems", Calspan Report No. WG-6021-A-2, 1978

1. The molecule must not be a fast V-T relaxant for CO (or N₂). In all analysis, it is assumed the lasant species does not significantly quench the vibrationally excited donor via V-T collisions.

2. The rate of E-V transfer $k_{0 \rightarrow m}^{V \rightarrow E}$ must be sufficiently rapid to overcome quenching losses from the upper laser state. As can be seen from Eq. (6-3), it is desirable that

$$k_{0 \rightarrow m}^{V \rightarrow E} [X_2(v=i)] [A_2^2(v=0)]$$

be as large as possible in comparison to $k_{\text{QUENCH}} [M]$.

3. As can be seen from Eqs. (6-3) and (6-4), a long radiative lifetime τ_{RAD} laser, enhances the population inversion, as is well-known for many laser systems. However, the necessity of realizing useful gain in a reasonable pathlength (via Eq. (6-8)) places an upper limit on τ_{RAD} .

4. Collisional quenching of the lower laser level must be rapid, i.e., from Eq. (6-4), for a total population inversion:

$$\tau_{\text{RAD}} k_{\text{QUENCH}}^2 [M] > 1.$$

5. Vibration - vibration (V-V) transfer from the donor molecule to vibrational levels of the lower electronic state of the acceptor, and subsequent V-V pumping among the acceptor states, should be minimal.

6. The electronic transition chosen should, of course, be at a desirable visible or UV wavelength.

7. The electronic transition chosen should leave $B_{v''} > B_{v'}$; this will give the highest small signal gain, according to Equation (6-8).

Within the framework of the model just described, we have used Eqs. (6-3), (6-4) and (6-8) to estimate the possible small signal gain obtainable with the CO/NO β VE transfer laser. Table 9 summarizes the available rate data for this system. Using these data, small signal gain on the NO β ($v = 0 \rightarrow 8$) transition at 300°K is calculated by the following procedure:

i) The concentration of NO required to maintain equal populations in the upper and lower laser levels, $[A_2^1(v = m)] = [\text{NO } B^2\Pi(v = 0)] = [A_2^2(v = n)] = [\text{NO } X^2\Pi_\nu(v = 8)]$ is calculated from Eq. (6-4). Note that NO-NO collisions are by far the most effective V-T relaxer of the lower laser level ($[M] = [\text{NO}]$). This gives a required NO concentration of $8.1 \times 10^{17} \text{ cm}^{-3}$.

ii) We assume $[\text{CO}] = 10 [\text{NO}]$, and that the population distribution of CO vibrational states is that of the fully V-V pumped distributions of Figure 12, (Case 1). We further assume that the dominant $E \rightleftharpoons V$ process is close to resonance. In the notation of Eq. (6-3), these assumptions give $[X_2] \approx [\text{CO}] = 8.1 \times 10^{18} \text{ cm}^{-3}$, $[X_2(v=i)]/[X_2(v=0)] \approx [\text{CO}(v \approx 27)]/[\text{CO}(v=0)] \approx 5 \times 10^{-4}$, and $k_{0 \rightarrow m}^{V \rightarrow E} \approx k_{m \rightarrow 0}^{E \rightarrow V}$ into the NO $B^2\Pi(v = 0)$ state.

iii) The rate of V-E transfer, $k_{0 \rightarrow m}^{V \rightarrow E}$, is unknown at this time. Accordingly, we express the V-E transfer rate in terms of an unknown probability of V-E transfer per CO ($v = 27$) - NO ($X^2\Pi_\nu$) collision, P_{VE} , i.e.,

$$k_{0 \rightarrow m}^{V \rightarrow E} = P_{VE} Z_{\text{CO-NO}}$$

where $0 \leq P_{VE} \leq 1$, and $Z_{\text{CO-NO}}$ is the CO-NO gas kinetic collision frequency, as listed in Table 1. The rate of collisional quenching of the NO $B^2\Pi(v=8)$ state, k'_{QUENCH} , is taken as the measured NO-NO V-T quenching rate as given in Table 9.

TABLE 9

SUMMARY OF RATE DATA FOR CO/NO/Ar SYSTEM

	PROCESS	PROBABILITY	LIFETIME (seconds)	REF.
1.	CO(v=0) + CO(v=1) → CO(v=1) + CO(v=0)	1.5 (-2)		11
2.	CO(v=0) + CO(v=12) → CO(v=1) + CO(v=11)	1.0 (-4)		11
3.	CO(v=9) + CO(v=10) → CO(v=10) + CO(v=11)	1.0 (0)		11
4.	CO(v=1) + NO(v=0) → CO(v=0) + NO(v=1)	1.0 (-4)		12
5.	CO(v=12) + NO(v=0) → CO(v=11) + NO(v=1)	3.0 (-3)		12
6.	CO(v=1) + NO → CO(v=0) + NO	6.7 (-5)		13
7.	NO(v=1) + NO(v=1) → NO(v=0) + NO(v=2)	1.3 (-2)		14
8.	NO(v=1) + NO → NO(v=0) + NO	2.6 (-4)		14
9.	CO(v=2) → CO(v=0) + 2 hν ₀		3.4	15
10.	CO(v=1) → CO(v=0) + hν ₀		3.3 (-2)	15
11.	NO(v=2) → NO(v=0) + 2 hν ₀		1.17	16
12.	NO(v=1) → NO(v=0) + hν ₀		7.7 (-2)	16
13.	NO(v=1) + Ar → NO(v=0) + Ar	4.7 (-8)		14
14.	NO(B ² Π) → NO(X ² Π) + hν		3.16 (-6)	17
15.	NO(A ² Σ ⁺) → NO(X ² Π) + hν		1.78 (-7)	17
16.	NO(B ² Π, v'=0) + NO → NO(other states) + NO	4.7 (-1)		18
17.	NO(B ² Π, v'=0) + Ar → NO(other states) + Ar	9.7 (-4)		18

NOTE: In the gain estimates of the report, it has been assumed that:

- All diatomic - diatomic collisions (NO-NO, NO-CO, CO-CO) occur at a collision frequency of $3 \times 10^{-10} (T/300)^{1/2} \text{ cm}^3 \text{ sec}^{-1}$. All diatomic-argon collisions have a frequency of $2.7 \times 10^{-10} (T/300)^{1/2} \text{ cm}^3 \text{ sec}^{-1}$.
- Vibration - translation (V-T) energy transfer processes involving transitions between vibrational states $V \rightarrow V-1$, for $V > 1$, are related to the transition probability for $V=1 \rightarrow 0$, P_{10} , by

$$P_{V \rightarrow V-1} = V P_{10} .$$

iv) The small signal gain estimates based on the above procedure are plotted, using Eq. (6-8), in Figures 35 to 37. Gain on the $\text{NO } B^2 \Pi (v = 0) X^2 \Pi_v (v = 8)$ transition is plotted versus rotational quantum number of the upper laser level, J' , for various values of the $V \rightarrow E$ transition probability, P_{VE} . Gains have been calculated for room temperature (Figure 35) and reduced temperatures (Figure 36, 200°K, Figure 37, 100°K). It should be noted, however, that the same room temperature kinetic rates have been used in all calculations; there are no data for lower temperatures.

In these gain estimates, curves are shown for equal upper and lower laser level populations ($\text{NO}_u / \text{NO}_l = 1$), and for two total inversion cases ($\text{NO}_u / \text{NO}_l = 1.1, 1.2$). If we consider that small signal gains of the order of 0.1% per cm. and greater would result in a practicable laser, these estimates suggest the $V \rightarrow E$ transfer probability must be greater than 10^{-2} for room temperature operation, but can be somewhat less than this at reduced temperatures. Overall, transfer laser action appears feasible, unless the $V - E$ transfer rate is slow.

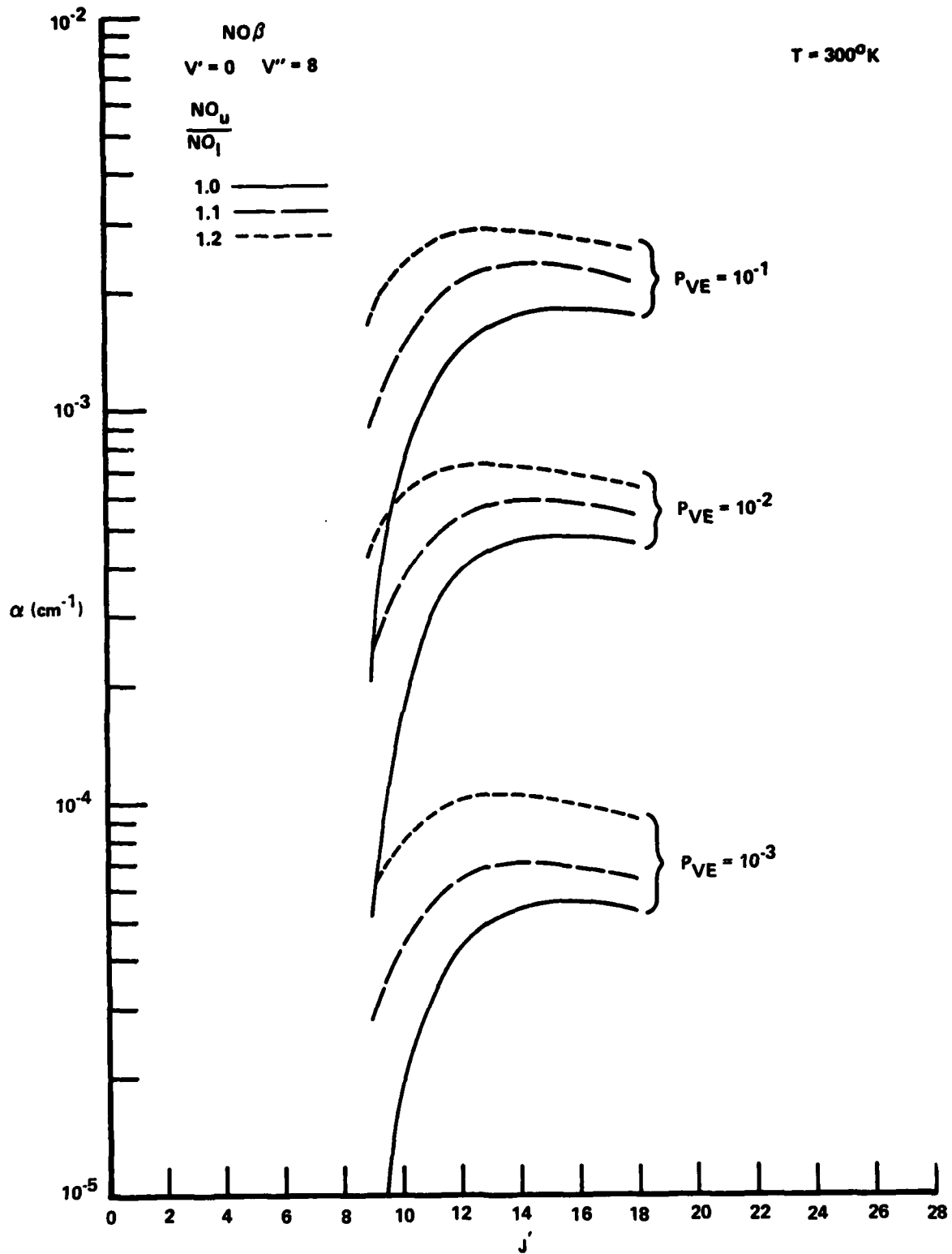


Figure 35 ESTIMATED CO-NO β TRANSFER LASER GAIN, T = 300°K

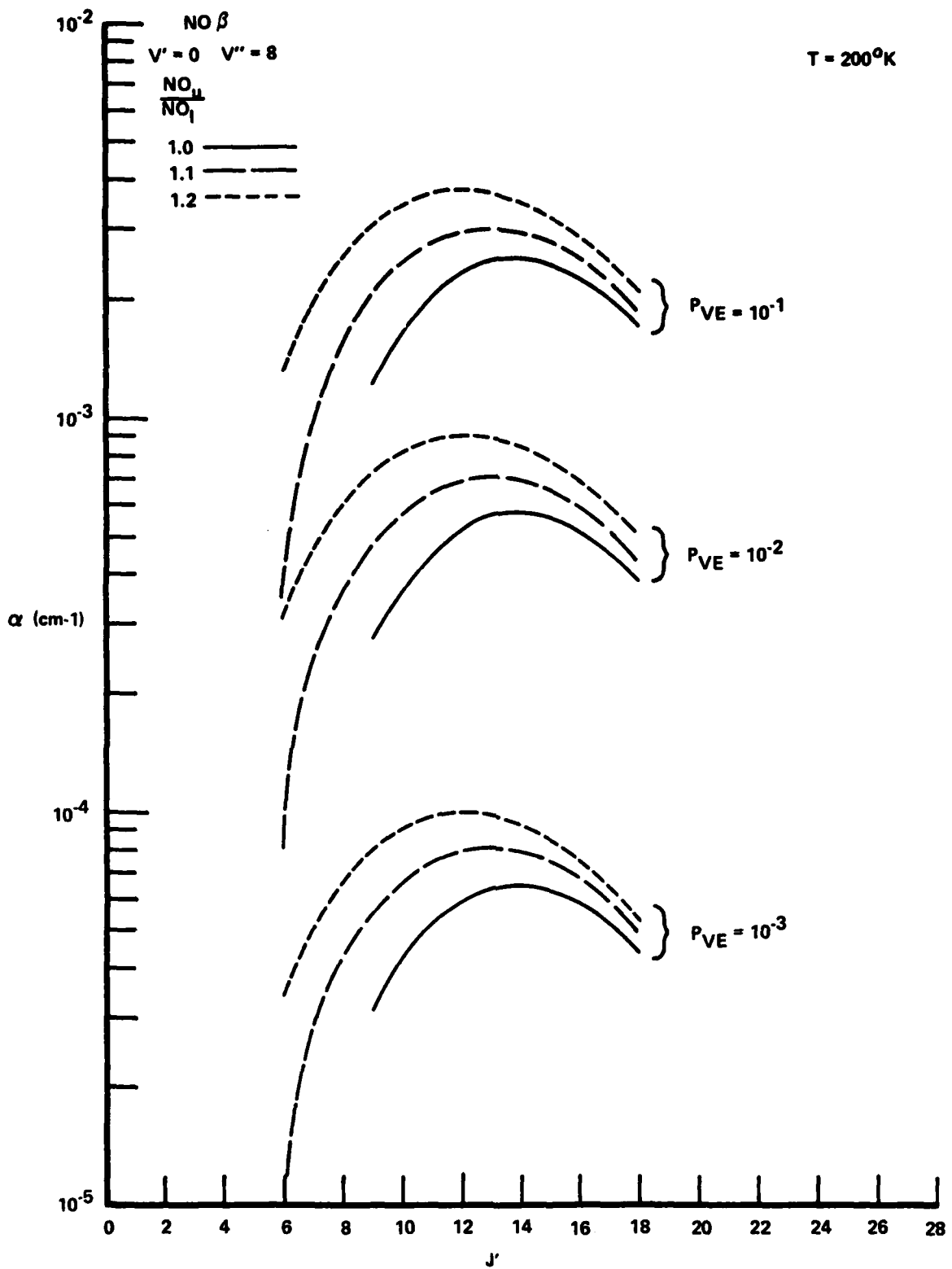


Figure 36 ESTIMATED CO-NO β TRANSFER LASER GAIN, $T = 200^\circ K$

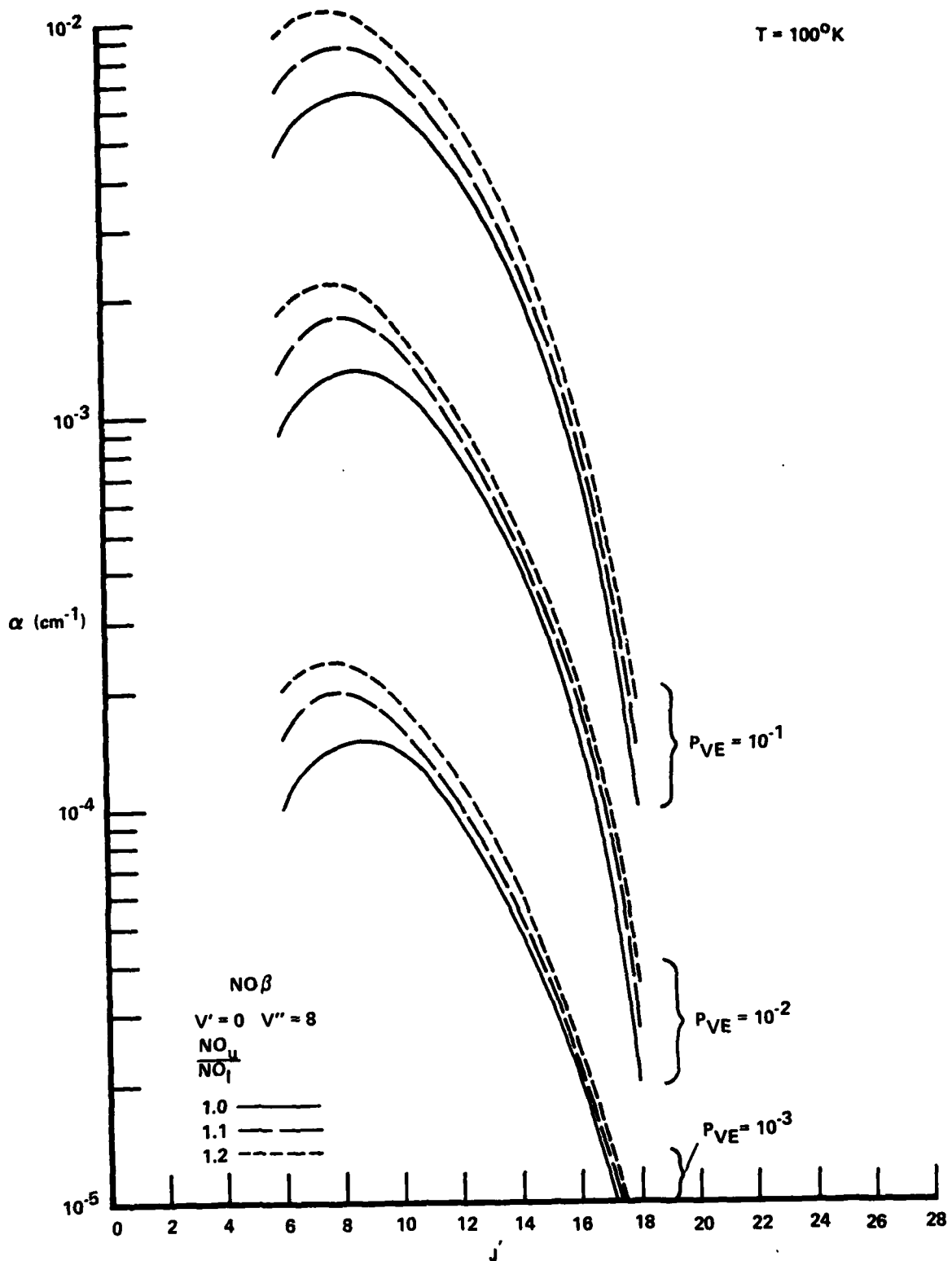


Figure 37 ESTIMATED CO-NO β TRANSFER LASER GAIN, T = 100°K

REFERENCES

1. Nikitin, E.E., Theory of Thermally Induced Gas Phase Reactions, Indiana Univ. Press, 1966.
2. Kieffer, J.H., Joosten, H.P.G., and Breshears, W.D., Chem. Phys. Lett. 30, 424 (1975).
3. Johnston, H. and Birks, K., Accounts Chem. Res. 5, 327 (1972).
4. Symposium on Current Status of Kinetics of Elementary Gas Reactions: Predictive Power of Theory and Accuracy of Measurement, J. Phys. Chem. 83, No. 1, 1979.
5. Bailey, W.F., and Cuscadden, A., J. Physique Colloque C7 Supplement Aun 7, 40 July 1979.
6. Bailey, W.F., Ph.D. Thesis, Air Force Institute of Technology, Wright-Patterson Air Force Base, Ohio 1978.
7. Rich, J.W., Bergman, R.C., and Lordi, J.A., AIAA J. 13, 95 (1975).
8. Lordi, J.A., Falk, T.J., and Rich, J.W., "Analytical Studies of the Kinetics of Electrically Excited, Continuously Operating CO Flow Lasers", AIAA Paper No. 74-563, AIAA 7th Fluid and Plasma Dynamics Conference, Palo Alto, California, June 17-19, 1974.
9. Rich, J.W., Lordi, J.A., Gibson, R.A., and Kang, S.W., "Supersonic Electrically Excited Laser Development", Calspan Report No. WG-5164-A-3, June 1974.
10. Lacina, W.B., et al., IEE J. Quant. Elec. QE-9, 120 (1973).
11. Smith, N.S., Hassan, H.A., McDuville, R.M., "Analysis of High-Flow Electric Discharge CO Laser Systems", AIAA Paper No. 74-180, AIAA 12th Aerospace Sciences Meeting, Washington, D.C., January 30 - February 1, 1974.
12. Center, R.E. and Caledonia, G.E., Appl. Phys. Lett. 19, 211 (1971).
13. Rich, J.W., J. Appl. Phys. 42, 2719 (1971).
14. Suchkov, A.F., and Shebeko, Yu. N., Sov. J. Quant. Electron. 9, 565 (1979).
15. Letokhov, V.S., Ann. Rev. Phys. Chem. 28, 133 (1977).
16. Gordiets, B.F., and Mamedov, Sh. S., Sov. J. Quant. Electronics 5, 1082 (1976).

17. Basov, N.G., Belenov, E.M., Gavrilina, L.K., Isakov, V.A., Markin, E.P., Oraevskii, A.N., Romanenko, V.I., and Ferapontov, N.B., JETP Lett. 20, 277 (1974); 19, 190 (1974); Basov, N.G., and Belenov, E.M., Isakov, V.A., Markin, E.P., Oraevskii, A.N., Romanenko, V.I., and Ferapontov, N.B., Sov. J. Quant. Electron. 5, 510 (1975); JETP 41, 1017 (1976).
18. Manuccia, T.J., and Goesling, C.E., Appl. Phys. Lett. 31, 575 (1977).
19. Manuccia, T.J., and Clark, M.D., Appl. Phys. Lett. 28, 372 (1976).
20. Hancock, G., and Smith, I.W.M., Chem. Phys. Lett. 8, 41 (1971).
21. Fisher, E.R., Rabitz, H., and Lam, S.H., "CO-He V-T Rates at High Quantum Numbers", Paper presented at 5th Conference on Chemical and Molecular Lasers, St. Louis, Mo. 1977.
22. Hancock, G., and Smith, I.W.M., Appl. Opt. 10, 1827 (1971).
23. Treanor, C.E., Rich, J.W., and Rehm, R.G., J. Chem. Phys. 48, 1798 (1968).
24. Rich, J.W., Bergman, R.C., and Williams, M.J., "Measurement of Kinetic Rates for Carbon Monoxide Laser Systems", Calspan Report No. WG-6021-A-1, November 1977.
25. Milliken, R.C., J. Chem. Phys. 38, 2855 (1963).
26. Horn, K.P., and Oettinger, P.E., J. Chem. Phys. 54, 3040 (1971).
27. Mantz, A.W., Nichols, E.R., Alpert, B.D. and Rao, K.N., Journal of Molecular Spectroscopy 35, 325-328, (1970).
28. Roh, W.B. and Rao, K.N., J. Mol. Spectrosc. 49, 317 (1974).
29. Young, L.A. and Eachus, W.J., J. Chem. Phys. 44, 4195 (1966).
30. Lightman, A.J. and Fisher, E.R., Appl. Phys. Lett. 29, 593 (1976); Fisher, E.R., Private Communication (1977).
31. Lam, S.H., J. Chem. Phys. 67, 2577 (1977).
32. Brechignac, Ph., Chem. Phys. 34, 119 (1978).
33. Powell, H.T., J. Chem. Phys. 59, 4937 (1973).
34. Caledonia, G.E. and Center, R., J. Chem. Phys. 55, 552 (1971).
35. Drozdowski, W.S., Young, R.M., Bates, R.D., Jr., and Hancock, J.K., J. Chem. Phys. 65, 1542 (1976).
36. Verter, M. and Rabitz, H., J. Chem. Phys. 64, 2939 (1976).

37. Djeu, N., Chem. Phys. Lett. 15, 392 (1972).
38. Lordi, J.A., and Rich, J.W., "A Theoretical Study of a High-Pressure, Tunable CO Laser", Report No. AFAL-TR-75-184, USAF Avionics Laboratory, December 1975.
39. Rich, J.W., Lordi, J.A., Gibson, R.A. and Kang, S.W., "Supersonic Electrically Excited Laser Development", Calspan Report No. WG-5164-A-3, June 1974.
40. Lordi, J.A., Falk, T.J., and Rich, J.W., "Analytical Studies of the Kinetics of Electrically Excited, Continuously Operating CO Flow Lasers", AIAA Paper No. 74-563, AIAA 7th Fluid and Plasma Dynamics Conference, Palo Alto, California, June 17-19, 1974.
41. Smith, Astrophysical J. 156, 791 (1969).
42. McCoy, B.J., and Carbonell, R.G., Chem. Phys. 20, 227 (1977).
43. Hogarth, W.L., and McElwain, D.L.S., Chem. Phys. 19, 429 (1977).
44. Collins, C.J., and Bowman, N.S., Isotope Effects in Chemical Reactions, ACS Monograph No. 167 (Van Nostrand-Reinhold, NY, 1970), p. 15, p. 15; Lukasik, J., and Ducing, J., Chem. Phys. Lett. 27, 203 (1974).
45. Provencher, G.M. and McKenney, D.J., Chem. Phys. Lett. 10, 365 (1971).
46. Reisler, H., Mangir, M. and Wittig, C., "The Kinetics of Free Radicals Generated by IR Laser Photolysis: I. Reactions of C_2 ($a^2\Pi_u$) with NO, Vinyl Cyanide, and Ethylene", Dept. of Elec. Eng., USC, 1979. To be published.
47. Suchard, S.N., "Spectroscopic Constants for Selected Heteronuclear Diatomic Molecules" Vol. II. Aerospace Corporation Report No. TR-0074(4641)-6, Vol. II, 1974.
48. Allen, R.A., "Air Radiation Tables: Spectral Distribution Functions for Molecular Band Systems" Avco Everett Research Lab. Report No. 236, 1966.
49. Lemont, S., and Flynn, G.W., Ann. Rev. Phys. Chem. 28, 261 (1972).
50. Patel, C.K.N., Phys. Rev. Lett. 12, 588 (1964).
51. Rich, J.W., Bergman, R.C., and Williams, M.J., "Measurement of Kinetic Rates for Carbon Monoxide Laser Systems", Calspan Report No. WG-6021-A-2, 1978.